EXPLORING CARRIER IMPACT ON IMMUNE RESPONSE TO NUCLEIC ACID NANOPARTICLES AND PROVIDING INSIGHTS INTO CONDITIONALLY ACTIVATED THERAPEUTIC NUCLEIC ACIDS

by

Yelixza Idalyss Avila

A dissertation submitted to the faculty of
The University of North Carolina at Charlotte
in partial fulfillment of the requirements
for the degree of Doctor of Philosophy in
Nanoscale Science

Charlotte

2024

Approved by:

_____
Dr. Kirill Afonin

_____
Dr. Brittany Johnson

_____
Dr. Juan Vivero-Escoto

_____
Dr. Jerry Troutman

_____
Dr. Vasily Astratov

ABSTRACT

YELIXZA IDALYSS AVILA. Exploring Carrier Impact on Immune Response to Nucleic Acid Nanoparticles and Providing Insights into Conditionally Activated Therapeutic Nucleic Acids.

(Under the direction of DR. KIRILL AFONIN)

In this work, the in vitro characterization profiles of delivery vehicles, specifically polyamidoamine (PAMAM) dendrimers, are assessed to investigate their impact on pre-established immune responses to immunostimulatory and immunoquiescent nucleic acid nanoparticles (NANPs). Isolated human peripheral blood mononuclear cells (PBMCs) were used as the universal model system for these investigations, providing a detailed understanding of the impact delivery vehicles play on NANP recognition. Additionally, to further identify mechanisms of immune recognition of these novel formulations, several engineered reporter cell lines were employed to understand the involvement of pattern recognition receptors relevant to nucleic acid detections in human cells.

Furthermore, we explore the design and in vitro assessment of conditionally activated reconfigurable nucleic acid nanoparticles (recNANPs). By further investigating dynamic recNANPs and their interactions with delivery vehicles and the immune system, we aim to gain deeper insights into these systems. This innovative platform will enable the development of refined design principles for therapeutic systems incorporating NANPs, allowing for the creation of more precise and optimized options.

ACKNOWLEDGMENTS

I would not be here today without the support of everyone who has ever believed in me. From the bottom of my heart, thank you to each of you. It has taken a village, and I would be remised to not acknowledge the aid and support of my mentors, friends, and family.

To begin, I would like to start by acknowledging my advisor, Dr. Kirill A. Afonin for being a constant support throughout my journey of graduate school. Your ability to always encourage any idea with infectious enthusiasm and crossed fingers went such a long way. You have taught me so much about research, radical confidence, and to always shoot my shot. The constant challenges have ensured my growth as a researcher and as a person. Thank you for welcoming me and my family into your lab with open arms and for supporting us as we grew. You believed in me the whole way through.

I also want to thank my dissertation members, Dr. Johnson, Dr. Vivero-Escoto, Dr. Troutman, and Dr. Astratov for their constant support and accommodation. There were plenty of times when I went to you all for support and advice, and you always delivered. Dr. Bernadette Donovan-Merkert, thank you for seeing us all as individuals and genuinely supporting us in every way possible.

I am also grateful for everyone at the Nanotechnology Characterization Lab – Dr. Dobrovolskaia, Dr. Newton, and Ed – for sharing their research expertise, taking time to train me, and for sharing their wisdom with me. My time there contributed an insurmountable amount of knowledge, data and information for my dissertation.

I would also like to acknowledge the NIH for their support of my research and career track. Research reported in this publication was supported by the National Institute Of General Medical Sciences of the National Institutes of Health under Award Number F31GM146479. The content is solely the responsibility of the authors and does not necessarily represent the official views of the National Institutes of Health.

Thank you to everyone at UNC Charlotte helped with the submission process, as well as navigating our way through it all (Peter, Paul, Rebecca, Ida, Joconda).

To our prep room ladies, thank you so much for your constant supply of smiles and support, and for always being excited with us whenever a new package came in – Brenda and Cindy.

To my peers and friends alike from the program, this experience was one that was made easier because of your support, weirdness, and laughs. Many of you opened your homes, hearts, and families up to us, and for that I'll forever be thankful. To all our lab alumni, thank you for your infinite source of wisdom and guidance, you all gave me something to aspire to everyday. To those who came after me, I know that each of you will become top-notch scientists and are already well on your way to doing so.

To my *pollitos* (Laura, Brandon, and Jose), thank you for coming in each day, challenging me as a mentor and scientist. Each of you has added to my life, and in times of struggle, you all provided motivation and normalized excellence as part of our everyday routine. A million dollars will never be enough. To Melanie, Jalen, and Jaden, although you have moved on from the lab in your individual pursuits, your impacts are long lasting. Thank you all for making my time as your mentor such an enriching and fulfilling experience.

To Armando, my biggest supporter, thank you for choosing to live life with me, and for understanding the life of a graduate student and researcher. Thank you for always believing in me, even when I didn't want to believe in myself. Thank you for pushing me to get back up every single time. Throughout this journey, you have seen me become not only a scientist and doctorate, but also a mother to our son, Leo. For you both, I do my best every day. I can't wait for our next adventure.

DEDICATION

I dedicate my dissertation work to my family.

Los quiero mucho. Gracias por todo el apoyo. Desde mi corazón, les doy mil gracias a cada uno de ustedes.

Descansa en paz, papi

TABLE OF CONTENTS

LIST OF TABLES ix

LIST OF FIGURES x

LIST OF ABBREVIATIONS xiv

1 CHAPTER 1: INTRODUCTION 1

1.1. EXPLORING THERAPEUTIC POTENTIAL: NUCLEIC ACID NANOTECHNOLOGY IN BIOMEDICINE 1

1.2. IDENTIFYING CHALLENGES AND OPPORTUNITIES: BRIDGING THE GAP IN NUCLEIC ACID THERAPIES AND TECHNOLOGIES 3

1.3. NAVIGATING DELIVERY CHALLENGES: STRATEGIES FOR EFFICIENT NUCLEIC ACID NANOPARTICLE TRANSPORT INTO CELLS 4

1.4. MITIGATING UNINTENDED CONSEQUENCES: UNDERSTANDING OFF-TARGET EFFECTS IN NUCLEIC ACID THERAPIES 5

1.5. UNDERSTANDING THE IMMUNOLOGICAL LANDSCAPE: IMMUNE RECOGNITION OF NUCLEIC ACID NANOPARTICLES 5

1.6. ADVANCING NUCLEIC ACID THERAPEUTICS: STRATEGIES FOR ENHANCED PRECISION, EFFICACY, AND OVERCOMING CHALLENGES 8

2 CHAPTER 2: INDUCTION OF CYTOKINES BY NUCLEIC ACID NANOPARTICLES (NANPS) DEPENDS ON THE TYPE OF DELIVERY CARRIER 12

2.1. INTRODUCTION 12

2.2. RESULTS 14

2.3. DISCUSSION 25

2.4. MATERIALS AND METHODS 28

2.5. CONCLUSIONS 33

3 CHAPTER 3: EXPLORING DENDRIMER-NUCLEIC ACID NANOPARTICLE INTERACTIONS: IMPACT ON IMMUNE RECOGNITION AND DIFFERENTIAL COMPLEXING OF DNA AND RNA 37

3.1. INTRODUCTION 37

3.2. RESULTS AND DISCUSSION 40

3.3. METHODS 47

3.4. CONCLUSIONS 51

4 CHAPTER 4: RECONFIGURABLE NUCLEIC ACID NANPARTICLES: ACTIVATED BY INTRACELLULAR BIOMARKERS FOR THE RELEASE OF THERAPEUTIC RNAI INDUCERS 56

4.1. INTRODUCTION 56

4.2. RESULTS AND DISCUSSION 59

4.3. METHODS 63

4.4. CONCLUSION 66
5 CHAPTER 5: CONCLUSIONS 72
FUTURE PROSPECTS 72
REFERENCES 76
APPENDIX A: Previously published material 90

LIST OF TABLES

Table 1. Summary of the hydrodynamic diameters for G5-NH2 PAMAM dendrimers. 14
Table 2. Summary of the zeta potentials for G5-NH2 PAMAM dendrimers. 15

LIST OF FIGURES

Figure 1. Therapeutic landscape of nanomedicines. Nanomedicines are being explored for various therapeutic fields, including chemotherapy, immunotherapy, nucleic acid therapy, radiation therapy, photothermal therapies, and postoperative treatments[7]. 1
Figure 2. Structure and connectivity of nucleic acids (made in Biorender). 2
Figure 3. Delivery Vehicle/carrier candidates for nucleic acids and their desired properties. 4
Figure 4. Illustration depicting the activation of immune outputs after recognition of a pathogen (made in Biorender). 6
Figure 5. PBMCs → treatment → cytokines produced and released → immune response data (made in Biorender). 8
Figure 6. Physicochemical characterization of the G5-NH2 PAMAM dendrimers. The averaged intensity (A) and volume (B) distribution plots as measured by dynamic light scattering and the averaged zeta potential distribution (C). The hydrodynamic size was measured before and after filtration through a 0.02 μm filter. Zeta potential was measured both at its native pH and after adjustment to neutrality. 14
Figure 7. DNA and RNA cube characterization. 3D models, native-PAGE results, and representative AFM images of (A) DNA cubes and (B) RNA cubes. 15
Figure 8. NANPs complexed with G5-NH2 dendrimers. (A) Transmission electron microscopy images of Lipofectamine 2000 (L2K), G5-NH2 dendrimers, and DNA and RNA cubes complexed to either L2K or G5-NH2 dendrimers. (B) Resulting fluorescence profiles from nuclease resistance assays. (C) Mean fluorescence intensity associated with the in vitro uptake of Alexa 488-labeled DNA and RNA cubes in MDA-MB-231 cells. Each bar shows the mean response and standard deviation (N = 3). Statistical significance between the DNA and RNA cubes delivered with G5-NH2 versus all other treatments is denoted by **** where $p < 0.0001$. (D) Brightfield and GFP microscopy images of MDA-MB-231 cells transfected with DNA cubes complexed to G5-NH2 dendrimers and RNA cubes complexed to G5-NH2 dendrimers. 17
Figure 9. Experimental flow of the complexation of DNA and RNA cubes with either G5-NH2 dendrimers or L2K and their further analysis in PBMCs. 18
Figure 10. Cytokine induction by DNA and RNA cubes as a function of the delivery carrier. PBMC from three healthy human donor volunteers (F4Z5, G2K9, and M9K9) were treated with negative control (NC), positive control (PC), DNA cubes, or RNA cubes for 24 h. Prior to the addition to PBMC cultures, DNA cubes and RNA cubes were complexed with lipofectamine 2000 (L2K), G5 amine-terminated PAMAM dendrimers (G5-NH2) or used without complexation (no carrier). Culture supernatants were analyzed for the presence of cytokines, chemokines, and interferons using multiplex ELISA as described in the Materials and Methods. The data are presented based on the function of cytokines, including (A) type I and type III interferons, (B) danger signals and cytokines commonly associated with trauma and cytokine storm, (C) type II interferon and type II interferon-inducible protein, and (D) chemokines. Each bar shows the mean response and standard deviation (N = 2). Other cytokines from this study are presented on Figure 15. 21
Figure 11. Correlation analysis of cytokine response. The data from the multiplex cytokine analysis including those presented in Figure 10 were analyzed using the GraphPad Prism software to determine a correlation or lack thereof between individual cytokines. (A) The Pearson correlation matrix assumes a Gaussian distribution (parametric analysis). In this analysis, values between ±0.5 and ±1 refer to a high degree of correlation, whereas values

close to ±1 mean perfect correlation; negative values (in red) refer to the negative correlation, whereas positive values (in blue) mean positive correlation. (B) The Spearman correlation matrix assumes no Gaussian distribution (non-parametric analysis). In this analysis, values of ±1 mean perfect correlation; the closer the value is to zero, the weaker the association is; negative values (in red) and positive values (in blue) refer to the negative and positive correlation, respectively. 23
Figure 12. Uptake of fluorescently labeled DNA and RNA cubes by peripheral blood cells. PBMCs from three healthy human donor volunteers (F4Z5, G2K9, and M9K9) were either left untreated or incubated with Alexa 488-labeled DNA cubes or RNA cubes for 24 h. Prior to the addition to PBMC cultures, DNA cubes and RNA cubes were complexed with Lipofectamine 2000 (L2K), G5 amine-terminated PAMAM dendrimers (G5-NH2) or used without complexation (no carrier). After a wash to remove excess particles, the cells were analyzed by flow cytometry as described in the Materials and Methods. (A) Analysis of the percentage of positive cells indicates the overall proportion of the cells in either the lymphocyte or monocyte population associated with the fluorescent signal that is greater than that in the carrier alone or untreated cells. (B) Analysis of geometric mean fluorescent intensity (GMFI) reveals the degree of a fluorescent signal associated with the individual cells in the lymphocyte or monocyte populations. Green fluorescence is delivered to the cells by DNA and RNA oligonucleotides labeled with Alexa 488 prior to their assembly into DNA and RNA cubes, respectively. Each bar shows the mean response and standard deviation (N = 2). 25
Figure 13. Complexation of DNA duplex with G5-NH2 dendrimers at various N/P ratios. DNA duplexes labeled with Alexa 488 (labeled in green font) were combined with G5-NH22 dendrimers (labeled in blue font) at different negative charge (N) to positive charge (P) ratios as shown above. The samples were then analyzed by agarose gel electrophoresis. 35
Figure 14. Cell viability assay of MDA-MB-231 cells treated with NANPs and G5 NH2 dendrimers. Viability of MDA-MB-231 cells after being exposed to DNA cube G5-NH2 dendrimer complexes which was evaluated at 72 hours. All samples remained above an 80% viability. 36
Figure 15. Cytokine induction by DNA and RNA cubes as a function of the delivery carrier. PBMC from three healthy human donor volunteers (F4Z5, G2K9, and M9K9) were treated with negative control (NC), positive control (PC), DNA cubes, or RNA cubes for 24 hours. Prior to the addition to PBMC cultures, DNA cubes and RNA cubes were complexed with lipofectamine 2000 L2K), G5 amine-terminated PAMAM dendrimers (G5-NH2) or used without complexation (no carrier). Culture supernatants were analyzed for the presence of cytokines, chemokines, and interferons using multiplex ELISA as described in Materials and Methods. The data for other cytokines grouped based on their function (i.e., type I and type III interferons, danger signals and cytokines commonly associated with trauma and cytokine storm, type II interferon and type II interferon inducible protein, and chemokines are presented on Figure 5. Each bar shows the mean response and standard deviation (N = 2). 36
Figure 16. Experimental workflow of NANPs and dendrimer complexing and in vitro assessment. A) DNA or RNA cubes will be complex to each dendrimer generation. B) Binding will be characterized by electromobility shift assays, and nuclease protection assays. C) Complexed NANPs and dendrimers will be run through in vitro characterization profiles of uptake and immune activation. D) Acquired data will be assessed and analyzed. 39
Figure 17. Binding assays of DNA duplexes to dendrimers at increasing N/P ratios – from left to right. Table with dendrimer characteristics for each generation. 40

Figure 18. Nuclease protection assay of each generation of dendrimer. A) Schematic representation of the nuclease protection assay experiment. B) The legend for each of the generations and controls. C) Nuclease protection results for dendrimers plus duplex at an N/P of 1. D) Nuclease protection results for dendrimers plus duplex at an N/P of 2. 41
Figure 19. Comparison of DNA and RNA Cube Uptake in HEK-293FT Cells Across Dendrimer Generations. A) Microscopy images: Images depict uptake of DNA and RNA cubes labeled with Al488 fluorophore in HEK-293FT cells. B) Flow cytometry data: Percentage of HEK-293FT cells positive for Al488 fluorescence at each dendrimer generation is presented, indicating uptake efficiency. 42
Figure 20. Using human reporter cell lines to investigate immune response of dendriplexes at the endosomal and cytosolic level. A) hTLR3 cells were transfected at a final concentration of 10 nM cube construct complexed to each dendrimer generation at N/P of 2. B) hTLR7 cells were transfected at a final concentration of 10 nM cube construct complexed to each dendrimer generation at N/P of 2. C) hTLR9 cells were transfected at a final concentration of 10 nM cube construct complexed to each dendrimer generation at N/P of 2. D) RIG-I cells were transfected at a final concentration of 10 nM cube construct complexed to each dendrimer generation at N/P of 2. 43
Figure 21. PBMC results of interferon response to DNA vs RNA cubes complexed to dendrimers generations 3-7. From top to bottom: Type I IFNs (IFN-α and IFN-β), Type II IFN-λ, and Type III IFN-γ. From left to right: Donors 1 through 3, showing the concentration of each IFN produced in response to treatment. 46
Figure 22 Uptake of DNA and RNA cubes complexed to dendrimers into HEK-293FT cells. Cubic NANPs were complexed to dendrimers at either an N/P of 1 or 2 and transfected into cells at a final NANP concentration of 20 nM for a period of 24 hours to coincide with the TLR investigation protocols. 54
Figure 23. Cell viability of HEK-293FT cells. HEK-293FT cells were transfected with either DNA or RNA cube dendriplexes for a period of 24 hours at either an N/P of 1 or 2. Final NANP concentration was 20 nM. 54
Figure 24. Cell viability of reporter cell lines: hTLR 3, hTLR 7, hTLR 9, and RIGI cells. Cells were transfected with either DNA or RNA cube dendriplexes for 24 hours and then tested for any impacts on cell viability. Transfections were completed at an N/P of 2 and for a period of 24 hours to coincide with QUANTI-Blue and QUANTI-Luc testing. 55
Figure 25. Cytokine induction by DNA and RNA cubes when complexed to dendrimers generations 3-7. PBMCs from three healthy human donor volunteers were treated with a negative and positive control, and RNA or DNA cube dendriplexes for 24 hours. Prior to the transfection, DNA and RNA cubes were complexed with lipofectamine 2000 (L2K), or amine-terminated PAMAM dendrimers. Supernatants were then analyzed for the presence of cytokines, chemokines, and interferons using multiplex ELISA assays. 55
Figure 26. Modular four-stranded reconfigurable nucleic acid nanoparticles (recNANPs) for conditional activation of therapeutic RNAi responses upon interaction with a trigger mRNA. (a) Working principle of molecular beacons (MBs). (b) Working principles of split RNAi inducers. (c-d) Proposed design of recNANPs which act as a simple NOT logic gate (c) and allow for conditional activation of RNAi (d). In (d), 2D schematics and predicted 3D structures are shown for all constructs. 59
Figure 27. In vitro characterization of recNANPs. (a) Schematic of recNANPs and native-PAGE (with EtBr staining or Alexa 488 labeled recNANPs) for assessment of assembly and working principles of recNANPs. (b) Atomic force microscopy (AFM) of recNANPs and

recNANPs incubated with target sequence, showing the morphology changes for inactive and activated state. 61
Figure 28. Cellular and specificity in activation of recNANPs. (a-b) Microscopy of uptake in PANC-1 and HEK-293FT cells of labeled DS RNAs and recNANPs after 72 hours of incubation. (c) Relative expression of Survivin in PANC-1 and HEK-293FT cells. Expression of Survivin in (d) PANC-1 and (e) HEK-293FT cells after treatment with DS RNA and recNANPs with media replaced after 24 hours for total of 72 hours incubation, analyzed by western blots. Representative immunoblots demonstrate changes in expressions of Survivin at the predicted size of 16.5 kDa (SI Fig. S4-S5). Each bar represents the mean of N=3 biological repeats ± SEM. Asterisks indicate statistical significance (one-ways ANOVA, $p<0.0001$). 63
Figure 29. Assembly conditions of recNANPs. (A) recNANPs (Surv) and (B) recNANPs (BCL2) at 4-8-12-16-37 and 45°C from 0 to 10 minutes Figure S2. Relative stability of recNANPs when stored at 4°C, room temperature (RT), and 50°C for durations ranging from 24 to 72 hours, using native PAGE (8%). (A and B) The stability of speed-vac-dried recNANPs and duplexes were investigated when stored at 4°C and 50°C, with the recNANPs assembled using dried duplexes stored from 24 to 72 hours. (C and D) Similarly, duplexes in solution were examined when stored at RT and 50°C, with recNANPs assembled using these stored duplexes from each time points. (E and F) Dried assembled recNANPs was evaluated when stored at 4°C and 50°C from 24 to 72 hours, as well as the stability of recNANPs in solution stored at 4°C, RT, and 50°C at corresponding time points (G and H). 69
Figure 30. Relative expression of Survivin in HEK-293FT and PANC-1 and relative cell viability. A) Western blat analysis of Surv expression in HEK-293FT and PANC-1 cells. B) Expression quantification of Surv in HEK-293FT and PANC-1 cells. C) Cell viability in each cell line. Data presented as mean ± SEM (N=3). 70
Figure 31. Detection of Survivin expression in PANC-1 cells and cell viability under treatment with 25 and 50nM DS RNAs or recNANPs with media changed 24 hours after transfection and total incubation of 72 Hours. (A) Immunoblotting for detection of Survivin in PANC-1 cells. (B) Correlation of cell viability to each treatment in PANC-1 cells. Data presented as Mean ± SEM (N=3). 70
Figure 32. Detection of Survivin expression in HEK-3293FT cells and cell viability under treatment with 25 and 50nM DS RNAs or recNANPs with media changed 24 hours after transfection and total incubation of 72 Hours. (A) Immunoblotting for detection of Survivin in HEK-3293FT cells. (B) Correlation of cell viability to each treatment in HEK-3293FT cells. Data presented as Mean ± SEM (N=3). 71
Figure 33. Detection of Survivin expression in PANC-1 and HEK-293FT cells and cell viability under different concentrations of DS RNAs and recNANPs after 48 hours incubation. (A-B) Immunoblotting for detection of Survivin in PANC-1 cells from 1 to 25nM with cells viability under same treatments. (C-D) Immunoblotting of PANC-1 and HEK-293FT with their viability when treated at 2.5 to 7.5nM for 48 hours. Data presented as Mean ± SEM (N=3). 71

LIST OF ABBREVIATIONS

3WJ	3-way junction
AB	Assembly buffer
AL488	Alexa Fluor 488
APS	Aminopropyl silatrane
ASO	Anti-sense oligonucleotide
BBB	Blood brain barrier
BCL2	B-cell lyphoma 2
BSA	Bovine serum albumin
cGAS	Cyclic GMP-AMP synthase
CNS	Central nervous sytem
CO2	Carbon dioxide
CpG	Cytosine phosphate guanosine
DAMP	Damage associated molecular pattern
ddH2O	Double deionized water
DMEM	Delbuco's modified eagle medium
DNA	Deoxyribonucleic acid
DS	Dicer substrate
DSBCL2	Dicer substrate against BCL2
dsRNA	Double-stranded RNA
DSSURV	Dicer substrate against Survivin
DTT	Dithiothreitol
ELISA	Enzyme linked immunosorbent assay
EU	Endotoxin unit
FBS	Fetal bovine serum
FDA	Food and drug administration
FRET	Förster resonance energy transfer
GFP	Green fluorescent protein
gMFI	Geometric mean fluorescence
IFN I	Type one interferon
IFN-α	Interferon alpha
IFN-β	Interferon beta
IL-1B	Interleukin 1B
IL-6	Interleukin 6
IL-8	Interleukin 8
IWB	Iowa black quencher
KCl	Potassium chloride
L2K	Lipofectamine 2000
LAL	Limulus amoebocyte assay
Li	Lithium
lncRNA	Long non-coding ribonucleic acid
LPS	Lipopolysaccaride
MDA5	Melanoma differentiation-associated protein 5
MgCl2	Magnesium chloride
MIP-1α	Macrophage inflammatory protein alpha
miRNA	Micro ribonucleic acid
mRNA	Messenger ribonucleic acid
MW	Mesoporous silica nanoparticle
N/P	Amine to phosphate ratio

NaCl	Sodium chloride
NANP	Nucleic acid nanoparticle
nm	Nanometer
nM	Nanomolar
PAGE	Polyacrylamide gel electrophoresis
PAMAM	Polyamidoamine
PAMP	Pathogen associated molecular pattern
PBMC	Peripheral blood mononuclear cell
PCR	Polymerase chain reaction
pDNA	Purified deoxyribonucleic acid
PRR	Pattern recognition motif
recNANP	Reconfigurable nucleic acid nanoparticle
RIGI	Retinoic inducible gene
RISC	Ribonucleic acid induced silencing complex
RNA	Ribonucleic acid
RNAi	Ribonucleic acid interference
rNTP	Ribonucleotide triphosphate
RT	Room Temperature
RT-PCR	Reverse transcriptase polymerase chain reaction
shRNA	Short hairpin ribonucleic acid
siRNA	Small interfering ribonucleic acid
ssDNA	Single stranded deoxyribonucleic acid
ssRNA	Single stranded ribonucleic acid
STING	Stimulator of interferon genes
SURV	Survivin
T7 RNAP	R7 ribonucleic acid polymerase
TB	Tris-borate buffer
TBE	Tris-borate ethylenediaminetetraacetic acid buffer
TEM	Transmission electron microscopy
TLR	Toll-like receptor
TNA	Therapeutic nucleic acid
TNFα	Tumor necrosis factor alpha
μL	Microliter
μM	Micromolar
UV	Ultraviolet
w/w	Weight by weight

1 CHAPTER 1: INTRODUCTION

The field of nucleic acid nanotechnology is rapidly expanding, promising profound implications across a spectrum of applications, encompassing biological and computational fields[1-4]. Nucleic acids are a set of biological materials that possess inherent versatility, rendering them indispensable in a diverse range of applications. As such, the field of nucleic acid nanotechnology is endeavoring to capitalize on the functional and structural characteristics of nucleic acids to harness and unlock the potential of these natural biopolymers[5-8].

1.1. EXPLORING THERAPEUTIC POTENTIAL: NUCLEIC ACID NANOTECHNOLOGY IN BIOMEDICINE

Nanotechnologies are being explored across various biomedical domains such as diagnostics, therapeutics, immunotherapies, and vaccine development. Various subclasses of nanoscale technologies are under development for therapeutic interventions, including metallic nanoparticles, polymeric nanoparticles, and biologically inspired nanoparticles[9-12]. Their integration as novel therapeutics is attributed to the unique phenomena that occur at the nanoscale, ensuring a high payload when utilizing nanomaterials[13] Applicable treatment avenues include cancer therapeutics, immune-oncology, antibiotics, vaccines, cardiovascular disease[14], imaging, and diagnostics. (Figure 1).

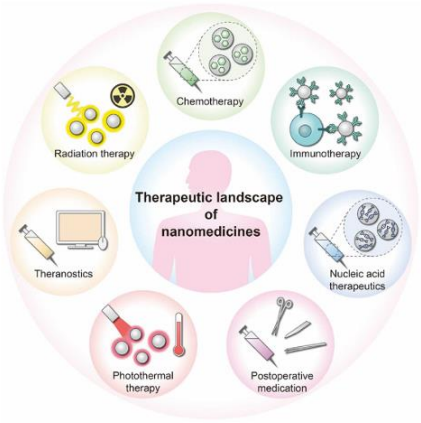

Figure 1. Therapeutic landscape of nanomedicines. Nanomedicines are being explored for various therapeutic fields, including chemotherapy, immunotherapy, nucleic acid therapy, radiation therapy, photothermal therapies, and postoperative treatments[11].

Nucleic acid nanoparticles (NANPs) represent a promising frontier in biomedical research, owing to their biocompatibility and customizable attributes derived from the programmability of nucleic acids and their sequences. This programmability enables precise control over the structure and function of NANPs, making them highly adaptable for various biomedical applications[1, 15-17].

The chemical structure of nucleic acids – deoxyribose and ribonucleic acids - is categorized into the three main segments that comprise a nucleic acid – the nucleobase, pentose sugar, and the phosphate backbone (Figure 2). The phosphate backbone is negatively charged at neutral pH and is identical in both DNA and RNA. The phosphate backbone covalently links to the pentose sugar group. A key indicator of DNA vs RNA molecules is the additional 2' -hydroxyl group in RNA, which contributes to different interactions with delivery vehicles. For example, the 2'-hydroxyl group is polar and contributes to RNA's reactivity being higher than that of DNA. Furthermore, these 2'-hydroxyl groups also contribute to the orientation of RNA, resulting in a different helical structure than DNA. The different shape and twist of the helical structure impacts the secondary structure of RNA.

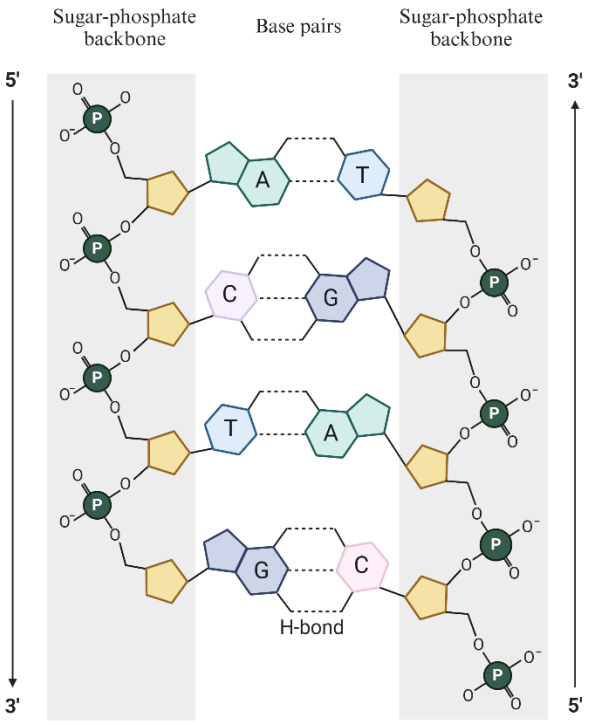

Figure 2. Structure and connectivity of nucleic acids (made in Biorender).

Nucleic acid nanoparticles take shape from the exploitation of naturally occurring building materials found in cells, the nucleotides. Wherein each nucleotide has a cognate pair that it builds a bond that is complimentary, and if we combine such nucleotides in a sequence that form through phosphate linkages in the backbone of the nucleotide. Then in turn, we design a sequence of base pairs that naturally prefer specific orientations depending on the order of the sequence. Furthermore, studies have shown that there

are naturally occurring structural moieties that correspond to the sequences and can be replicated in the lab[18-21]. As such, nucleic acid nanoparticles are programmed to utilize specific structural components to make intentional scaffolds[22-26].

Different therapeutic applications that harness the use of nucleic acid nanoparticles include RNA interference, gene therapy, antisense oligonucleotide (ASO) therapy, mRNA delivery, and CRISPR/Cas9 systems. Each system listed utilizes and targets the machinery found in cells to enforce and carry out the intended result. An example of cellular machinery that can be harnessed through nucleic acid nanotechnology is RNA interference (RNAi). RNAi is a naturally cellular mechanism that results in the down regulation of a targeted protein, and it is being harbored by scientists for the development of therapeutic approaches and platforms[27-30]. The mechanism calls for the use of an activating modality referred to as short interfering RNA (siRNA) that is complimentary to the protein of interest that will then get processed by the RNA induced silencing complex (RISC), resulting in down regulation of the protein. Since the discovery of this mechanism, great strides have been taken in utilizing the process to develop clinical level siRNAs. As such there have been a total of four clinically approved siRNA platforms since 2018: Onpattros[31], Givosiran[32], Lumasiran[33], and Inclisiran[34]. Although the previously listed platforms are all composed of nucleic acids, the ways in which they enact their therapeutic functions are unique. Researchers can design and incorporate these functions into nucleic acid nanoparticle scaffolds to target different mechanistic pathways contributing to diseased states.

1.2. IDENTIFYING CHALLENGES AND OPPORTUNITIES: BRIDGING THE GAP IN NUCLEIC ACID THERAPIES AND TECHNOLOGIES

Some of the primary challenges associated with nucleic acid therapies stem from their limited ability to enter cells without a delivery vehicle, resulting in off-target effects and the potential for immune system activation upon introduction into biological systems[1, 35, 36].

Furthermore, achieving efficient and targeted delivery of nanoparticles is hindered by the need to overcome biological barriers such as the cellular membrane[37-40]. Optimization of specificity is essential to minimize undesired effects in off-target cells or tissues. Moreover, nucleic acids can elicit immune responses in the body, potentially leading to side effects such as inflammation or reduced effectiveness. Addressing these challenges is critical for enhancing the safety and efficacy of nucleic acid therapies.

1.3. NAVIGATING DELIVERY CHALLENGES: STRATEGIES FOR EFFICIENT NUCLEIC ACID NANOPARTICLE TRANSPORT INTO CELLS

The field of nucleic acid nanoparticle delivery represents a critical area of research due to the pressing need for effective solutions to enable the utilization of these platforms. Delivery systems encompass a diverse range of carriers, including polymeric, inorganic, lipid, and viral vectors (Figure 3). Researchers often engineer hybrid particles that integrate multiple strategies to create efficient and multifunctional platforms[38, 41-51].

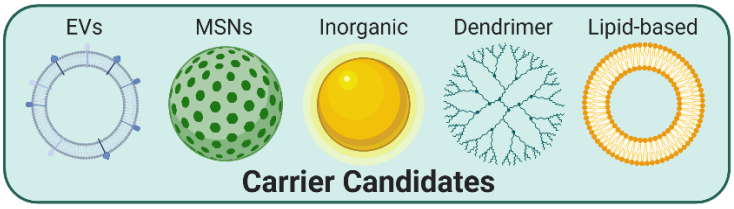

Figure 3. Delivery Vehicle/carrier candidates for nucleic acids and their desired properties.

The literature underscores the multifaceted nature of factors influencing the biological fate of nanoparticles. Effective delivery vehicles must prioritize biocompatibility, ensuring efficient particle delivery characterized by high carrying capacity and stability pre- and post-conjugation or complexation with nucleic acid counterparts. Moreover, delivery systems should minimize immune responses while facilitating targeted delivery of therapeutic nucleic acids. Size, charge, and morphology emerge as critical determinants impacting nanoparticle cellular uptake, emphasizing the need to carefully consider these attributes to optimize the performance and efficacy of nucleic acid nanoparticle delivery systems[39, 40, 43, 46, 51-58].

1.4. MITIGATING UNINTENDED CONSEQUENCES: UNDERSTANDING OFF-TARGET EFFECTS IN NUCLEIC ACID THERAPIES

Off-target effects are a significant concern in the use of therapeutic nucleic acids, referring to unintended consequences resulting from their introduction. These effects may occur if the therapeutic is delivered into unintended cells, exhibits toxicity, disrupts natural signaling pathways, or activates unintended biological mechanisms, potentially leading to adverse outcomes. To address these challenges, researchers employ various strategies such as optimizing delivery systems to enhance targeting specificity, designing nucleic acid sequences with improved selectivity, and utilizing advanced screening methods to identify potential off-target interactions early in the development process. Despite these efforts, off-target effects remain a complex and multifaceted issue, highlighting the ongoing need for rigorous investigation and refinement of nucleic acid therapeutics to ensure their safety and efficacy in clinical applications.

1.5. UNDERSTANDING THE IMMUNOLOGICAL LANDSCAPE: IMMUNE RECOGNITION OF NUCLEIC ACID NANOPARTICLES

The immune response to nucleic acid nanoparticles is an ongoing area of investigation, crucial for understanding the immune response elicited by therapeutic nucleic acids and their delivery vehicles. Activation of the immune system in response to foreign substances presents significant implications for therapeutic efficacy and patient safety. The immune system has evolved to respond to specific danger or pathogenic molecular patterns, termed pathogen or danger-associated molecular patterns (PAMPs or DAMPs)[59]. By pattern recognition receptors (PRRs), activation by foreign nucleic acids can trigger interferon responses and the release of proinflammatory cytokines, potentially leading to inflammatory reactions and adverse effects (Figure 4).

Immunotoxicity remains a significant consideration in the development of nucleic acid therapeutics, especially as researchers continue to explore new delivery systems and formulations.

However, it's important to recognize that advancements in the field have led to the development of more sophisticated delivery strategies and better understanding of immune responses to nucleic acids. While immunotoxicity remains a consideration, researchers are actively working to mitigate these risks through improved design of nucleic acid therapeutics, such as the use of modified nucleic acid sequences, targeted delivery systems, and immune evasion strategies.

Managing immunogenicity is paramount in optimizing the biocompatibility and therapeutic potential of nucleic acid nanoparticles. Ongoing research endeavors focus on developing strategies to mitigate immunogenic responses, such as modifying nanoparticle formulations or incorporating immunomodulatory agents, to enhance the safety and efficacy of nucleic acid-based therapeutics. As the field progresses, continuous efforts in understanding the immune response to nucleic acid nanoparticles and refining delivery approaches will be crucial for realizing their full therapeutic potential.

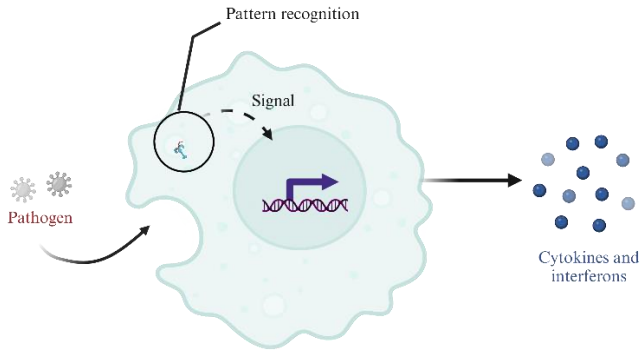

Figure 4. Illustration depicting the activation of immune outputs after recognition of a pathogen (made in Biorender).

As previously mentioned, pattern recognition receptors (PRRs) are types of receptors that recognize specific molecular structures on the surface of pathogens. PRRs are responsible for the production of nonspecific anti-infection, antitumor, and other immunoprotective responses[60]. Upon recognition of specific ligands, PRRs will initiate downstream signaling pathways to enact their immunological effects. Immunological effects come in the form of recruiting and releasing cytokines, hormones, chemokines, growth factors, and result in the induction of inflammation, formation of an inflammatory microenvironment, and initiation of immune killing[61]. Interestingly, PRRs are widely distributed

throughout intracellular compartments, endosomal membranes, in the cytoplasm, and the cell membrane[62, 63].

Toll like receptors (TLRs) are one of the earliest discovered PRRs of innate immune system and are shown to play a significant role in inflammatory response. TLRs are comprised of three main regions – extracellular, transmembrane, and intracellular[64]. Each region is responsible for different functions in relation to recognition and resulting immune response. The extracellular region of the receptors contains leucine-rich repeats that contribute to the recognition of the specific ligands, the intracellular regions contribute signal transduction by binding to different receptor proteins in the cytoplasm[65]. The corresponding signal transduction amplifies anti-pathogen infection by the transcription of genes that produce and secrete a variety of pro-inflammatory and antiviral factors.

Notably, another PRR, RIG-I-like receptors (RLRs), are intracellular and cytoplasmic, responsible for the recognition and response to viral nucleic acids to activate an antiviral response. RIG-I mediates an antiviral response to double stranded RNA, as well as to 5’-triphophate RNA of viruses[66].

Peripheral blood mononuclear cells (PBMCs) serve as pivotal components of the immune system, playing a crucial role in alerting the body to potential threats. Comprising various cell populations such as lymphocytes, monocytes, natural killer cells, dendritic cells, neutrophils, basophils, and eosinophils, PBMCs are obtained from blood samples and offer a comprehensive view of the body's immune response. Upon activation, PBMCs produce cytokines, which can be analyzed using enzyme-linked immunosorbent assay (ELISA) to generate an immunological profile. Leveraging PBMCs as a model provides several advantages, including easy accessibility via blood samples.

Numerous studies have utilized PBMCs to investigate the immune responses elicited by nucleic acid nanoparticles (NANPs). This wealth of research has laid the foundation for the development of predictive tools employing artificial intelligence, which can anticipate cytokine and chemokine production based on the sequences of nucleic acid structures[17, 24, 26, 39, 67-73]. PBMCs offer valuable insights into the type of

immune response induced upon transfection or treatment with NANP/carrier complexes, as illustrated in Figure 5.

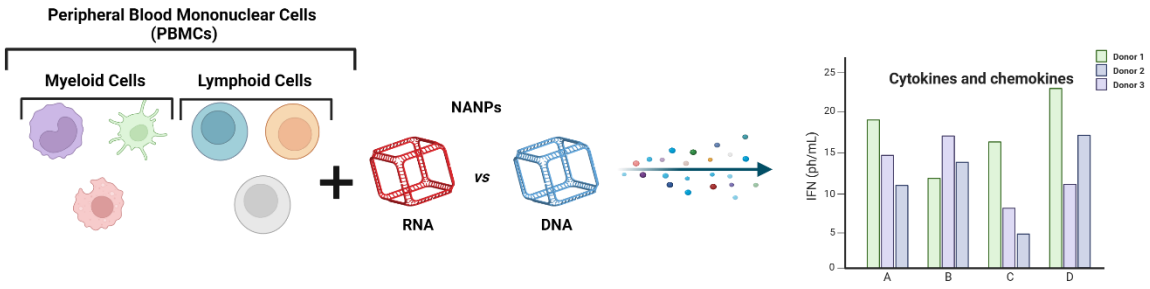

Figure 5. PBMCs → treatment → cytokines produced and released → immune response data (made in Biorender).

Cytokines and chemokines are the output signals that are responsible for pro-inflammatory responses by the immune system and are a result of activation by PAMPs and DAMPs (Figure 5). Chemokines are a part of the immune surveillance system in place by the immune system. Interferons are released in response to pathogens and tumor cells. Interferons (IFNs) are grouped into three main groups – Type I (IFN-α, IFN-ß), type II (IFN- γ), and type III (IFN-λ). Type I IFNs are biomarkers that get released to interfere with viral replication and are expressed in response to microbial products[74]. Type II IFNs are also involved in the action of killing pathogens. Interleukins promote inflammation and an increase in body temperature to inhibit the proliferation and growth of pathogens[75].

1.6. ADVANCING NUCLEIC ACID THERAPEUTICS: STRATEGIES FOR ENHANCED PRECISION, EFFICACY, AND OVERCOMING CHALLENGES

The work presented here investigates the feasibility of influencing biological responses, including immune reactions, and uptake into cells, by modifying the nanoparticle carriers used for nucleic acid nanoparticles. By tailoring the physicochemical properties of carriers (size, shape, and charge), we seek to understand their influence on the modulation of their interaction with the immune system, potentially attenuating or augmenting immune responses as desired. Furthermore, therapeutic specificity with our nucleic acid nanoparticles was endeavored by engineering nanoparticles with dynamic reconfiguration

capabilities. This approach aims to introduce conditional activation to the therapeutic platform, introducing specific targeting mechanisms. The goal of this work was to increase the precision and efficacy in therapeutic delivery, paving the way for more effective biomedical applications.

The following works aim to expand on the themes introduced in the preceding sections, addressing key aspects such as delivery and specificity. Through in-depth exploration and analysis, these works will contribute to a comprehensive understanding of the impact of delivery vehicles and application of conditionally activated nucleic acid nanoparticles.

Chapter Two explores the use of two different carriers for nucleic acid nanoparticles and investigates their impact on nanoparticle uptake into cells, as well as their influence on immune responses using human peripheral blood mononuclear cells. The carriers examined in this section include NH2-terminated polyamidoamine dendrimers and lipofectamine 2000. Polyamidoamine dendrimers are cationic, hyperbranched polymeric nanoparticles, while lipofectamine 2000 is a lipid nanoparticle commonly employed for nucleic acid transfection into cells.

This research significantly contributes to the field by elucidating the differential effects of carrier type on immune responses to nucleic acid nanoparticles, which had been previously characterized for their immune recognition properties. Our findings reveal distinct immunological responses when employing dendrimers as carriers compared to lipofectamine 2000. These observations highlight the importance of carrier selection in modulating immune responses to nucleic acid nanoparticles and underscore the potential impact of carrier properties on therapeutic outcomes.

Chapter Three further investigates and expands upon the research presented in Chapter Two by incorporating additional generations of dendrimers to elucidate their impact on immune responses to cubic nucleic acid nanoparticles. The study systematically varies the size, shape, and charge of carriers across dendrimer generations three through seven, spanning sizes from 2 to 100 nm. Notably, the research reveals that higher generations of dendrimers appear to suppress immune responses to nucleic acid

nanoparticles, suggesting a potential mechanism for immune evasion. These findings shed light on the complex interplay between carrier characteristics and immune responses, offering insights into strategies for optimizing nanoparticle design in biomedical applications.

By demonstrating the influence of carrier type and generation on immune responses, this study provides valuable insights into the design and optimization of nanoparticle-based therapeutics. Understanding how carrier characteristics affect immune interactions is critical for enhancing the efficacy and safety of nucleic acid nanoparticle delivery systems. Moving forward, further investigation into the underlying mechanisms driving these differential immune responses will be essential for advancing the development of targeted and immunocompatible nanoparticle therapies.

Chapter Four presents the design and validation of a novel modular hybrid nucleic acid nanoparticle (NANP) for conditional activation, aimed at precise therapeutic targeting. This four-component particle incorporates a molecular beacon (MB) that specifically recognizes an oncogenic mutation, serving as the recognition step. Upon recognition of the target mutation, a conformational change is triggered, leading to the release of the therapeutic component, dicer substrate (DS) RNAs, facilitating the therapeutic step. Specifically, our construct targets mutated KRAS oncogenes in pancreatic cancer cells, enabling selective activation in diseased states.

Our study demonstrates the efficacy of our NANP in downregulating Survivin, an inhibitor of apoptosis, associated with cancer cell survival. Moreover, our modular design allows for customization with different triggers, targets, and therapeutic moieties, rendering the NANP versatile and adaptable to diverse therapeutic applications. For instance, by extending the molecular beacon, multiple DS RNAs targeting distinct cellular mechanisms can be incorporated, enhancing the therapeutic potential against various diseases.

Chapter Five concludes with a discussion of the overarching findings and implications of the research presented in the thesis. The discussion synthesizes the key insights obtained from the work presented,

providing a comprehensive understanding of the influence of carrier characteristics on immune responses to nucleic acid nanoparticles. Moreover, the discussion explores potential avenues for future research and the translational potential of the findings for developing targeted and immunocompatible nanoparticle-based therapies. By summarizing the main findings and their broader implications, Chapter Five offers valuable insights for researchers and practitioners in the field of nucleic acid nanotechnology.

2 CHAPTER 2: INDUCTION OF CYTOKINES BY NUCLEIC ACID NANOPARTICLES (NANPS) DEPENDS ON THE TYPE OF DELIVERY CARRIER

2.1. INTRODUCTION

The field of RNA and DNA nanotechnology is rapidly growing. In the past decade, researchers have established various approaches to synthesize RNA and DNA nanoassemblies of different sizes, shapes, and compositions and generated proof-of-concept data intended for the use of these materials in biology and medicine [24-26, 53, 76-82]. A growing library of nucleic acid nanoparticles (NANPs), the design of which takes advantage of natural RNA (and DNA) motifs and canonical Watson–Crick base pairings, have been demonstrated to assemble into precise nanoscaffolds exemplified by hexagonal rings[83], various polygons[84], and fibrous structures[85], to name a few[4]. A variety of NANPs are now being investigated for broad applications in detection and diagnostics[86-88], targeting specific disease sites[89], and as therapeutic approaches[80, 90-92] for various illnesses. As the technology approaches the stage of preclinical development and clinical translations, many researchers in the field have consolidated their efforts to overcome translational gaps and accelerate the transition of DNA and RNA nanoassemblies from bench to clinic[1, 17, 93-96]. Among these efforts is the understanding of the immunological properties of NANPs as a new class of therapeutic nucleic acids.

Our group has recently reported that biomarkers for NANP immunorecognition are type I and type III interferons (IFNs), which are produced by human primary blood cells only after NANPs are delivered with a widely used lipid-based carrier (Lipofectamine 2000 or L2K); otherwise, without a delivery agent, NANPs are not efficiently internalized and do not induce an IFN response[69]. Among other structure–activity relationships, we demonstrated that the IFN-inducing capability of NANPs depends on their composition (RNA-based NANPs are more potent than their DNA counterparts), shape (globular structures are more potent than planar particles, which in turn are more potent than fibrous NANPs), and size[69]. This relationship is well-exemplified by DNA and RNA cubes, which are both six-stranded 3D

NANPs similar in size, shape, and sequence. While both DNA and RNA cubes have been demonstrated to serve as nanoscaffolds for carrying therapeutic nucleic acids into cells, the difference in their DNA versus RNA composition has been shown to yield greater IFN induction for RNA cubes when compared to their DNA analogs[97]. The most remarkable finding of our earlier studies was that despite general knowledge regarding the involvement of toll-like receptors (TLRs) in the recognition of DNA and RNA, TLR7, known as a receptor for single-stranded RNA, played a key role in the immune recognition of both DNA and RNA cubes. Altogether, the results of our studies allowed us to hypothesize that both the quality (i.e., the repertoire of cytokines) and quantity (i.e., the magnitude of the cytokine response) of the immune response to NANPs can be manipulated not only by changing NANPs' physicochemical properties and composition, but also by using different types of carriers [69, 74].

As a candidate for such a delivery platform, polyamidoamine (PAMAM) dendrimers are cationic, hyperbranched, globular structures. Amine-terminated PAMAM dendrimers, like the ones used in this study, have been proposed as an effective delivery platform for gene therapy by complexation with siRNAs, biological molecules, and drugs[41, 44, 49, 98-100]. Different generations of the PAMAM dendrimers have been shown to successfully carry nucleic acids such as plasmids, siRNAs, and miRNAs into different cancer cell lines[101-103]. Once inside the cells, the siRNAs were able to activate RNA interference and silence their specific target mRNAs in both in vitro and in vivo proof-of-concept models[48]. The dendrimer–nucleic acid complexes form through electrostatic interactions between the positively charged amine group terminals of the dendrimers and the negatively charged phosphate groups of the nucleic acids[104].

Herein, we present the results confirming the hypothesis that immunostimulation by NANPs can also be manipulated by the type of carrier. Specifically, we compared the cytokine induction by DNA and RNA cubes delivered to human peripheral blood mononuclear cells (PBMCs) using either L2K (the carrier used in our previous studies) or generation 5 amine-terminated (G5-NH2) polyamidoamine (PAMAM) dendrimers. The results of DNA and RNA cubes' physicochemical characterization, complexation with

G5-NH2 PAMAM dendrimers, resistance to nucleases, and delivery to cancer cells and PBMCs are also presented.

2.2. RESULTS

2.2.1. Physicochemical Characterization of Dendrimers

Hydrodynamic sizes were measured by dynamic light scattering (DLS) for the dendrimer as is (no filtering) and after filtration through a 0.02 µm filter. The intensity, volume distribution, and zeta potential plots are shown in Figure 6 and summarized in Table 1. Before filtration, several peaks are observed in the intensity-weighted distribution plot (Figure 6A), with the most dominant size population being ~7 nm, as determined by the volume-weighted distribution plot (Figure 6B). After filtration, these larger size populations (consisting of aggregates) are removed and a monomodal size distribution centered at 7 nm (Int-Peak) is observed.

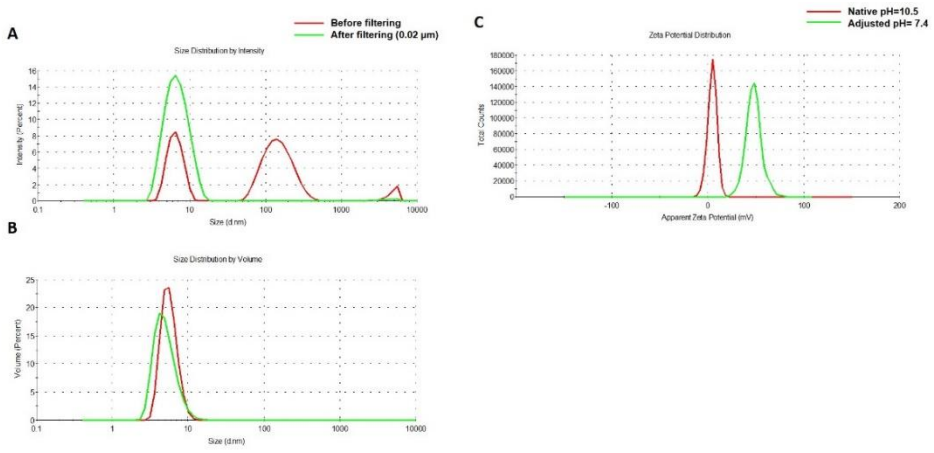

Figure 6. Physicochemical characterization of the G5-NH2 PAMAM dendrimers. The averaged intensity (A) and volume (B) distribution plots as measured by dynamic light scattering and the averaged zeta potential distribution (C). The hydrodynamic size was measured before and after filtration through a 0.02 µm filter. Zeta potential was measured both at its native pH and after adjustment to neutrality**.**

Table 1. Summary of the hydrodynamic diameters for G5-NH2 PAMAM dendrimers.

Sample	Z-Avg, nm	PdI	Int-Peak, nm	%Int	Vol-Peak, nm	%Vol
Before filtering	30.4 ± 11.0	0.759 ± 0.188	156.5 ± 11.4	59.7 ± 2.0	5.7 ± 0.1	100 ± 0
After filtering	6.3 ± 0.1	0.143 ± 0.022	7.0 ± 0.1	99.1 ± 1.1	5.1 ± 0.1	100 ± 0

The zeta potential distributions for the dendrimer are shown in Figure 6C and summarized in Table 2. Zeta potential was measured both at its native pH and after adjustment to neutrality (Figure 6C). At its native pH (10.5), the dendrimer is neutral (+4.6 mV) due to the surface primary amines existing as NH2. Note, zeta potentials from –10 to +10 mV are generally considered neutral. The zeta potential becomes highly cationic (+48.2 mV) after pH adjustment to 7.4 as the surface primary amines are protonated and exist as NH3+.

Table 2. Summary of the zeta potentials for G5-NH2 PAMAM dendrimers.

Sample	pH	ZP, mV
G5-NH_2	10.5 (Native)	+4.6 ± 0.9
G5-NH_2	7.4	+48.2 ± 3.4

2.2.1. NANP Synthesis and Characterization

To demonstrate the ability of G5-NH2 dendrimers to serve as a carrier of NANPs, representative DNA and RNA cubic NANPs were chosen as a proof of concept for all experiments. These NANPs have been previously characterized and have been demonstrated to be delivered into cells using a variety of delivery platforms. While both exhibit the same globular shape and relative size, their difference in composition in terms of being made of either DNA or RNA makes for a noticeable divergence in their immunostimulation, with RNA cubes serving as potent stimulators of IFNs. DNA and RNA cubes were assembled in endotoxin-free conditions and were visualized via non-denaturing polyacrylamide gel electrophoresis (native-PAGE) to verify their assembly and additionally visualized via atomic force microscopy (AFM) to ensure sample uniformity (Figure 7).

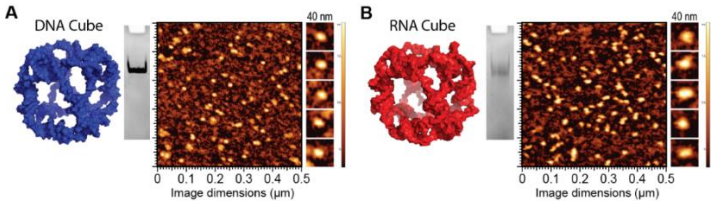

Figure 7. DNA and RNA cube characterization. 3D models, native-PAGE results, and representative AFM images of (A) DNA cubes and (B) RNA cubes.

2.2.3. NANP Complexation with G5-NH2 Dendrimers

The electrostatically-driven complexation of G5-NH2 dendrimers to NANPs was assessed using the number of primary amines available per dendrimer (N) and the number of phosphates available on the backbone of a DNA duplex (P) to calculate complexation at the N/P ratio. Once DNA duplexes were complexed to G5-NH2 dendrimers at different N/P ratios and incubated for 30 min, the samples were visualized via agarose gel electrophoresis (supporting Figure 13) to determine the ratio at which the DNA duplex migration was impeded. This ratio was then used to determine the amounts of G5-NH2 needed to bind NANPs.

L2K and G5-NH2 dendrimers were visualized individually with transmission electron microscopy (TEM) and then again with the addition of cubic NANPs (Figure 8A). To investigate whether NANPs could be complexed to and protected by the G5-NH2 dendrimers, a nuclease resistance assay was conducted. To run this assay, a DNA duplex, decorated with a fluorophore/quencher pair, was complexed to G5-NH2 dendrimers and treated with DNase. The change in fluorescence over time for the G5-NH2-complexed dendrimers was compared to uncomplexed duplexes (Figure 8B). Contrarily to the uncomplexed duplexes, G5-NH2-complexed duplexes were protected from nuclease digestion for an extended period of time (one hour). The delay in fluorescence increase of the G5-NH2-complexed duplexes indicated that the dendrimers protected the duplexes from nuclease degradation, thus again confirming the complexation between nucleic acid constructs and dendrimers.

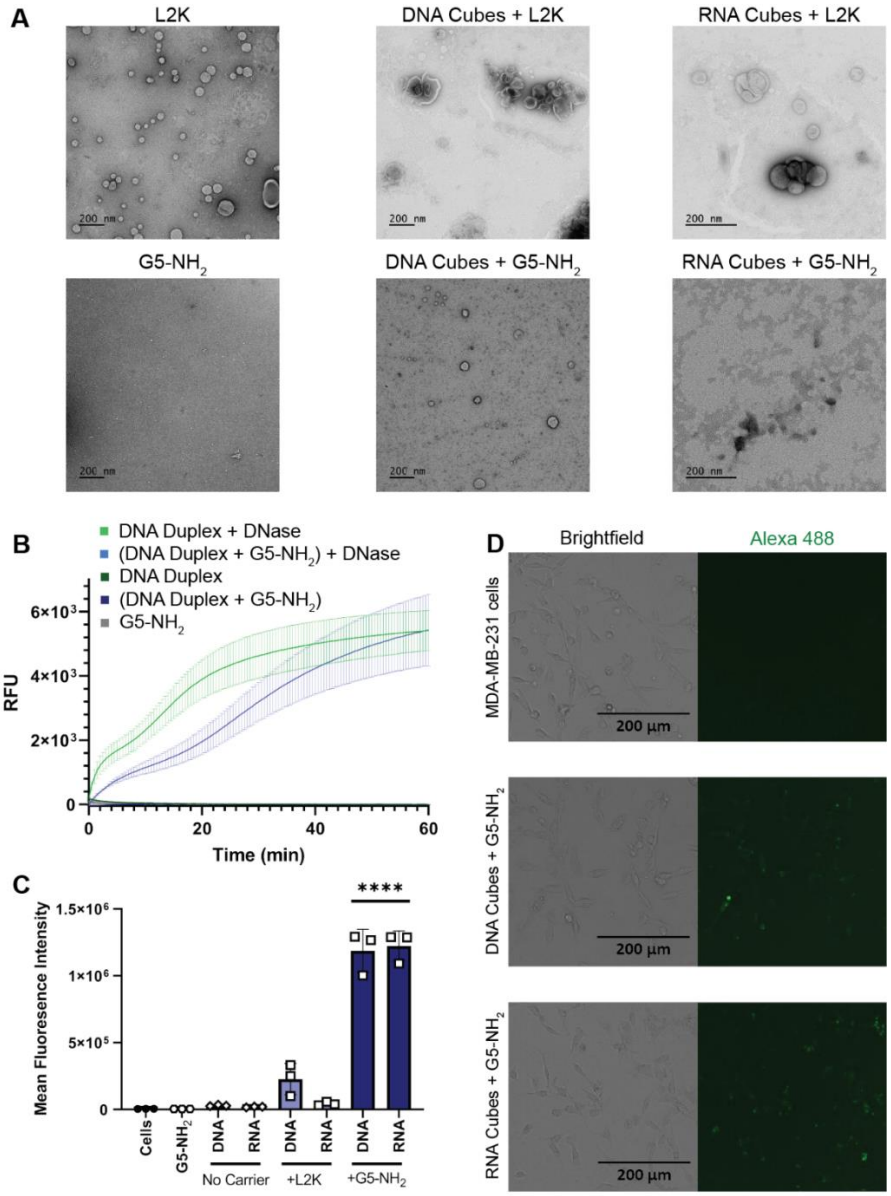

Figure 8. NANPs complexed with G5-NH2 dendrimers. (A) Transmission electron microscopy images of Lipofectamine 2000 (L2K), G5-NH2 dendrimers, and DNA and RNA cubes complexed to either L2K or G5-NH2 dendrimers. (B) Resulting fluorescence profiles from nuclease resistance assays. (C) Mean fluorescence intensity associated with the in vitro uptake of Alexa 488-labeled DNA and RNA cubes in MDA-MB-231 cells. Each bar shows the mean response and standard deviation (N = 3). Statistical significance between the DNA and RNA cubes delivered with G5-NH2 versus all other treatments is denoted by **** where $p < 0.0001$. (D) Brightfield and GFP microscopy images of MDA-MB-231 cells transfected with DNA cubes complexed to G5-NH2 dendrimers and RNA cubes complexed to G5-NH2 dendrimers.

To evaluate DNA and RNA cubes' uptake efficiency by a cancer cell line when complexed to either dendrimers or L2K, Alexa 488-labeled cubes were used to track the complexes introduced into the human breast cancer cell line MDA-MB-231 (Figure 8C, D). The uptake results provided information on the

overall general uptake of the G5-NH2 cubes in an adherent cell line that is customarily used to assess NANP uptake with other carriers. The cells appeared to uptake the G5-NH2-complexed cubic NANPs significantly more than those observed for the L2K-complexed NANPs. Uptake of the complexes was observed through the increase in mean fluorescence intensity of the treated cells.

2.2.4. Cytokine Response in PBMCs Depends on the Type of Carrier and Correlates with NANP Uptake by the Cells

To understand whether the spectrum and the magnitude of the cytokine response to DNA and RNA cubes depend on the type of carrier, we conducted experiments using human PBMCs (Figure 9). NANPs were added to PBMC cultures either without a carrier or after complexation with either L2K or G5-NH2 dendrimers, and the supernatants were analyzed for the presence of 29 cytokines. Owing to the pleiotropic function of cytokines, we used the broadest panel available; and for the purpose of this manuscript, when analyzing the results, we grouped cytokines based on their known roles in various biological responses as will be detailed below. Analysis of culture supernatants revealed that NANPs used without a carrier and G5-NH2 dendrimers alone did not induce any cytokines (Figure 10 and Figure 15).

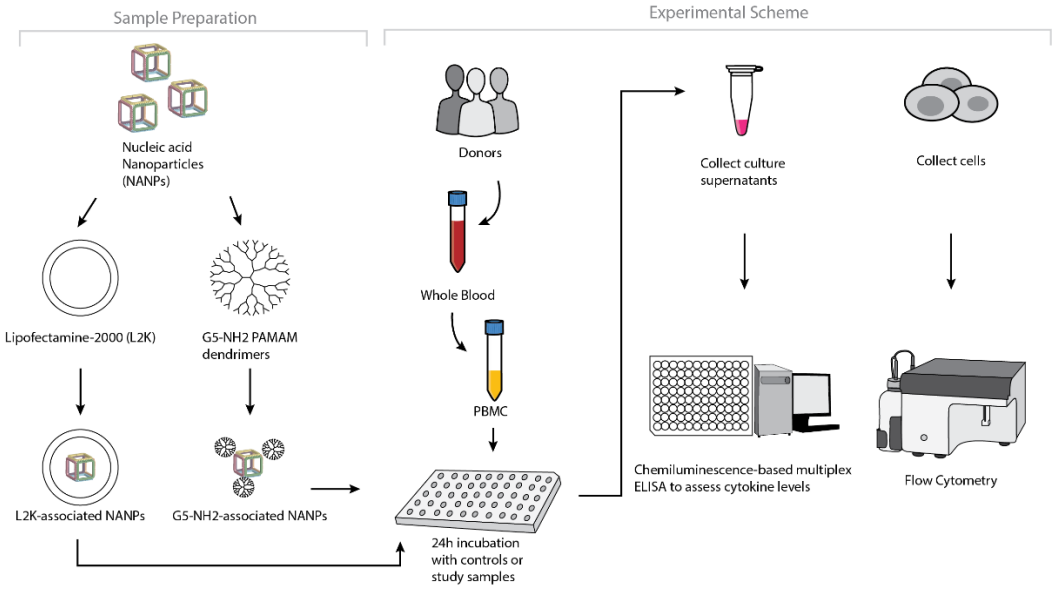

Figure 9. Experimental flow of the complexation of DNA and RNA cubes with either G5-NH2 dendrimers or L2K and their further analysis in PBMCs.

After the complexation with L2K, both DNA and RNA cubes induced type I and type III interferons, known for their role in anti-viral and anti-tumor effects; these responses were stronger in the RNA cube-treated group than in the DNA cube-treated group (Figure 10A). Unlike L2K-complexed NANPs, particles complexed with amine-terminated dendrimers did not induce type I and type III IFNs (Figure 10A).

A striking difference, however, was observed for cytokines that are known as danger signals (IL-1α) and those commonly associated with stress, trauma, and cytokine storm (IL-1 β, IL-6, TNFα). In this case, L2K-complexed NANPs did not produce a response, whereas dendrimer-delivered NANPs induced the aforementioned stress and danger-related cytokine biomarkers (Figure 10B). Similar to the effect on type I and type III IFNs observed in the L2K-delivered NANPs, RNA cubes delivered using dendrimers were more potent in inducing stress-related cytokines than DNA cubes; no cytokines were detected in the samples treated with DNA or RNA cubes without a carrier (Figure 10A, B). Interestingly, L2K alone induced IL-1α and IL-1β and, in PBMCs from one donor, low levels of TNFα and IL-6; however, this effect was neutralized by the complexation with RNA and DNA cubes (Figure 10B).

Low levels of type II interferon (IFNγ), known for its role in T cell-mediated immunity, were observed in the L2K-delivered NANP group and similar between DNA cubes and RNA cubes (Figure 10C). IFNγ-induced protein (IP-10), however, was detected only in the L2K-delivered NANP group (Figure 10C). Similar to the data with other cytokines, DNA and RNA cubes used without a carrier did not induce type II IFN and IFNγ-induced protein (Figure 10C).

Analysis of chemokines (IL-8, MIP-1α, MIP-1β, MCP-1, MCP-2, and RANTES) revealed that L2K alone induced all chemokines except for MCP-2, and this effect was neutralized by complexation with NANPs; dendrimers alone did not induce any of these chemokines (Figure 10D). Interestingly, induction of IL-8, MIP-1α, MCP-1, and RANTES was similar between L2K- and dendrimer-delivered NANPs and was stronger in RNA cubes than in DNA cubes (Figure 10D). In contrast, the induction of MCP-2 was observed only in L2K-complexed NANPs, but not in dendrimer-complexed NANPs and was again higher

with RNA cubes than with DNA cubes (Figure 10D). The pattern of MCP-2 induction (Figure 10D) matched closely with that of type I and type III IFNs (Figure 10A). Other cytokines (IL-2, IL4, IL-5, IL-22, IL-10, IL-12, and IL-21) were also detected; the induction of some of these biomarkers (e.g., IL-2 and IL-15) was donor-dependent (Figure 15).

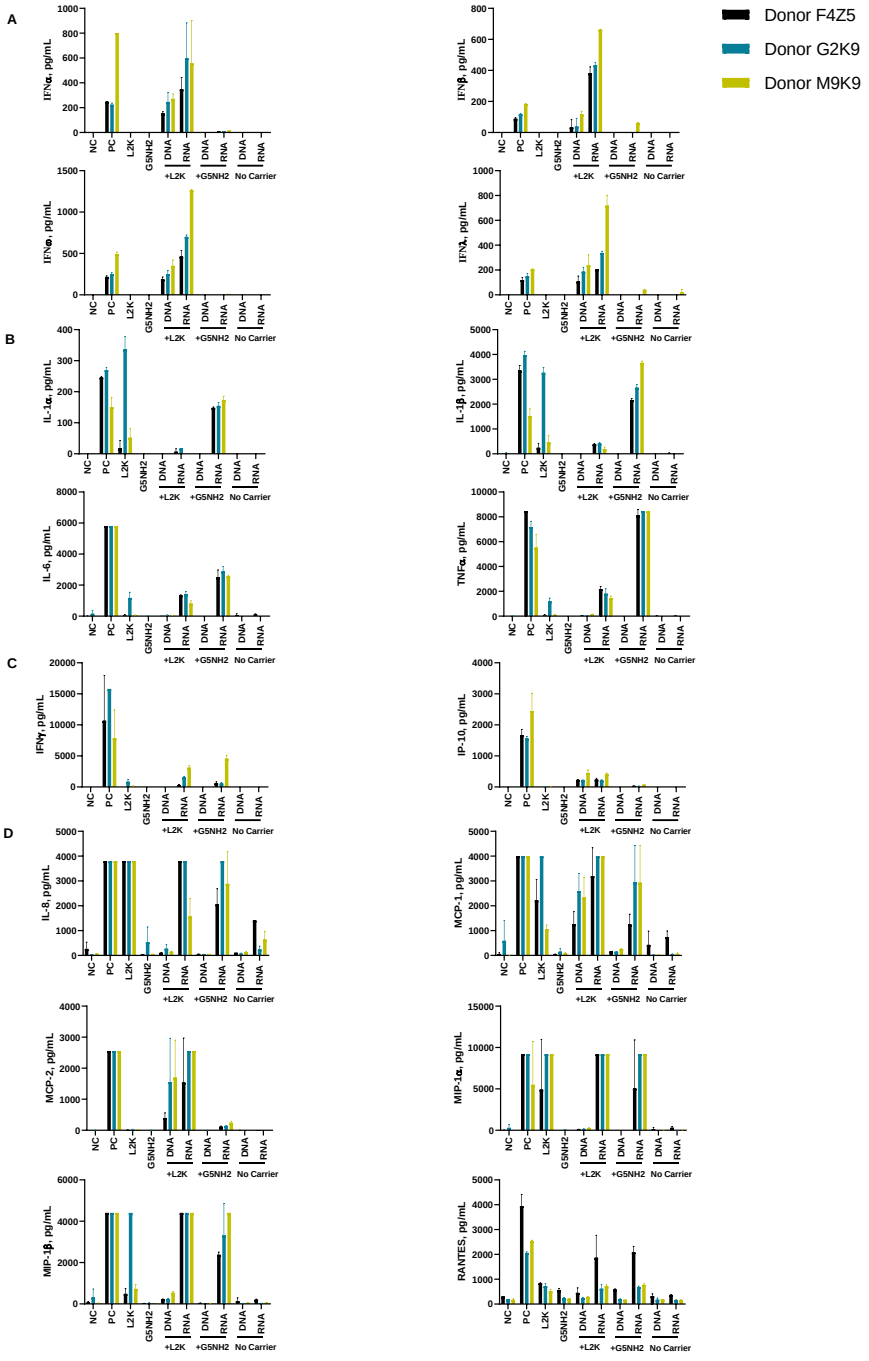

Figure 10. Cytokine induction by DNA and RNA cubes as a function of the delivery carrier. PBMC from three healthy human donor volunteers (F4Z5, G2K9, and M9K9) were treated with negative control (NC), positive control (PC), DNA cubes, or RNA cubes for 24 h. Prior to the addition to PBMC cultures, DNA cubes and RNA cubes were complexed with lipofectamine 2000 (L2K), G5 amine-terminated PAMAM dendrimers (G5-NH2) or used without complexation (no carrier). Culture supernatants were analyzed for the presence of cytokines, chemokines, and interferons using multiplex ELISA as described in the Materials and Methods. The data are presented based on the function of cytokines, including (A) type I and type III interferons, (B) danger signals and cytokines commonly associated with trauma and cytokine storm, (C) type II interferon and type II interferon-inducible protein, and (D) chemokines. Each bar shows the mean response and standard deviation (N = 2). Other cytokines from this study are presented on Figure 15.

To understand whether detected cytokines provide positive or negative regulation loops that influence their expression, we conducted a correlation analysis. Since the number of donors was limited, we applied two matrices—the Pearson matrix, which assumes a Gaussian distribution (Figure 11A), and the Spearman matrix, which assumes a non-Gaussian distribution (Figure 11B). With L2K-delivered DNA cubes, a positive correlation was observed between type II IFN (IFNγ) and cytokines and chemokines IL-6, IL-8, MCP-1, MCP-2, and IL-2, and between type I and type III IFNs (IFNα, IFNβ, IFNω, IFNλ) and cytokines and chemokines MCP-1, MCP-2, TNFα, IL-4, and IL-22 (Figure 11A, DNA cubes-L2K). A negative correlation in the same group was detected between type I and type III IFNs and chemokine RANTES (Figure 11A, DNA cubes-L2K). With L2K-delivered RNA cubes, a positive correlation was observed between individual cytokines IL-1α, IL-1β, IL-6, IL-8, and IL-2; IFNγ and chemokines MCP-1, MCP-2, MIP-1α, and MIP-1β; type I and type III IFNs; chemokines MCP-1, MCP-2, MIP-1α, and MIP-1β and type I and type III IFNs; and between IL-4 and IL-22 (Figure 11A, RNA cubes L2K). A negative correlation was observed between cytokines IL-1α, IL-1β, IL-6, and IL-8 and all IFNs, IL-4, and IL-22 (Figure 11A, RNA cubes-L2K). With dendrimer-delivered DNA cubes, a positive correlation was observed between individual cytokines IL-1α, IL-1β, IL-6, and IL-8; between individual type I and type III IFNs; IL-4, IL-15, and IL-22; and between IFNγ and MCP-1, MCP-2, type I and type III IFNs, IL-4, IL-15, IL-22, IL-12, and IP-10 (Figure 11A, DNA cubes-G5-NH2). Negative correlation in the same treatment group was observed between IL-1α, IL-1β, IL-6, IL-8, and all IFNs, IL-12, IL-21, IP-10, IL-4, IL-15, IL-22, MCP-1, MCP-2, and RANTES; and between individual cytokines IL-4, IL-15, and IL-22 (Figure 11A, DNA cubes-G5-NH2). With dendrimer-delivered RNA cubes, a positive correlation was observed between IFNγ and IL-12, MCP-1, type I and type III IFNs, IL-4, IL-14, and IL-22; between IL-6, IL-1α, IL-1β, and IL-8; MIP-1α, MIP-1β, RANTES, and TNFα; between type I and type III IFNs and IL-4, IL-15, and IL-22; and between individual type I and type III IFNs (Figure 11A, RNA cubes-G5-NH2). Negative correlation in this treatment group was observed between IL-1α, IL-1β, IL-6, and IL-8, and MIP-1α, MIP-1β, IL-4, IL-15, and IL-22; between TNFα and IFNγ, IP-10, MCP-1, MCP-2, MIP-1α, MIP-1β, and type I and type III IFNs; between IL-2 and IL-4, IL-15, and IL-22 (Figure 11A, RNA cubes-

G5-NH2). While the correlation indices for individual cytokines were different in the Spearman matrix, the overall conclusions about negative and positive correlation did not change (Figure 11B).

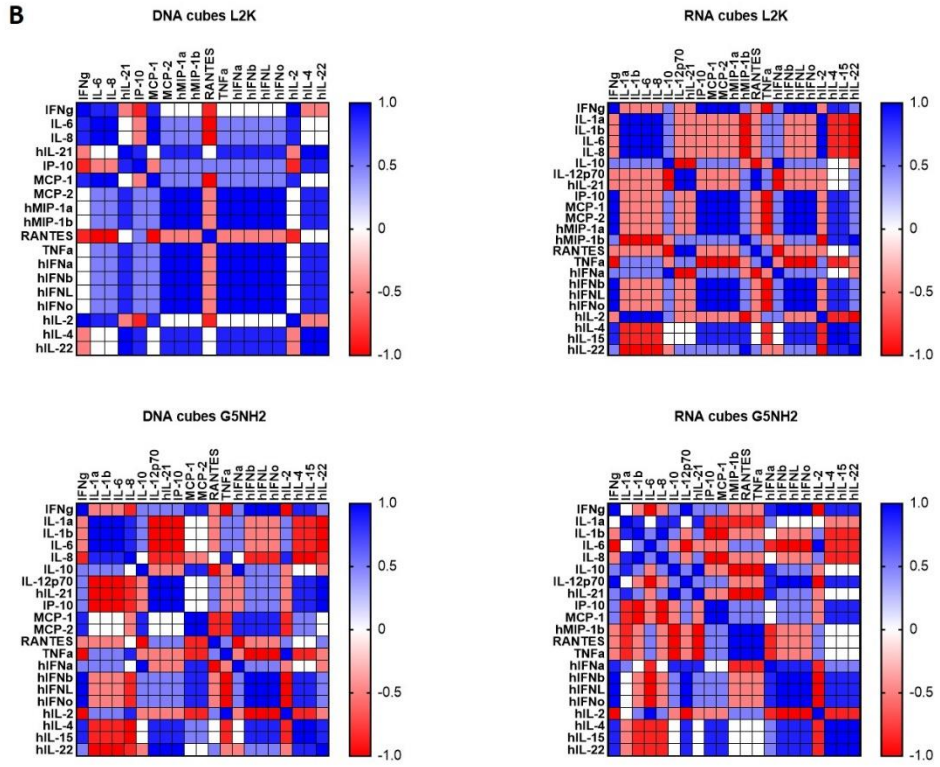

Figure 11. Correlation analysis of cytokine response. The data from the multiplex cytokine analysis including those presented in Figure 10 were analyzed using the GraphPad Prism software to determine a correlation or lack thereof between individual cytokines. (A) The Pearson correlation matrix assumes a Gaussian distribution (parametric analysis). In this analysis, values between ±0.5 and ±1 refer to a high degree of correlation, whereas values close to ±1 mean perfect correlation; negative values (in red) refer to the negative correlation, whereas positive values (in blue) mean positive correlation. (B) The Spearman correlation matrix assumes no Gaussian distribution (non-parametric analysis). In this analysis, values of ±1 mean perfect correlation; the closer the value is to zero, the weaker the association is; negative values (in red) and positive values (in blue) refer to the negative and positive correlation, respectively.

Next, we tested NANP uptake by blood cells. PBMCs from the same donors as those used for cytokine analysis were exposed to carriers alone (L2K or G5-NH2 dendrimers), DNA cubes or RNA cubes without a carrier, or DNA cubes or RNA cubes complexed with either L2K or with dendrimers (Figure 12). The NANPs used in this study contained a green fluorescent label (Alexa 488) covalently attached to one oligonucleotide of each six-stranded assembly of the DNA and RNA cubes. Percent of positive cells shows the proportions of cells in the analyzed population of lymphocytes or monocytes that were associated with green fluorescence, which, in turn, is indicative of the particle uptake and/or association

with the cellular membrane. When L2K or dendrimers were used as delivery carriers for NANPs, between 40 and 90% of monocytes demonstrated a greater fluorescent signal as opposed to 10–30% of lymphocytes (Figure 12A). The uptake of NANPs in L2K and dendrimer-complexed groups was comparable in both monocytes and lymphocytes; a greater uptake of DNA cubes vs. RNA cubes complexed with L2K was noticed (Figure 12A, lymphocytes). No uptake of RNA and DNA cubes delivered without a carrier was seen in lymphocytes and monocytes treated with RNA cubes, while about 40% of the monocytes exposed to DNA cubes without a carrier demonstrated green fluorescence (Figure 12A, monocytes).

When geometric mean fluorescent intensity (GMFI), indicative of the magnitude of NANP uptake by individual cells, was measured, no significant uptake of naked RNA and DNA cubes was noticed in either lymphocytes or monocytes (Figure 12B). No or very low levels of uptake were registered for both DNA and RNA cubes complexed with L2K in lymphocytes (Figure 12B, lymphocytes). The lymphocyte uptake of RNA and DNA cubes complexed with dendrimers was greater than that after the complexation with L2K, and the uptake of DNA cubes complexed with dendrimers was greater than that of the RNA cubes delivered using dendrimers (Figure 12B, lymphocytes). The uptake of both DNA and RNA cubes by monocytes was also greater in the dendrimer group than in the L2K group; in both groups, the uptake of DNA cubes was higher than that of the RNA cubes (Figure 12B, monocytes). In all groups where the uptake was registered, the signal was an order of magnitude higher in monocytes than in lymphocytes (Figure 12B).

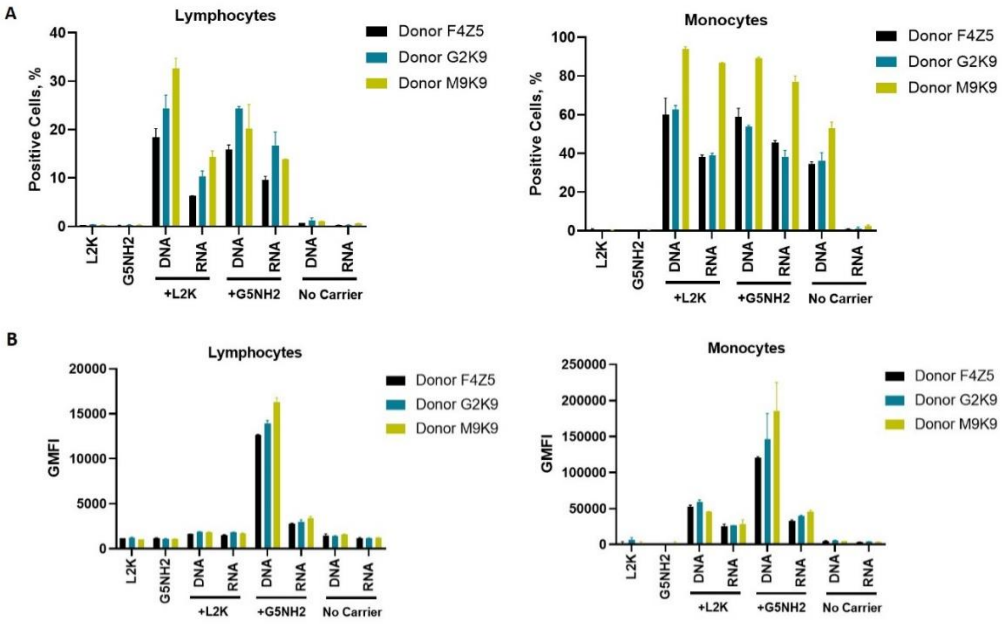

Figure 12. Uptake of fluorescently labeled DNA and RNA cubes by peripheral blood cells. PBMCs from three healthy human donor volunteers (F4Z5, G2K9, and M9K9) were either left untreated or incubated with Alexa 488-labeled DNA cubes or RNA cubes for 24 h. Prior to the addition to PBMC cultures, DNA cubes and RNA cubes were complexed with Lipofectamine 2000 (L2K), G5 amine-terminated PAMAM dendrimers (G5-NH2) or used without complexation (no carrier). After a wash to remove excess particles, the cells were analyzed by flow cytometry as described in the Materials and Methods. (A) Analysis of the percentage of positive cells indicates the overall proportion of the cells in either the lymphocyte or monocyte population associated with the fluorescent signal that is greater than that in the carrier alone or untreated cells. (B) Analysis of geometric mean fluorescent intensity (GMFI) reveals the degree of a fluorescent signal associated with the individual cells in the lymphocyte or monocyte populations. Green fluorescence is delivered to the cells by DNA and RNA oligonucleotides labeled with Alexa 488 prior to their assembly into DNA and RNA cubes, respectively. Each bar shows the mean response and standard deviation (N = 2).

2.3. DISCUSSION

Physicochemical properties of PAMAM dendrimers used in this study were consistent with those described earlier[105-107]. The DNA and RNA cubes are complexed to G5-NH2 dendrimers through electrostatic interactions between the negatively charged phosphate groups of the nucleic acid cubes and the positively charged amine surface groups from the dendrimers. The N/P ratio of cubes to G5-NH2 dendrimers was determined by using a gel retardation assay showing that complete binding occurs at a 1.5 N/1 P ratio. This was shown by the neutralization of the nucleic acids on the gel through the decrease in migration along the gel. A nuclease resistance assay was also used to determine the ability of dendrimers to protect NANPs from nuclease degradation. The results in Figure 8B show that when DNA and RNA

cubes are complexed to G5-NH2 dendrimers, the rate of digestion by nucleases is lowered and prolonged for up to 60 min.

The observed induction of type I (IFNα and IFNβ) and type III IFNs (IFNλ) by DNA and RNA cubes complexed with L2K but not by those used without any carrier, the higher potency of IFN induction by RNA cubes vs. DNA cubes (Figure 10A), and the correlation with the uptake by monocytes (Figure 7) are in agreement with our earlier studies[69, 74]. Since type I IFNs' main function is to prevent viral replication in cells and that of type III IFNs is to support anticancer immunity, the data point to the potential utility of L2K-mediated delivery of NANPs in stimulating anti-viral and anti-tumor immune responses. Our hypothesis that by changing the carrier used to deliver NANPs to the blood cells one may control the spectrum and the magnitude of the cytokine responses was verified in the present study. The induction of type I and type III IFNs and proinflammatory cytokines associated with stress and damage are in direct contrast between NANPs delivered using L2K and those complexed with dendrimers (compare DNA cubes and RNA cubes complexed with L2K to those complexed with dendrimers in Figure 10A,B). Cationic dendrimers were shown in multiple studies to affect the integrity of cellular membranes [105-111]. We also reported earlier that many nanoparticles are immunomodulatory in that a combination of otherwise non-reactive particles produces a detectable biological response [36, 112, 113]. Our results, therefore, suggest that NANPs delivered by cationic dendrimers are perceived by immune cells as danger signals, hence the induction of IL-1α, IL-6, and IL-8 [93]. Cationic nanoparticles activate the inflammasome, thereby contributing to the secretion of mature IL-1β, expression of which is induced by other stimuli [114-116]. The induction of IL-1β observed in supernatants from cells treated with NANP–dendrimer complexes is consistent with this knowledge; the data suggest that NANPs induce IL-1β expression whereas cationic dendrimers activate the inflammasome to produce mature IL-1β proteins. The induction of type II IFN (IFNγ) by L2K- and dendrimer-complexed NANPs (Figure 10C) is new data; to our knowledge, this phenomenon has not been previously reported. IFNγ is produced by activated T cells and its main function is to activate macrophages and various other cell types and to coordinate a cooperation between

activated T cells and other host cells. Therefore, these data point to the potential utility of NANPs for controlling adaptive immunity. The induction of chemokines by L2K alone (Figure 10D) is not unexpected; we reported earlier that lipid-based nanoparticles commonly induce chemokines via a mechanism involving oxidative stress [36, 112, 113, 117]. While this induction complicates the interpretation of chemokine results in the NANPs-L2K group, the data suggest that complexation with DNA and RNA cubes neutralizes this effect (Figure 9D), which is consistent with the expected change in the L2K's overall charge after its electrostatic complexation with NANPs. The induction of other cytokines (IL-2, IL-4, IL-15, IL-22, IL-10, IL-12, and IL-21) was also observed (Figure S15); in some cases (e.g., IL-2 and IL-15), the induction was donor-dependent suggesting that individual variability in NANP-mediated cytokine signaling including the expression of receptors involved in NANP recognition exists. Such interindividual variability is not surprising since both qualitative and quantitative variations in individuals' immune responses have been described before [118-122].

Correlation analysis revealed the complexity of the cytokine network in that both positive and negative correlation was observed between type I, type II, and type III IFNs, chemokines, and various interleukins and TNFα (Figure 11). These observations are consistent with the current knowledge of the cytokines' pleiotropic function and their ability to regulate their expression via both homo- and hetero-stimulatory mechanisms. Cytokine-mediated refractory states have also been reported [123], and it is possible that NANP delivery using different carriers can induce different refractory states, and NANPs' physicochemical properties can further contribute to these effects. It is important to note that the correlation analysis reveals the strength of the relationship between individual cytokines and is helpful in guiding the mechanistic studies; it is not meant to analyze a quantitative difference between study samples. Furthermore, due to the limited number of donors used in our study, the current correlation analysis should be considered preliminary and used to generate ideas for subsequent mechanistic studies involving PBMC from a greater number of donors.

These data also point to communication between different cell types such as monocytes (the main producers of TNFα, IL-1, IL-6, IL-8, and MIP-1), plasmacytoid dendritic cells (the main source of type I and type III IFNs), and T lymphocytes (the main producers of chemokines MCP and RANTES, type II IFN, and IL-2). Most importantly, the negative and positive correlation patterns differ between DNA and RNA cubes and between L2K- and dendrimer-delivered NANPs. These data further support the original hypothesis about the NANPs' ability to stimulate immune responses that might differ both quantitatively and qualitatively depending on the type of carrier used to deliver these particles to the immune cells. It would be interesting to compare routes of uptake and molecular pathways induced by the same types of NANPs after complexation with different carriers; this is the focus of the future research in this field.

The cytokine data (Figure 10 and Figure 11) correlate with NANP uptake by immune cells, which was studied by flow cytometry (Figure 12). The greater rates of NANP uptake by monocytes are consistent with the well-known phagocytic function of these cells [124]. The uptake of naked NANPs is negligible, which explains the lack of cytokine induction by RNA and DNA cubes used without a carrier. Since the melting temperature of DNA cubes is about 37 °C, an increase in the percentage of positive monocytes observed after the exposure to naked DNA cubes is likely due to the disassembly of these particles in the culture medium followed by an interaction of individual DNA oligonucleotides with cells.

2.4. MATERIALS AND METHODS

2.4.1. Materials

Generation 5 amine-terminated PAMAM dendrimers were purchased from Dendritech (Midland, MI, USA). Lipofectamine 2000 and all cell culture reagents were from Invitrogen (Carlsbad, CA, USA). Reagents for the preparation of buffers were purchased from Sigma-Aldrich (St. Louis, MO, USA).

2.4.2. Physicocheimcal Characterization of Dendrimers

A Malvern Zetasizer Nano ZS instrument (Southborough, MA, USA) with a back-scattering detector (173°) was used for measuring the hydrodynamic size (diameter) in the batch mode. NIST-NCL joint

protocol PCC-1 was followed (https://ncl.cancer.gov/resources/assay-cascade-protocols). Samples were prepared at a concentration of 3 mg/mL in 10 mM NaCl. Samples were measured as is (no filtering) and after filtration through a 0.02 μm filter. Samples were measured at 25 °C in a quartz microcuvette. Traces in the figures represent the average of ten measurements. Hydrodynamic diameters are reported as the intensity-weighted average and as the volume-weighted average over a particular range of size populations corresponding to the most prominent peak. The Int-Peak value is used as the hydrodynamic diameter of a particular species. The Vol-Peak and %Vol values are used to approximate relative amounts of various species in the formulation. A Malvern Zetasizer Nano ZS instrument (Southborough, MA, USA) was used to measure zeta potentials at 25 °C for all samples. NCL protocol PCC-2 was followed (https://ncl.cancer.gov/resources/assay-cascade-protocols). Samples were prepared at a concentration of 3 mg/mL in 10 mM NaCl. Sample pH was measured before loading into a pre-rinsed folded capillary cell. Measurements were made at both native pH and after adjustment to near neutral pH using 1 N standardized HCl. An applied voltage of 151 V was used. Traces in the figures represent the average of three measurements.

2.4.3. Preparation of NANPs

All sequences are available in the Supporting Information. The strands of DNA for DNA cubes or the DNA templates to produce RNA cubes were purchased from Integrated DNA Technologies (Coralville, IA, USA). RNA cube templates were then PCR-amplified using MyTaq™ Mix from Bioline (London, UK). Purification of the PCR products was done by using a DNA Clean and Concentrator™ kit from Zymo Research (Irvine, CA, USA). T7 RNA polymerase promoters from the PCR products were used to produce RNAs through in vitro run-off transcription with T7 RNA polymerase (80 mM HEPES-KOH (pH 7.5), 2.5 mM spermidine, 50 mM DTT, 25 mM MgCl2, 5 mM rNTP). The reaction was incubated at 37 °C for 3.5 h when RQ1 RNase-free DNase (Promega, Madison, WI, USA) was added. Denaturing 8 M urea polyacrylamide gel electrophoresis (PAGE 15%) was used to purify the reactions. RNA bands were visualized under short wavelength UV, cut, and eluted in a crush and soak buffer (300 mM NaCl, 89 mM

tris-borate (pH 8.2), 2 mM EDTA) overnight. RNA was precipitated in 2× volume of 100% ethanol for 3 h at −20 °C. 90% ethanol was used to wash the samples after centrifugation at 14,000 RCF for 30 min and twice for 10 min. The supernatant was disposed of and samples were then vacuum-dried and dissolved in double-deionized water (17.8 MΩ*cm). DNA and RNA cubes were each assembled using a one-pot assembly by combining each of the purified monomers at equimolar concentrations in double-deionized and endotoxin-free water. Solutions were then heated to 95 °C and cooled to 45 °C where assembly buffer (89 mM tris-borate (pH 8.2), 2 mM MgCl2, 50 mM KCl) was added after 2 min. DNA and RNA cubes were heated at 45 °C for an additional 20 min prior to storage at 4 °C throughout all experiments.

2.4.4. Physicochemical Characterization of NANPs

To analyze the DNA and RNA cube assemblies, 8% non-denaturing native-PAGE (37.5:1) was used in the presence of 89 mM tris-borate (pH 8.2) and 2 mM MgCl2. The gels were run for 20 min (Mini-PROTEAN® Tetra system Bio-Rad, Hercules, CA, USA) at 4 °C and 300 V. Gels were washed with double-deionized water and stained for 5 min with ethidium bromide for visualization using a ChemiDoc MP system (Bio-Rad) (Hercules, CA, USA). The resulting single bands for each cubic NANP demonstrate its complete assembly. Atomic force microscopy (AFM) of DNA and RNA cubes was performed on a freshly cleaved 1-(3-aminopropyl)silatrane-modified mica surface using a MultiMode AFM Nanoscope IV system (Bruker Instruments, Santa Barbara, CA, USA) in tapping mode.

2.4.5. Complexing NANPs and Dendrimers

Gel retardation assays were performed to assess the level at which the positively charged G5-NH2 dendrimers could neutralize the negative charge of Alexa 488-labeled DNA duplexes. DNA duplexes and G5-NH2 dendrimers were complexed at various N/P ratios and incubated for 30 min at room temperature before being run on a 2% agarose gel for 30 min at 75 V. The gel was imaged using a ChemiDoc MP system (Bio-Rad). To determine the G5-NH2 dendrimers' ability to protect nucleic acids from nuclease degradation, a double-stranded DNA carrying Alexa 488 (5′) and an Iowa Black Quencher (3′) on

complementary strands was complexed to the G5-NH2 dendrimers at the 1.5 N/1 P ratio. When samples were treated with DNase, digested DNA would result in separation of the fluorophore and quencher and subsequent increase in detection of fluorescence. DNAs were incubated with the G5-NH2 dendrimer for 30 min at room temperature. The complexes were then treated with 3 µL of RQ1 RNase-Free DNase (Promega, Madison, WI, USA) and immediately placed into a Bio-Rad C1000 Touch Thermal Cycler with a CFX96 Real-Time System (Hercules, CA, USA) Fluorescence was read every 30 s and the resulting curves were normalized to changes from the baseline fluorescence of the non-treated controls.

2.4.6. Transmission Electron Microscopy

After complexation, 5 µL of each sample was dropped onto a carbon-coated 400 mesh Cu/Rh grid (Ted Pella, Redding, CA, USA) and stained with 5 µL of 1% uranyl acetate (Polysciences, Warrington, PA, USA) which was prepared in filtered distilled water. A FEI Talos L120C TEM with a Gatan 4 k × 4 k OneView camera was used to image the grids.

2.4.7. Uptake by Cancer Cell Line MDA-MB-231

To assess uptake of the complexed cubes and dendrimers by a cancer cell line, MDA-MB-231 cells were used. The cells were cultured in DMEM containing 10% heat-inactivated FBS, 100 U/mL penicillin, and 100 µg/mL streptomycin at a density of 40,000 cells per well in a 24-well plate and incubated at 37 °C and 5% CO2 in a humidified incubator. After 24 h, the cells were transfected with Alexa 488-labeled cubes and the dendrimer complex at a final concentration of 50 nM of cubes for a period of 24 h. To compare, Alexa 488-labeled cubes were alternatively complexed with L2K (0.5 µL per well) for 30 min at room temperature and transfected into cells at a final concentration of 50 nM of cubes. After the incubation period, the cells were imaged with an EVOS FL Auto Imaging System (Thermo Fisher Scientific) (Carlsbad, CA, USA). The cells were then washed with phosphate buffered saline (PBS) and detached with 0.25% trypsin–EDTA (Thermo Fisher Scientific, Waltham, MA, USA). The detached cells were replenished with media, centrifuged for 5 min at 300× g, and the cell pellet was resuspended in PBS.

The cells were analyzed with flow cytometry (BD Accuri C6). Cell viability of the MDA-MB-231 cells post-transfection with the cubes and G5-NH2 dendrimers was measured using an MTS assay (Cell Titer 96® AQueous One Solution Cell Proliferation Assay from Promega, Madison, WI, USA). MDA-MB-231 cells were plated in a 96-well plate and then transfected with cube–dendrimer complexes at concentrations of 5, 10, 20, 50, and 100 nM. Cell viability was assessed by measuring the relative absorbance of the transfected cells with respect to the non-transfected cells at 490 nm using a Tecan ULTRA microplate reader.

2.4.8. Research Donor Blood

Blood was collected from healthy donor volunteers under NCI-Frederick protocol OH9-C-N046. Each donor was assigned a random number. Blood was collected into vacutainers containing Li-heparin as an anticoagulant and processed to isolate PBMC within 2 h after donation.

2.4.9. In Vitro Cytokine Release

PBMC isolation and cytokine analysis were performed as described previously [66]. Briefly, NANPs alone, NANPs after complexation with Lipofectamine 2000 or generation 5 amine-terminated PAMAM dendrimers, and positive or negative controls were added to PBMC cultures, and the incubation continued overnight at 37 °C in an incubator with 5% CO2. Complexation with Lipofectamine was done using the protocol described by us earlier [66]. For complexation with dendrimers, stocks of NANPs and dendrimers were incubated at room temperature for 30 min, then diluted in the complete cell culture medium (RPMI supplemented with 10% heat-inactivated FBS, 2 mM L-glutamine, 100 U/mL penicillin, and 100 μg/mL streptomycin). The final concentration of NANPs in the culture was 10 nM for all tested conditions (without a carrier, complexed with L2K, and complexed with dendrimers). After the incubation, the culture supernatants were collected and centrifuged at 18,000× g for 5 min. The supernatants were then analyzed by multiplex ELISA (Quansys Biosciences, Logan, UT, USA) to determine levels of individual cytokines.

2.4.10. Uptake by Flow Cytometry

PBMCs were either left untreated or incubated in the presence of DNA and RNA cubes alone, complexed with Lipofectamine, or complexed with G5 amine-terminated dendrimers. After 24 h of incubation, the cells were washed to remove the excess particles, reconstituted in the flow cytometry buffer, and analyzed using a Novocyte cytometer (ACEA Biosciences, San Diego, CA, USA). All cubes used for experiments were labeled with Alexa 488 (Integrated DNA technologies, Coralville, IA, USA). The final particle concentration was 10 nM, the same as was used in the cytokine experiments. The cells were separated according to their forward and side scatter, and the live populations of lymphocytes and monocytes were gated into the green fluorescent channel for the detection of particle uptake. The data analysis was performed using the FCS Express software (DeNovo Software Inc., Pasadena, CA, USA).

2.4.11. Statistical Analysis

Data are presented as the means ± standard deviation (SD) in all studies. For statistical analysis, a one-way analysis of variance (ANOVA) followed by Tukey's multiple comparison test was performed using GraphPad Prism version 9.0.0 for Windows, GraphPad Software, San Diego, CA, USA, www.graphpad.com. A p-value of less than 0.05 was considered statistically significant.

2.5. CONCLUSIONS

This study demonstrates that amine-terminated PAMAM dendrimers can be used as delivery carriers for nucleic acid nanoparticles. As a proof of concept, the uptake of two representative NANPs (DNA and RNA cubes) was demonstrated in a human cancer cell line prior to in human PBMCs. Most importantly, the uptake by different immune cells present in the peripheral blood and subsequent cytokine responses differ both quantitatively and qualitatively when NANPs are delivered to the blood cells using different carriers such as L2K and dendrimers.

Author Contributions

Y.I.A., M.C., E.C., H.S.N., M.R., and J.X. conducted experiments and analyzed data. K.A.A. and M.A.D. designed and supervised the study and analyzed data. J.D.C. and N.J.L. reviewed and analyzed data. All authors discussed the progress of research, interpreted data, and wrote the manuscript. All authors have read and agreed to the published version of the manuscript.

Sequences used in this work.

One strand per NANP was modified with an Alexa 488 label to assess uptake by fluorescence.

Six-stranded DNA cube:

5’- GGCAACTTTGATCCCTCGGTTTAGCGCCGGCCTTTTCTCCCACACTTTCACG

5’- GGGAAATTTCGTGGTAGGTTTTGTTGCCCGTGTTTCTACGATTACTTTGGTC

5’- GGACATTTTCGAGACAGCATTTTTTCCCGACCTTTGCGGATTGTATTTTAGG

5’- GGCGCTTTTGACCTTCTGCTTTATGTCCCCTATTTCTTAATGACTTTTGGCC

5’- GGGAGATTTAGTCATTAAGTTTTACAATCCGCTTTGTAATCGTAGTTTGTGT

5’- GGGATCTTTACCTACCACGTTTTGCTGTCTCGTTTGCAGAAGGTCTTTCCGA

Fluorescently labeled DNA cube strand:

5’- GGCGCTTTTGACCTTCTGCTTTATGTCCCCTATTTCTTAATGACTTTTGGCC/3AlexF488N/

Six-stranded RNA cube:

5’- GGCAACUUUGAUCCCUCGGUUUAGCGCCGGCCUUUUCUCCCACACUUUCACG

5’- GGGAAAUUUCGUGGUAGGUUUUGUUGCCCGUGUUUCUACGAUUACUUUGGUC

5’- GGACAUUUUCGAGACAGCAUUUUUUCCCGACCUUUGCGGAUUGUAUUUUAGG

5’- GGCGCUUUUGACCUUCUGCUUUAUGUCCCCUAUUUCUUAAUGACUUUUGGCC

5’- GGGAGAUUUAGUCAUUAAGUUUUACAAUCCGCUUUGUAAUCGUAGUUUGUGU

5’- GGGAUCUUUACCUACCACGUUUUGCUGUCUCGUUUGCAGAAGGUCUUUCCGA

Fluorescently labeled RNA cube strand:

5’-

GGCGCUUUUGACCUUCUGCUUUAUGUCCCCUAUUUCUUAAUGACUUUUGGCC/3AlexF488N

/

DNA duplex used in DNase protection assays:

5’- /5IABkFQ/TGACCCTGAAGTTCATCTGCACCACCGGTCACGGTCTCC

5’- GGAGACCGTGACCGGTGGTGCAGATGAACTTCAGGGTCATT/3AlexF488N/

DNA duplex used in complexation to determine N/P ratio:

5’- TGACCCTGAAGTTCATCTGCACCACCGGTCACGGTCTCC

5’- GGAGACCGTGACCGGTGGTGCAGATGAACTTCAGGGTCATT/3AlexF488N/

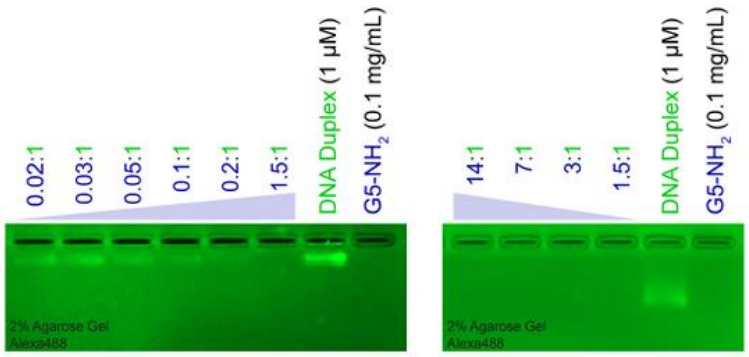

Figure 13. Complexation of DNA duplex with G5-NH2 dendrimers at various N/P ratios. DNA duplexes labeled with Alexa 488 (labeled in green font) were combined with G5-NH22 dendrimers (labeled in blue font) at different negative charge (N) to positive charge (P) ratios as shown above. The samples were then analyzed by agarose gel electrophoresis.

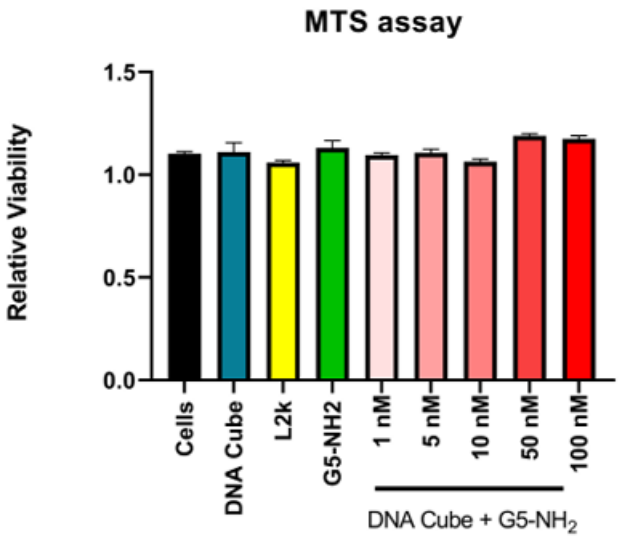

Figure 14. Cell viability assay of MDA-MB-231 cells treated with NANPs and G5 NH2 dendrimers. Viability of MDA-MB-231 cells after being exposed to DNA cube G5-NH2 dendrimer complexes which was evaluated at 72 hours. All samples remained above an 80% viability.

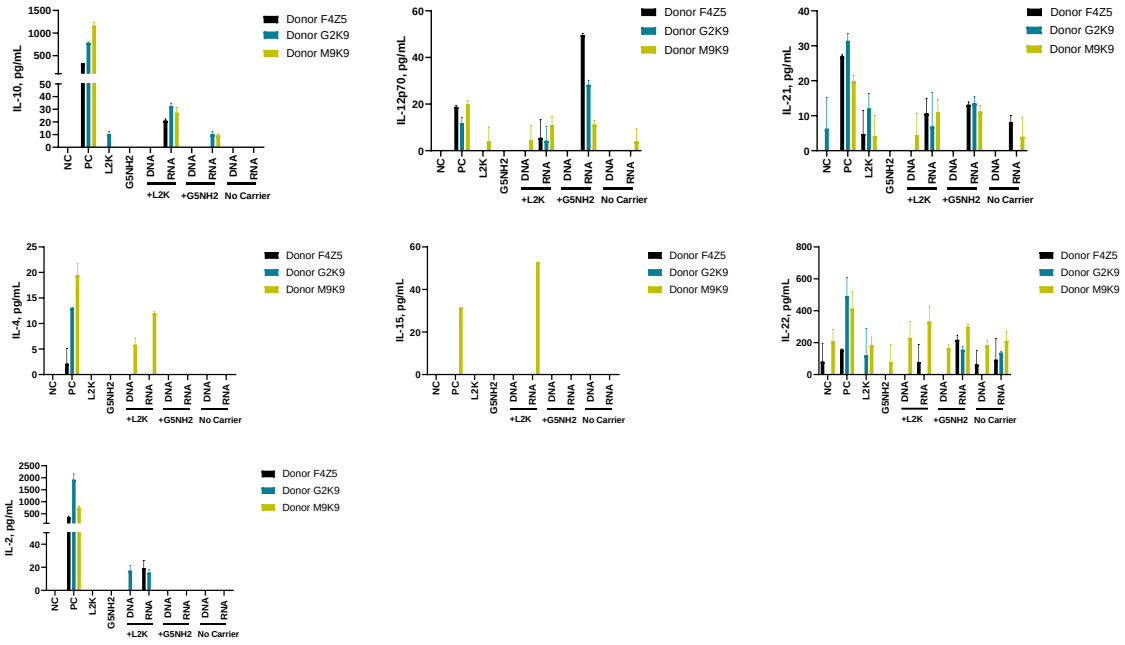

Figure 15. Cytokine induction by DNA and RNA cubes as a function of the delivery carrier. PBMC from three healthy human donor volunteers (F4Z5, G2K9, and M9K9) were treated with negative control (NC), positive control (PC), DNA cubes, or RNA cubes for 24 hours. Prior to the addition to PBMC cultures, DNA cubes and RNA cubes were complexed with lipofectamine 2000 L2K), G5 amine-terminated PAMAM dendrimers (G5-NH2) or used without complexation (no carrier). Culture supernatants were analyzed for the presence of cytokines, chemokines, and interferons using multiplex ELISA as described in Materials and Methods. The data for other cytokines grouped based on their function (i.e., type I and type III interferons, danger signals and cytokines commonly associated with trauma and cytokine storm, type II interferon and type II interferon inducible protein, and chemokines are presented on Figure 5. Each bar shows the mean response and standard deviation (N = 2).

3 CHAPTER 3: EXPLORING DENDRIMER-NUCLEIC ACID NANOPARTICLE INTERACTIONS: IMPACT ON IMMUNE RECOGNITION AND DIFFERENTIAL COMPLEXING OF DNA AND RNA

3.1. INTRODUCTION

Immunological profiling is emerging as a crucial approach for the advancement of therapeutic nucleic acids. The mRNA vaccine has underscored the significance of understanding the body's natural defense mechanisms, particularly in response to non-self-nucleic acids. It has become evident that many individuals exhibit robust immune responses to foreign nucleic acids, which can elicit a spectrum of immunological mechanisms leading to inflammation, stress, and other undesirable phenotypes. These responses are shaped by the prolonged exposure to various microorganisms, which educate the immune system to exhibit appropriate responses and prevent infections from causing harm. The immune system and its responses to therapeutic platforms play a pivotal role that considered for future designs[70, 71, 125, 126].

The choice of delivery vehicles for nucleic acids and other nanotechnologies is paramount, as it significantly influences the biological fate of the cargo. Effective delivery vehicles must not only facilitate cellular uptake but also shield the cargo from degradation and immune recognition, ensuring optimal therapeutic outcomes[52, 69, 70, 73, 94, 125]. Moreover, shielding the cargo from immune recognition helps minimize unwanted immune responses, thereby enhancing the safety and efficacy of the therapy. Overall, the selection of delivery vehicles is a critical consideration in the design of nanotherapeutic platforms, as it directly impacts the efficacy, safety, and success of the treatment strategy.

Polyamidoamine (PAMAM) dendrimers are synthetic polymeric nanoparticles that possess chemical modifications that facilitate interactions with therapeutic nucleic acids[127]. Amine-terminated PAMAM dendrimers, are synthesized to have positively charged surface groups that can bind to nucleic acid nanoparticles (NANPs) through electrostatic interactions[39]. Upon binding with dendrimers, the NANPs will have a higher delivery efficiency into cells[128].

Dendrimers, as polymeric nanoparticles, undergo growth during their synthesis, resulting in distinct generations. For example, generation zero is the dendrimer's core, which serves as the starting point. With each subsequent synthesis step, the dendrimer branches out from its surface terminal groups. This branching process results in a doubling of surface groups and overall size, defining a new generation of dendrimers. With the increase generation also comes an increase in carrying capacity and charge. In previous reports, the most clinically relevant generations are 3-5[41, 129-132]. However, recent studies have been revealing that the higher generations, 6 and 7, have the benefit of multivalency by providing the capability of binding more than one therapeutic payload to a single dendrimer because of their larger size and carrying capacity[132-136]. Furthermore, it has also been elucidated that higher generations of dendrimers provide protection from immune cell detection[137] by hindering recognition by the receptors of the immune system.

In this report, the use of PAMAM dendrimers is being investigated for their use as a delivery vehicle for nucleic acid nanoparticles to develop an understanding of the role that different dendrimer generations play in the delivery efficiency and immune responses of NANPs. In doing so, we aim to develop a repository of information on how size, shape, and charge influence the in vitro characterization profiles when reporting uptake efficiency and immune response using both immune reporter cell lines and peripheral blood mononuclear cells.

Moreover, the representative NANPs employed in these investigations are cubic in structure and are fabricated using either DNA or RNA. While each cube maintains the same structural framework, they exhibit variations in composition attributed to the distinct nucleotides utilized for DNA versus RNA assembly. Comprising six strands, these NANPs consist of a total of 120 intermolecular base pairs per cube. The connectivity between monomers is facilitated by the inclusion of eight three-way junctions (3WJ), each composed of nine single-stranded nucleotides[69, 138]. The cubic NANPs have 312 phosphate groups to make up the backbone of each strand; the negatively charged phosphate backbone will electrostatically interact with the positively charged amine-terminated dendrimers. Furthermore, different ratios of amine to phosphate (N/P) groups will be evaluated within this work.

Many of our previous works have investigated the immune recognition and responses to the cubes, consistently revealing that RNA cubes elicit significantly higher immunostimulatory effects compared to their DNA counterparts[16, 67, 69, 94]. In the current study, we aim to investigate how the complexation of these cubes with amine-terminated PAMAM dendrimers will influence cellular uptake and immune recognition of these well-characterized structures. By exploring the interplay between NANPs and dendrimers, we seek to reveal how their interaction modulates immune responses, furthering our understanding of their potential as therapeutic platforms and delivery vehicles.

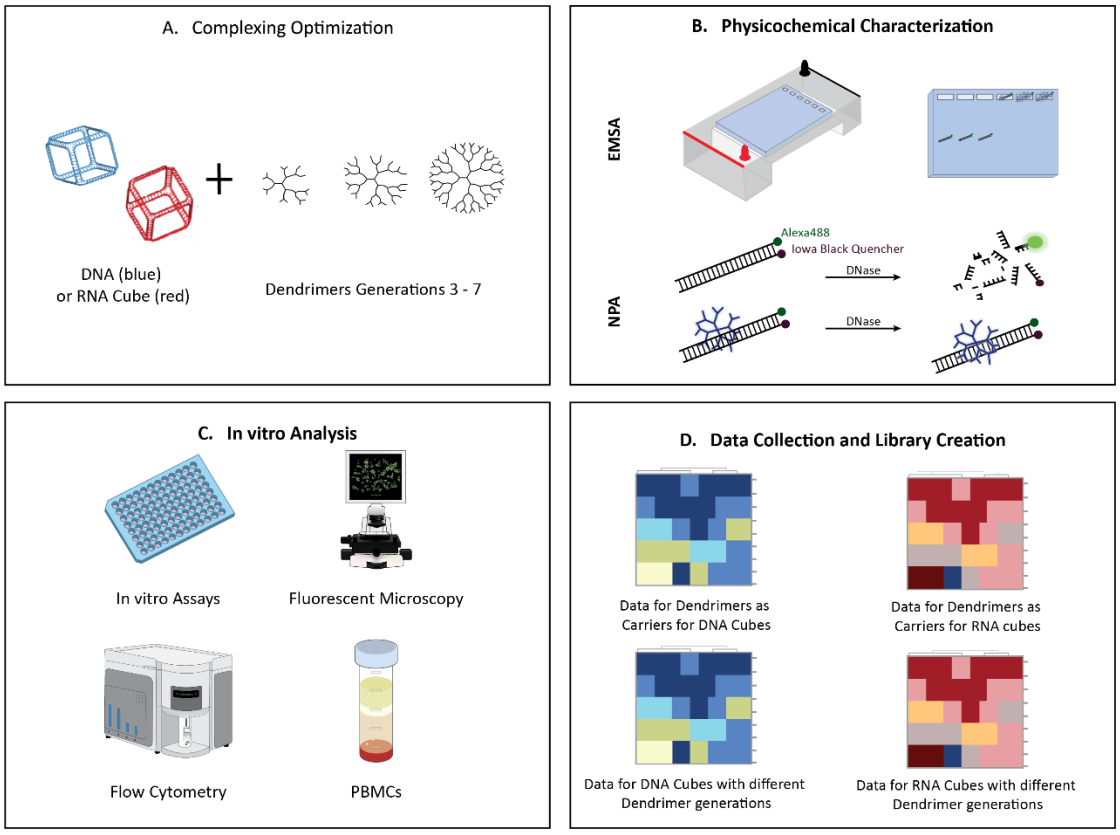

Figure 16. Experimental workflow of NANPs and dendrimer complexing and in vitro assessment. A) DNA or RNA cubes will be complex to each dendrimer generation. B) Binding will be characterized by electromobility shift assays, and nuclease protection assays. C) Complexed NANPs and dendrimers will be run through in vitro characterization profiles of uptake and immune activation. D) Acquired data will be assessed and analyzed.

The dendrimer generations investigated in this study were generations 3-7. Within this subset of dendrimers we investigated carriers ranging in size ranges from 3.6 to 8.1 nm and the number of surface

amine groups ranged from 32 to 512. The characteristics of the included dendrimers are shown in Figure 17. When compared to the cubic NANPs at 10 nm, each of the dendrimer generations is smaller. At 312 phosphates on the cubic DNA NANP, generations 6 and 7 are the only comparable generations in the number of surface groups.

3.2. RESULTS AND DISCUSSION

Binding assessment was determined by complexing dendrimers and DNA duplexes tagged with Al488 fluorophore. Formation of complexes (Figure 17) was found by using a constant concentration of fluorescently tagged duplex and varying the amount of dendrimer that was added to test various N/P ratios. Samples were then run through a 1.5% (w/v) agarose gel. Duplexes not complexed with dendrimers traveled freely through the gels, while the mobility of duplexes that were electrostatically complexed with dendrimers was limited and trapped in the wells. Complete hinderance for each generation was observed to vary at different N/P ratios across generations.

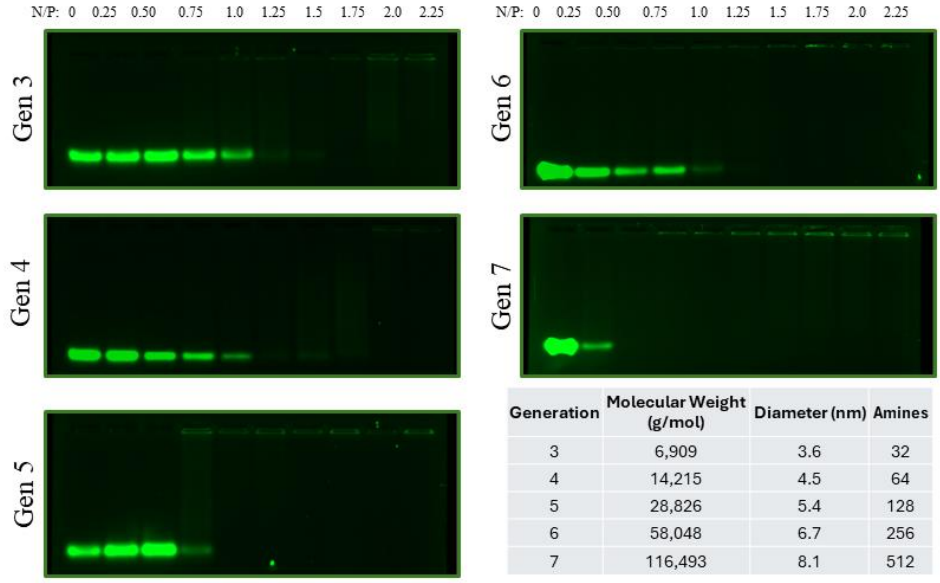

Generation	Molecular Weight (g/mol)	Diameter (nm)	Amines
3	6,909	3.6	32
4	14,215	4.5	64
5	28,826	5.4	128
6	58,048	6.7	256
7	116,493	8.1	512

Figure 17. Binding assays of DNA duplexes to dendrimers at increasing N/P ratios – from left to right. Table with dendrimer characteristics for each generation.

To evaluate the efficacy of different generations of dendrimers in protecting nucleic acids from enzymatic degradation, double-stranded DNA duplexes carrying an Alexa Fluor 488 (Al488) fluorophore (5' sense) and an Iowa Black Quencher (3' anti-sense) were complexed with each dendrimer generation at a N/P ratio of either 1 or 2. Subsequently, the complexes were treated with RQ1 DNase, and the fluorescence resulting from DNA digestion was measured at 60-second intervals (Figure 18).

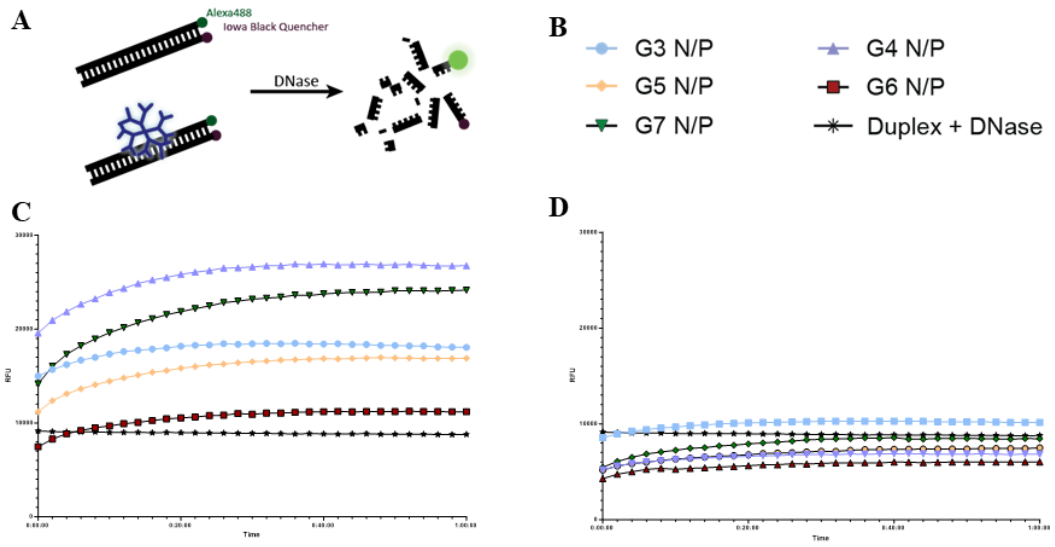

Figure 18. Nuclease protection assay of each generation of dendrimer. A) Schematic representation of the nuclease protection assay experiment. B) The legend for each of the generations and controls. C) Nuclease protection results for dendrimers plus duplex at an N/P of 1. D) Nuclease protection results for dendrimers plus duplex at an N/P of 2.

In uncomplexed samples, enzymatic digestion of the DNA duplex led to the separation of the fluorophore and quencher, resulting in increased fluorescence over time. Conversely, in samples complexed with dendrimers at an NP ratio of 2, no significant increase in fluorescence was observed, indicating effective shielding of the duplexes from enzymatic degradation by the dendrimers.

Notably, at an NP ratio of 1, only generation 6 dendrimers provided protection against enzymatic degradation. This observation underscores the generation-specific variations in the ability of dendrimers to protect nucleic acids from enzymatic attack.

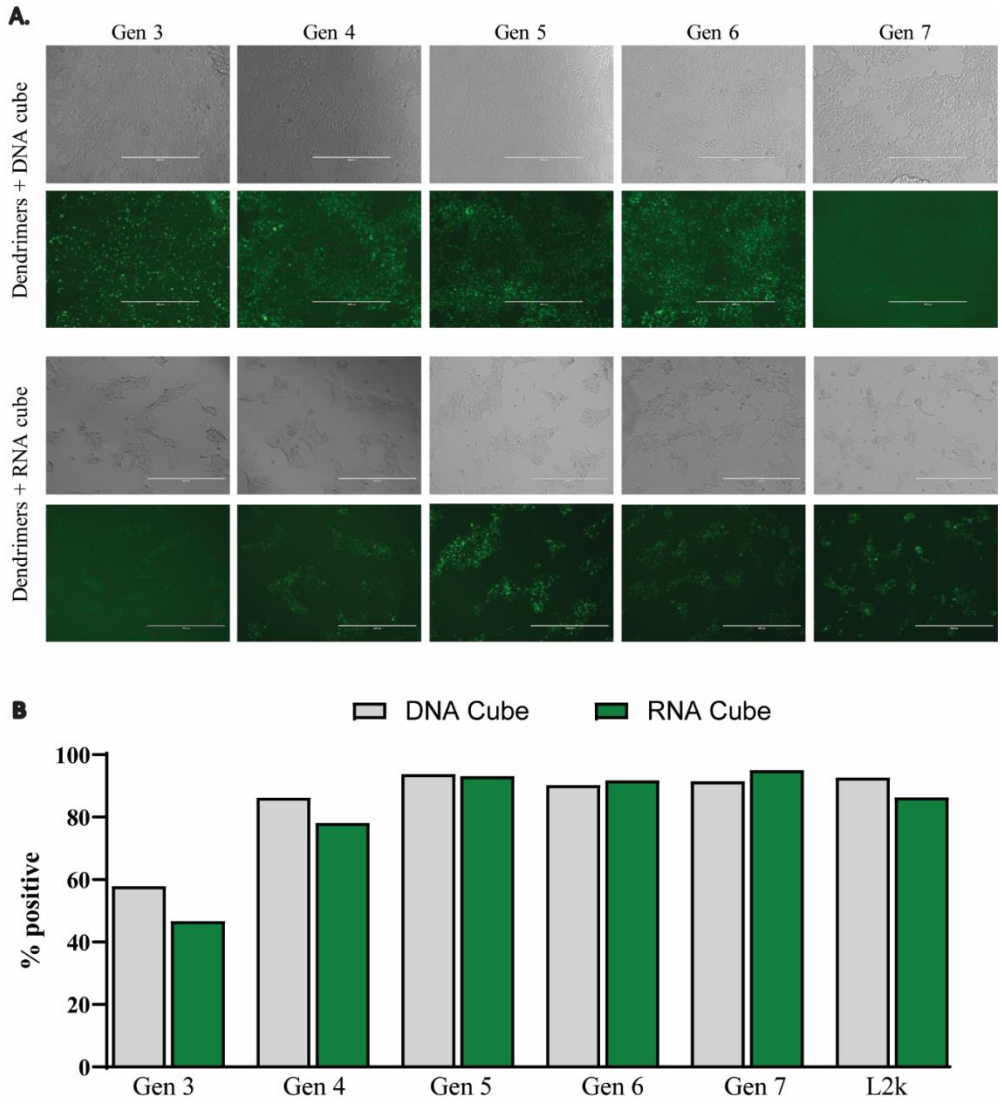

Figure 19. Comparison of DNA and RNA Cube Uptake in HEK-293FT Cells Across Dendrimer Generations. A) Microscopy images: Images depict uptake of DNA and RNA cubes labeled with Al488 fluorophore in HEK-293FT cells. B) Flow cytometry data: Percentage of HEK-293FT cells positive for Al488 fluorescence at each dendrimer generation is presented, indicating uptake efficiency.

To validate the intracellular uptake of our dendriplexes, dendrimers from each generation were complexed with either Alexa 488-labeled DNA or RNA cubes and subsequently introduced into human embryonic kidney (HEK-293FT) cells **(**Figure 19A). This cell line was chosen as a representative model to assess transfection efficiency in subsequent experiments involving human toll-like receptor cell lines (hTLRs). By employing HEK-293FT cells, we aimed to gain insights into the cellular uptake dynamics of our dendriplexes, laying the groundwork for evaluating their performance in immune cell lines. The uptake

efficiency of dendrimers complexed to cubes was assessed using fluorescence microscopy, followed by flow cytometry analysis. The percentage of cells positive for Al488, the tag used on our DNA or RNA cubes complexed to dendrimers at an N/P of 2, was determined by flow cytometry. The uptake studies revealed slight variation in the percent positive cells for generations 5, 6, and 7, observed across both DNA and RNA cubes. Interestingly, the uptake efficiencies of these generations were comparable to those observed with lipofectamine 2000 (L2K) as a carrier. However, lower generations (3 and 4) exhibited reduced efficiency for both cube types. Notably, DNA cubes in generations 3 and 4 displayed higher uptake efficiency compared to RNA cubes (Figure 19B). Furthermore, when testing an N/P ratio of 1 (Figure 22) across the different generations, there was variability in transfection efficiency when compared to N/P of 2. Also tested was the cell viability of the HEK-293FT cells when transfected with either cube complexed to each generation at N/P of 1 and 2. Figure 23 shows that there is no significant decrease in cell viability in any of the combinations. However, notably, for each generation, the N/P of 2 samples showed a slightly less viability than N/P of 1.

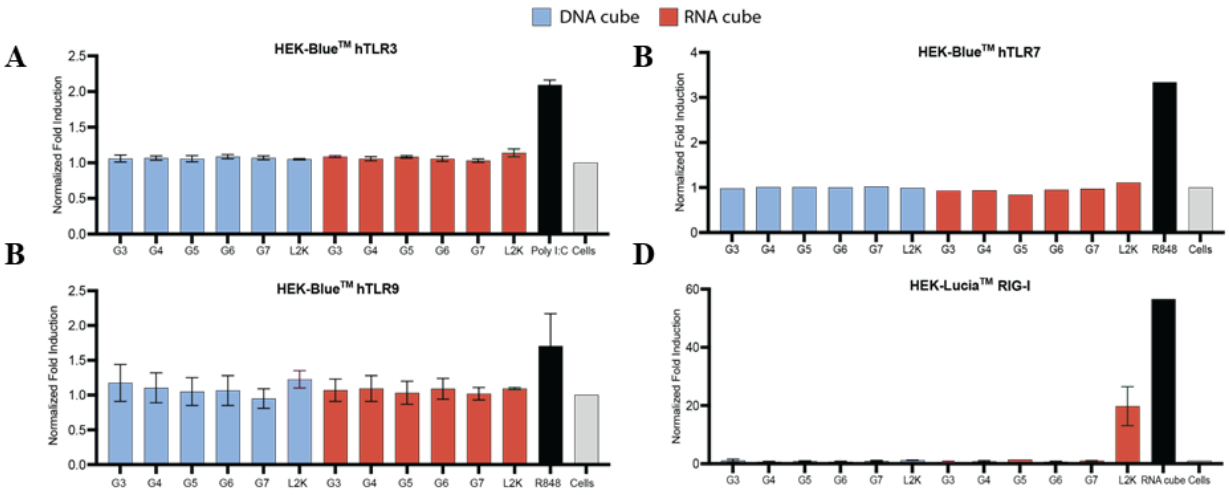

Figure 20. Using human reporter cell lines to investigate immune response of dendriplexes at the endosomal and cytosolic level. A) hTLR3 cells were transfected at a final concentration of 10 nM cube construct complexed to each dendrimer generation at N/P of 2. B) hTLR7 cells were transfected at a final concentration of 10 nM cube construct complexed to each dendrimer generation at N/P of 2. C) hTLR9 cells were transfected at a final concentration of 10 nM cube construct complexed to each dendrimer generation at N/P of 2. D) RIG-I cells were transfected at a final concentration of 10 nM cube construct complexed to each dendrimer generation at N/P of 2.

Immune recognition in human reporter cell lines: Toll-like receptors (TLRs) are specific pattern recognition receptors that have evolved to respond to distinct molecular patterns that can be associated with either danger or pathogen associated molecular patterns. Upon activation of TLRs, an intracellular signaling cascade is triggered, resulting in the activation of immune responses. TLRs are a key component of the innate immune system's ability to detect and respond to potential threats. We used HEK-293FT cells over-expressing human endosomal TLR 3, 7, 9, and cytosolic RIG-I to investigate the activation in response to our cubic NANPs when complexed to dendrimer generations 3-7, (Figure 20). The cells used are engineered to contain secreted embryonic alkaline phosphatase (SEAP) gene that is under the control of the IFN-β promoter fused to NF-kB and AP-1 binding sites[69]. SEAP can be easily detected and quantified using QUANTI-Blue™. RIG-I expressing cells will be reporting activity of the IRF pathway through the detection of luciferase which can be quantified as well, using QUANTI-Luc™.

TLR 3 detects double-stranded RNA, TLR7 recognizes single-stranded RNA, and TLR9 recognizes unmethylated CpG DNA motifs. Meanwhile, RIG-I detects double-stranded RNA with 5' triphosphate end.

Each of these pattern recognition receptors when tested against our DNA and RNA cubes did not show a significant response or activation after treatment with the dendriplexes (Figure 20). Most surprisingly, was the RIG-I results. The same RNA cube that was complexed to the dendrimers, was used as a positive control using lipofectamine 2000 (L2K) as the carrier, and the immune activation was significant. However, the dendrimers seem to hinder this response from taking place. A reason for the lack of immune response can be attributed to the dendrimer's impact on the molecular signature of the nucleic acids. Upon binding, it is possible that the surface groups of the dendrimers are blocking the TLR's ability to detect the nucleic acids. This phenomenon has been previously reported when using amine-terminated dendrimers at generations 3-5, wherein the dendrimers evaded complement activation by blocking pattern recognition[137].

We found that the immune reporting cell lines were not suitable for accurately depicting the immune response observed when testing peripheral blood mononuclear cells (PBMCs) with the same samples. This discrepancy can be attributed to the dendrimers utilizing another form up uptake into cells other than endocytosis, bypassing recognition in the endosomal TLRs. More mechanistic studies should be explored to reveal the mechanisms that are employed for uptake with each of the dendrimer generations when being used to deliver nucleic acid nanoparticles. The lack of responses from TLRs underscores the importance of utilizing physiologically relevant models, such as PBMCs, to assess the immune response more accurately to dendriplexes. Additionally, literature suggests that TLRs are not the sole source of immune activation, indicating that further mechanistic studies can be used to elucidate the pathways involved in cytokine and chemokines being released[125]. Furthermore, Figure 24 summarizes cell viability in each of the reporter cell lines, showing no significant impact or toxicity in any of the cell lines, for any of the combinations.

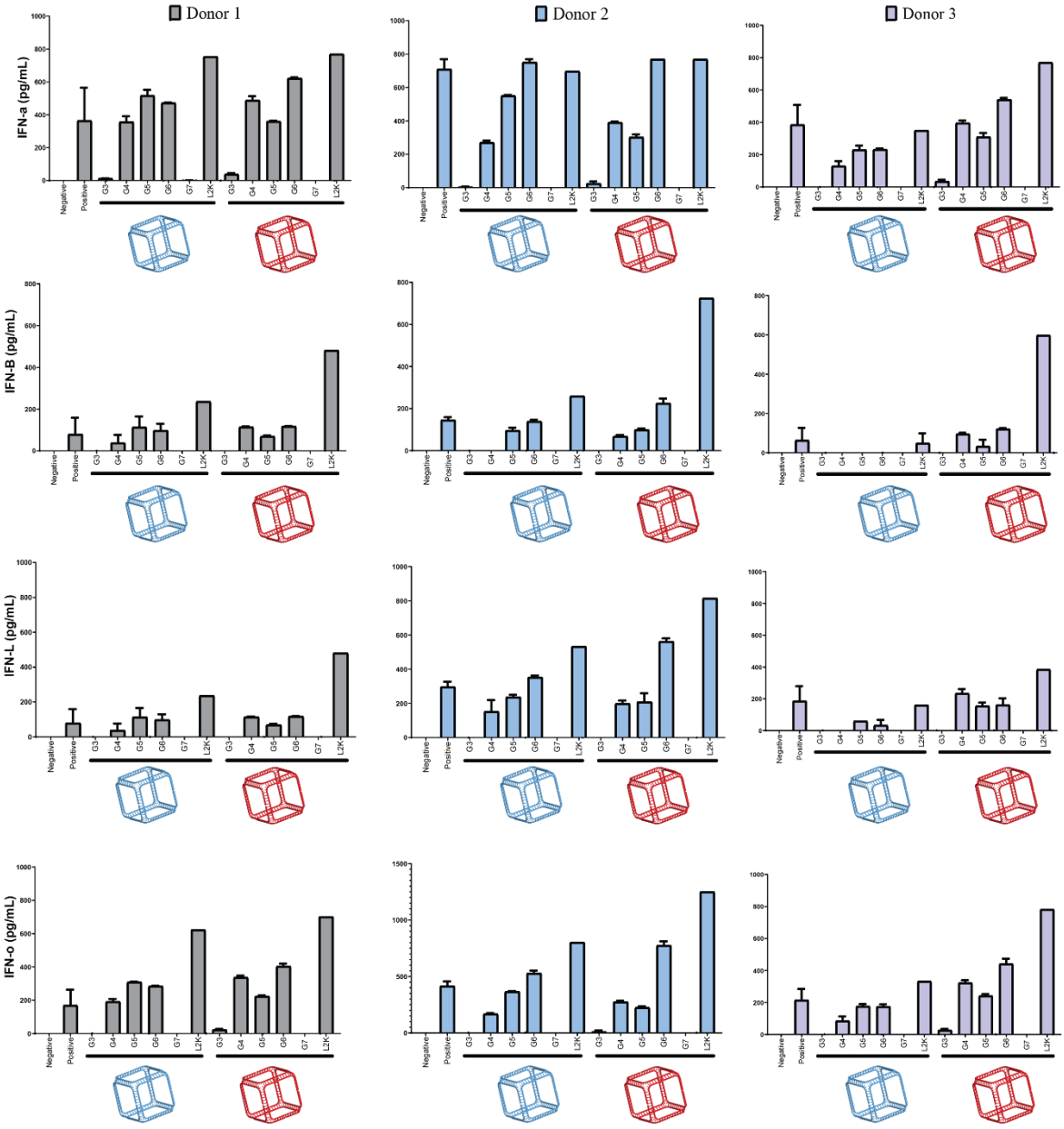

Figure 21. PBMC results of interferon response to DNA vs RNA cubes complexed to dendrimers generations 3-7. From top to bottom: Type I IFNs (IFN-α and IFN-β), Type II IFN-λ, and Type III IFN-γ. From left to right: Donors 1 through 3, showing the concentration of each IFN produced in response to treatment.

To investigate the NANP-dendrimer complex induced immune activation, we evaluated the cytokine and interferon induction using human peripheral blood mononuclear cells (PBMCs). The cells were incubated for 24 hours at a final NANP concentration of 10 nM. After incubation, the immunostimulatory activity of each dendriplex complex was assessed and quantified using multiplexed enzyme-linked immunosorbent

assays (ELISAs) to determine the concentration of interferons (α, ß, γ) and pro-inflammatory cytokines known for being expressed after exposed to nucleic acids (Figure 21). Consistent with previous studies, RNA cubes continued to have a higher activation than that of DNA cubes when delivered using L2K. However, when looking at the dendriplexes, for both DNA and RNA cubes, every generation had much less of an immune response than that of L2K. Figure 25 shows the heat map of the more expansive results resulting from the multiplex ELISAs.

3.3. METHODS

3.3.1. Preparation of NANPs

All sequences are available in the Supporting Information. The DNA strands for DNA cubes and the DNA templates to synthesize RNA cubes were purchased from Integrated DNA Technologies (Coralville, IA, USA). RNA cube templates were then PCR-amplified using MyTaq™ Mix from Bioline (London, UK). Purification of the PCR products was done by using a DNA Clean and Concentrator™ kit from Zymo Research (Irvine, CA, USA). T7 RNA polymerase promoters from the PCR products were used to produce RNAs through in vitro run-off transcription with T7 RNA polymerase (80 mM HEPES-KOH (pH 7.5), 2.5 mM spermidine, 50 mM DTT, 25 mM MgCl2, 5 mM rNTP). The reaction was incubated at 37 °C for 3.5 h when RQ1 RNase-free DNase (Promega, Madison, WI, USA) was added. Denaturing 8 M urea polyacrylamide gel electrophoresis (PAGE 15%) was used to purify the reactions. RNA bands were visualized under short wavelength UV, cut, and eluted in a crush and soak buffer (300 mM NaCl, 89 mM tris-borate (pH 8.2), 2 mM EDTA) overnight. RNA was precipitated in 2× volume of 100% ethanol for 3h at −20 °C. 90% ethanol was used to wash the samples after centrifugation at 14,000 RCF for 30 min and twice for 10 min. The supernatant was disposed of, and samples were then vacuum-dried and dissolved in double-deionized water (17.8 MΩ*cm). The DNA and RNA cubes were each assembled using a one-pot assembly by combining each of the purified monomers at equimolar concentrations in double-deionized and endotoxin-free water. Solutions were then heated to 95 °C and cooled to 45 °C where assembly buffer

(89 mM tris-borate (pH 8.2), 2 mM MgCl2, 50 mM KCl) was added after 2 min. DNA and RNA cubes were heated at 45 °C for an additional 20 min prior to storage at 4 °C throughout all experiments.

3.3.2. Physicochemical Characterization of NANPs

To analyze the DNA and RNA cube assemblies, 8% non-denaturing native-PAGE (37.5:1) was used in the presence of 89 mM tris-borate (pH 8.2) and 2 mM MgCl2. The gels were run for 20 min (Mini-PROTEAN® Tetra system Bio-Rad, Hercules, CA, USA) at 4 °C and 300 V. Gels were washed with double-deionized water and stained for 5 min with ethidium bromide for visualization using a ChemiDoc MP system (Bio-Rad) (Hercules, CA, USA). The resulting single bands for each cubic NANP demonstrate its complete assembly. Atomic force microscopy (AFM) of DNA and RNA cubes was performed on a freshly cleaved 1-(3-aminopropyl)silatrane-modified mica surface using a MultiMode AFM Nanoscope IV system (Bruker Instruments, Santa Barbara, CA, USA) in tapping mode.

3.3.3. Preparation of dendrimers

Amine-terminated PAMAM dendrimers were purchased from Dendritech, Inc. The stocks from Dendritech were dried overnight using SpeedVac at 30°C and then rehydrated at a stock concentration of 1 mg/mL using ET-Free H2O. For all following experiments, dendrimers were further diluted to a working stock of 0.1 mg/mL.

3.3.4 Calculating N/P Binding ratios

Amine to phosphate (N/P) ratios were found by using the known number of amine groups from each generation of dendrimers, which changed with each dendrimer, and the known number of phosphate groups in the DNA backbone of the duplex sequence used, 51. In equation 1, P is the number of variable phosphate groups. $N{:}\,P = \frac{51}{P}$

Equation 1 can be manipulated to find the concentration of dendrimer needed to get to the desired N:P ratio, when the duplex concentration is set, as shown in Equation 2.

$$uM\ of\ dendrimer = \frac{51 * x\ uM\ of\ duplex}{P * desired\ N{:}P}$$

To calculate the volume of DNA duplex needed based on the desired N:P ratio, equation 3 was used.

$$uL\ of\ duplex = \frac{desired\ N{:}P *\ P * uL\ of\ dendrimer}{51}$$

3.3.5. Complexing NANPs and Dendrimers

Binding assays were performed to assess the level at which the positively charged G5-NH2 dendrimers could neutralize the negative charge of Alexa 488-labeled DNA duplexes. DNA duplexes and G5-NH2 dendrimers were complexed at various N/P ratios and incubated for 30 min at room temperature before being run on a 1.5% agarose gel for 20 min at 250 V. The gel was imaged using a ChemiDoc MP system (Bio-Rad).

To determine the dendrimers' ability to protect nucleic acids from nuclease degradation, a double-stranded DNA carrying Alexa 488 (5′) and an Iowa Black Quencher (3′) on complementary strands was complexed to the dendrimers at N/P ratios of 1 and 2. DNA was incubated with the dendrimer for 30 min at room temperature. When samples were treated with DNase, digested DNA would result in the separation of the fluorophore and quencher and a subsequent increase in the detection of fluorescence. The complexes were then treated with 2 µL of RQ1 RNase-Free DNase (Promega, Madison, WI, USA) and immediately placed into the Tecan SPARK plate reader holding a constant temperature of 37°C. Fluorescence was read every 30 s, and the resulting curves were normalized to changes from the baseline fluorescence of the non-treated controls.

3.3.6. Uptake by HEK-293FT cells

To assess the uptake of the complexed cubes and dendrimers, HEK-293FT cells were used. The cells were cultured in DMEM containing 10% heat-inactivated FBS, 100 U/mL penicillin, and 100 µg/mL streptomycin at a density of 40,000 cells per well in a 24-well plate and incubated at 37 °C and 5% CO_2 in

a humidified incubator. After 24 h, the cells were transfected with Alexa 488-labeled cubes and the dendrimer complexes at a final concentration of 20 nM of cubes for a period of 24 h. To compare, Alexa 488-labeled cubes were alternatively complexed with L2K (2 µL per well) for 30 min at room temperature and transfected into cells at a final concentration of 20 nM of cubes. After the incubation period, the cells were imaged with an EVOS FL Auto Imaging System (Thermo Fisher Scientific) (Carlsbad, CA, USA). The cells were then washed with phosphate buffered saline (PBS) and detached with 0.25% trypsin–EDTA (Thermo Fisher Scientific, Waltham, MA, USA). The detached cells were replenished with media, centrifuged for 5 min at 300x g, and the cell pellet was resuspended in PBS. The cells were analyzed with flow cytometry (Attune NXT).

Cell viability of the by HEK-293FT cells post-transfection with the cubes and G5-NH2 dendrimers was measured using an MTS assay (Cell Titer 96® AQueous One Solution Cell Proliferation Assay from Promega, Madison, WI, USA). MDA-MB-231 cells were plated in a 96-well plate and then transfected with cube–dendrimer complexes at N/Ps of 1 and 2 with a final concentration of 20 nM cube. Cell viability was assessed by measuring the relative absorbance of the transfected cells with respect to the non-transfected cells at 490 nm using a Tecan® SPARK microplate reader.

3.3.7. Research Donor Blood

Blood was collected from healthy donor volunteers under NCI-Frederick protocol OH9-C-N046. Each donor was assigned a random number. Blood was collected into vacutainers containing Li-heparin as an anticoagulant and processed to isolate PBMC within 2 h after donation.

3.3.8. In Vitro Cytokine Release

PBMC isolation and cytokine analysis were performed as described previously. Briefly, NANPs alone, NANPs after complexation with Lipofectamine 2000 or PAMAM dendrimers, and positive or negative controls were added to PBMC cultures, and the incubation continued overnight at 37 °C in an incubator with 5% CO_2. Complexation with Lipofectamine was done using the protocol described by us earlier. For

complexation with dendrimers, stocks of NANPs and dendrimers were incubated at room temperature for 30 min, then diluted in the complete cell culture medium (RPMI supplemented with 10% heat-inactivated FBS, 2 mM L-glutamine, 100 U/mL penicillin, and 100 µg/mL streptomycin). The final concentration of NANPs in the culture was 10 nM for all tested conditions (without a carrier, complexed with L2K, and complexed with dendrimers). After the incubation, the culture supernatants were collected and centrifuged at 18,000× g for 5 min. The supernatants were then analyzed by multiplex ELISA (Quansys Biosciences, Logan, UT, USA) to determine levels of individual cytokines.

3.3.9. Toll-Like Reporter Cell Lines

In adherence to InvivoGen™ protocols, HEK-Blue™ hTLR3, HEK-Blue™ hTLR7, HEK-Blue™ hTLR9, and HEK-Lucia™ RIG-I cell lines were maintained at 37°C with 5% CO°2. Following the manufacture's guidelines, the seeding process involved using a 96-well flat-bottom Greiner plate. Specifically, HEK-Blue™ hTLR3, HEK-Blue™ hTLR7, and HEK-Lucia™ RIG-I cells were seeded at approximately 50,000 cells per well, while HEK-Blue™ hTLR9 cells were seeded at approximately 80,000 cells per well. All cell lines underwent same-day transfection with the respective dendrimer generation carrier treatment for RNA cube or DNA cube and positive control. Positive controls for each cell line included Poly I:C (2 µg/mL), R848 (5 µg/mL), and RNA cube (10 nM). The RNA cube used as a positive control was pre-incubated with lipofectamine 2000 (L2K) for 30 min before transfection, as well as the dendrimer treatments and their respective RNA and DNA cubes. Post-transfection, cells with their respective treatments were incubated at 37 °C with 5% CO 2 for 24 h prior to SEAP, IRF activation, and viability testing. For HEK-Blue™ cells, a QUANTI-Blue™ assay was conducted in accordance with the protocols to assess the SEAP activation of the treatments. For HEK-Lucia™ cells, a QUANTI-Luc™ assay was performed to evaluate IRF activation. Assay results were analyzed using a Tecan Spark® plate reader at an absorbance of 638 nm. All samples were normalized to cells alone to assess the treatments of three biological (N=3) repeats in duplicate.

3.4. CONCLUSIONS

Throughout our investigation into the five different generations of amine-terminated PAMAM dendrimers in conjunction with DNA or RNA nanoparticles (NANPs), we gained valuable insights into structure-activity relationships and their influence on immune responses. Through our experiments with reporter cell lines and human peripheral blood mononuclear cells, we elucidated how dendrimer generation can impact the characterization profile of NANPs and vice versa. Interestingly, we observed variations in how the same dendrimer generation influenced different NANPs, as well as how the same NANP was perceived differently across various dendrimer generations. These findings underscore the complex interplay between dendrimer properties and NANP behavior, shedding light on critical factors influencing their efficacy and immunogenicity.

Our findings reveal an intriguing discrepancy with existing literature regarding the impact of dendrimers on cell viability when complexed with our nucleic acid nanoparticles (NANPs). Contrary to previous reports, we observed no significant decrease in cell viability in HEK-293FT cells, even with dendrimers of higher generations (6 and 7). This unexpected result suggests that the cytotoxic effects commonly associated with dendrimers may be mitigated when they are complexed with our NANPs. One plausible explanation for this phenomenon is the reduction in the cationic properties of dendrimers upon complexation with NANPs through electrostatic interactions. This reduction in charge may alleviate the cytotoxicity typically associated with dendrimers, highlighting the importance of considering nanoparticle characteristics in modulating their biological effects. Further investigation into the underlying mechanisms driving this observed phenomenon is warranted to fully understand the implications for nanoparticle-based therapeutics.

Sequences used in this work.

One strand per NANP was modified with an Alexa 488 label to assess uptake by fluorescence.

Six-stranded DNA cube:

5’- GGCAACTTTGATCCCTCGGTTTAGCGCCGGCCTTTTCTCCCACACTTTCACG

5’- GGGAAATTTCGTGGTAGGTTTTGTTGCCCGTGTTTCTACGATTACTTTGGTC

5’- GGACATTTTCGAGACAGCATTTTTTCCCGACCTTTGCGGATTGTATTTTAGG

5’- GGCGCTTTTGACCTTCTGCTTTATGTCCCCTATTTCTTAATGACTTTTGGCC

5’- GGGAGATTTAGTCATTAAGTTTTACAATCCGCTTTGTAATCGTAGTTTGTGT

5’- GGGATCTTTACCTACCACGTTTTGCTGTCTCGTTTGCAGAAGGTCTTTCCGA

Fluorescently labeled DNA cube strand:

5’- GGCGCTTTTGACCTTCTGCTTTATGTCCCCTATTTCTTAATGACTTTTGGCC/Alexa 488/

Six-stranded RNA cube:

5’- GGCAACUUUGAUCCCUCGGUUUAGCGCCGGCCUUUUCUCCCACACUUUCACG

5’- GGGAAAUUUCGUGGUAGGUUUUGUUGCCCGUGUUUCUACGAUUACUUUGGUC

5’- GGACAUUUUCGAGACAGCAUUUUUUCCCGACCUUUGCGGAUUGUAUUUUAGG

5’- GGCGCUUUUGACCUUCUGCUUUAUGUCCCCUAUUUCUUAAUGACUUUUGGCC

5’- GGGAGAUUUAGUCAUUAAGUUUUACAAUCCGCUUUGUAAUCGUAGUUUGUGU

5’- GGGAUCUUUACCUACCACGUUUUGCUGUCUCGUUUGCAGAAGGUCUUUCCGA

Fluorescently labeled RNA cube strand:

5’-GGCGCUUUUGACCUUCUGCUUUAUGUCCCCUAUUUCUUAAUGACUUUUGGCC/Alexa 488/

DNA duplex used in DNase protection assays:

5’- /5IABkFQ/TGACCCTGAAGTTCATCTGCACCACCGGTCACGGTCTCC

5’- GGAGACCGTGACCGGTGGTGCAGATGAACTTCAGGGTCATT/Alexa 488/

DNA duplex used in complexation to determine N/P ratio:

5'- CGGTGGTGCAGATGAACTTCAGGGTCA/3aLEXf488n/3'

5'- ACCCTGAAGTTCATCTGCACCACCG

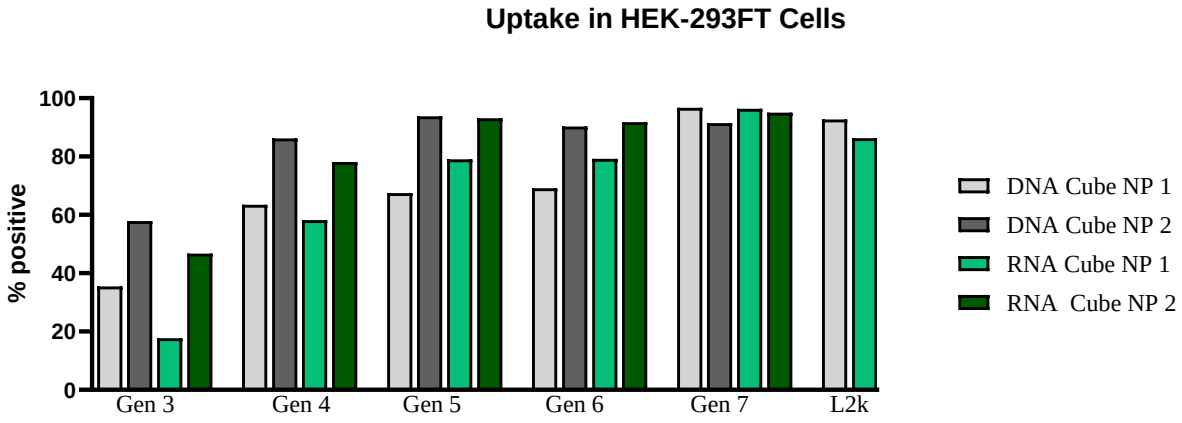

Figure 22 Uptake of DNA and RNA cubes complexed to dendrimers into HEK-293FT cells. Cubic NANPs were complexed to dendrimers at either an N/P of 1 or 2 and transfected into cells at a final NANP concentration of 20 nM for a period of 24 hours to coincide with the TLR investigation protocols.

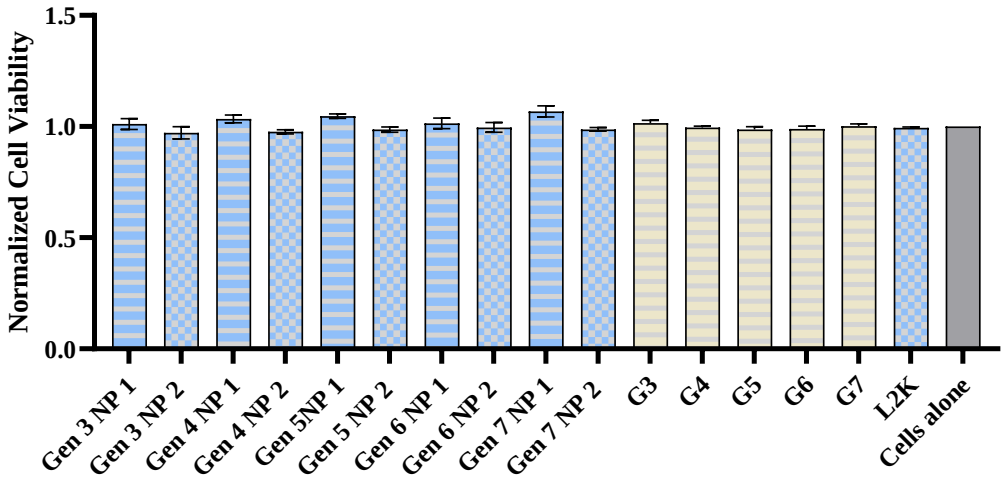

Figure 23. Cell viability of HEK-293FT cells. HEK-293FT cells were transfected with either DNA or RNA cube dendriplexes for a period of 24 hours at either an N/P of 1 or 2. Final NANP concentration was 20 nM.

.

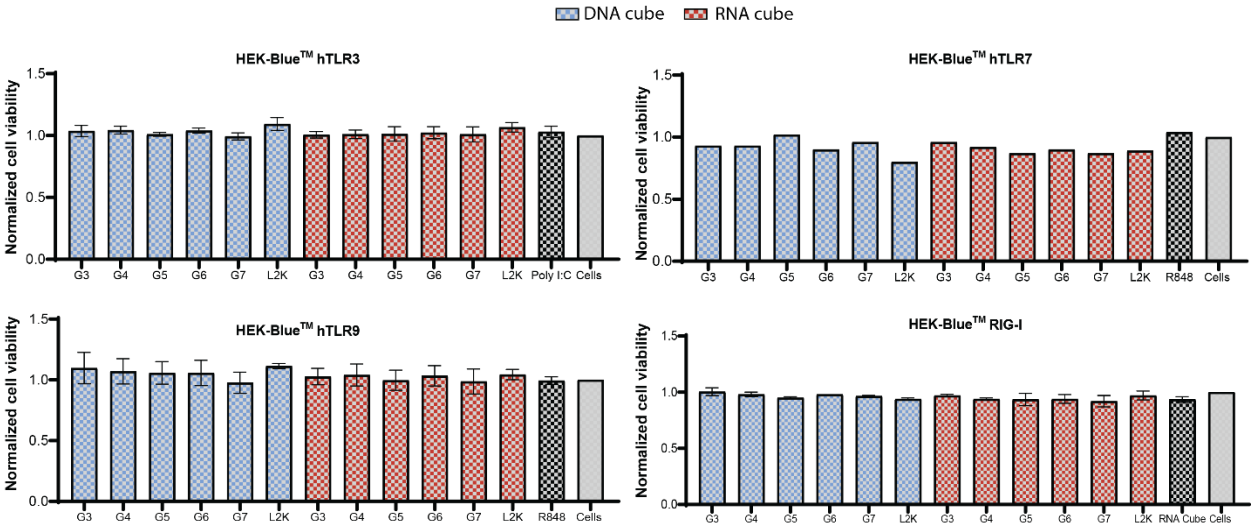

Figure 24. Cell viability of reporter cell lines: hTLR 3, hTLR 7, hTLR 9, and RIGI cells. Cells were transfected with either DNA or RNA cube dendriplexes for 24 hours and then tested for any impacts on cell viability. Transfections were completed at an N/P of 2 and for a period of 24 hours to coincide with QUANTI-Blue and QUANTI-Luc testing.

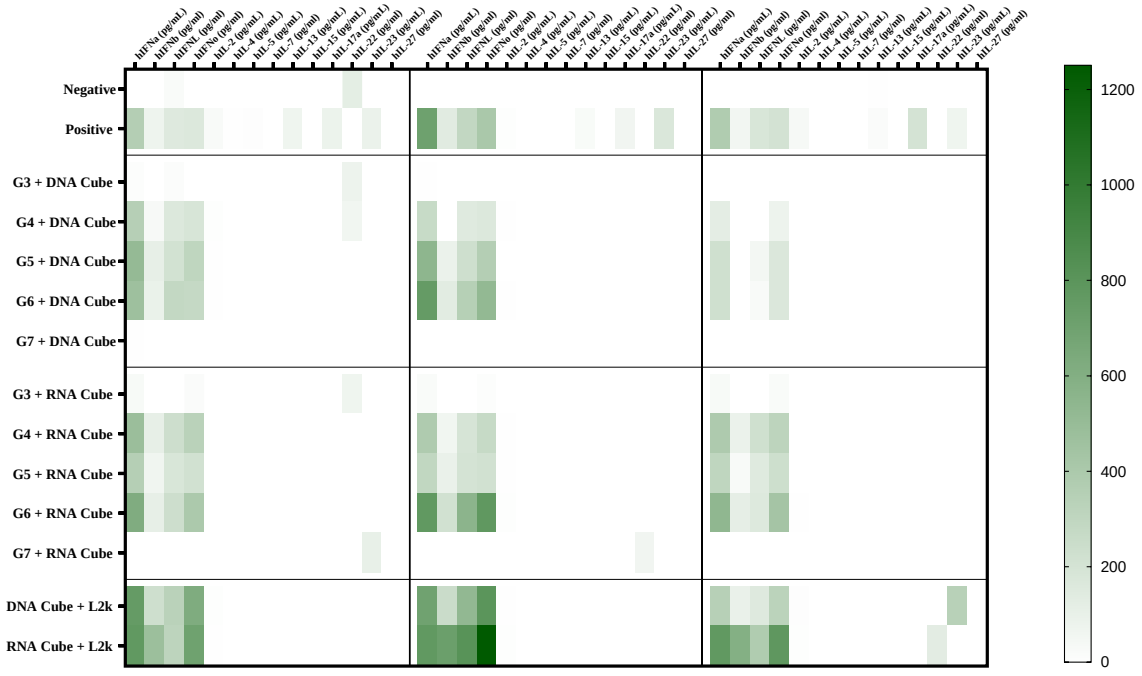

Figure 25. Cytokine induction by DNA and RNA cubes when complexed to dendrimers generations 3-7. PBMCs from three healthy human donor volunteers were treated with a negative and positive control, and RNA or DNA cube dendriplexes for 24 hours. Prior to the transfection, DNA and RNA cubes were complexed with lipofectamine 2000 (L2K), or amine-terminated PAMAM dendrimers. Supernatants were then analyzed for the presence of cytokines, chemokines, and interferons using multiplex ELISA assays.

4 CHAPTER 4: RECONFIGURABLE NUCLEIC ACID NANPARTICLES: ACTIVATED BY INTRACELLULAR BIOMARKERS FOR THE RELEASE OF THERAPEUTIC RNAI INDUCERS

4.1. INTRODUCTION

Limitations to Current Therapeutic Nucleic Acids. Therapeutic nucleic acids (TNAs) encompass a diverse array of functional biomolecules, including antisense oligonucleotides, RNAi inducers, aptamers, ribozymes, immunomodulatory oligonucleotides, mRNAs, and gene editing tools such as RNA guided CRISPR/Cas systems[16]. Despite their recent success, TNAs still encounter numerous challenges related to the shortage of suitable technologies for achieving target-specific delivery of personalized formulations while minimizing non-specific toxicity and off-target effects[42, 50, 139]. For RNAi therapies, such as siRNAs and miRNAs, these limitations primarily arise from their mechanism of action, which involves sequence-specific inhibition of gene expression. All existing RNAi therapeutics integrate the *diagnostic step*, wherein the RNA-induced silencing complex (RISC) loaded with exogenous RNAs binds to biomarker mRNA, with the *treatment step*, which involves silencing the function of the same mRNA. Although this approach is effective, with several FDA approvals[31-34], modularly separating the diagnostic and treatment steps would offer enhanced personalized therapeutic options and improve the safety profiles of TNAs.

Nucleic Acid Logic Systems. Certain diseases frequently stem from the dysregulation of gene expression or mutations[140-142]. The differentially expressed genes can serve as biomarkers, distinguishing corrupted cells from healthy tissues. Several design strategies were developed for nucleic acid nanodevices to recognize specific molecular inputs (*e.g.,* overexpressed mRNAs or miRNAs) and link them to the specific functional outputs[143-147]. However, these approaches rarely leverage the RNAi pathway for a therapeutic response. Previously, we developed and tested RNA logic gates exemplified by two-stranded RNA **recNANP**s tuned for conditional activation of RNAi in cancer cells[148]. These **recNANPs** were engineered to bind intracellular disease marker mRNAs, initiating conformational changes that lead to the release of shRNAs which upon dicing produced siRNAs and activated RNAi. While shown tfunctional in

the human cancer cells, the broader use of this approach was limited by poor modularity, a need for intense computational design, inability to release multiple siRNAs, and difficulties with scale-up production due to lengths and sequence limitations of RNA strands. Therefore, a modular, user-friendly platform is needed to establish a cost-efficient strategy adaptable to new biomarkers and multiple targets across various diseases.

Molecular Beacons for Diagnostics. A prominent illustration of conditional reporting for diseased biomarkers is molecular beacons (MBs) [149-153]. These probes (Fig 26a), crafted from short DNA oligos and their chemical analogs, possess the unique ability to detect and signal the presence of specific nucleic acid sequences that are the subject of investigation. MBs are designed in stem-loop structures with embedded fluorophore/quencher pairs that are separated once the MBs bind the target. This leads to heightened fluorescence, effectively reporting the disease. MBs play an essential role in medical diagnostics[154, 155]. This well-established technology has led to the development of hundreds of MBs targeting an array of biomarkers, **in vitro**. Thus, the versatility and specificity of validated MBs make them ideal candidates for incorporation into a diagnostic module of novel reconfigurable devices.

Split RNAi Inducers for Conditional Treatments. Building upon split-protein technology[156-158], we introduced a novel concept[159] that enabled the conditional activation of multiple functionalities within nucleic acid nanoparticles (NANPs) [76, 159-168]. This innovation relies on RNA/DNA hybrids that communicate with each other through sequence complementarity, triggering the activation of different functionalities both in vitro and in vivo[159]. The core idea involves splitting functional entities such as RNAi inducers, Förster resonance energy transfer (FRET) pair of dyes, and aptamers, into inactive RNA/DNA hybrids. These hybrids, equipped with complementary single-stranded toeholds, initiate re-association upon encountering their cognate partners, restoring the intended function *via* isothermal strand displacement (Fig 26b)[159, 169-173]. As a testament to the usability of our strategy, several teams have adapted and applied it in their research[167, 168, 174]. In this current work we implement the split-functionality NANPs as a treatment module in our devices.

Reconfigurable NANPs (recNANPs) with Biomarker-triggered Therapeutic Responses. Despite the existing assortment of NANPs and computational tools available for their design[95, 148, 175-180], it is important to note that most of them remain static in nature. They lack the capability to dynamically interact with biological systems and conditionally respond to intracellular environments. We introduce a system that melds together two well-established technologies within a single nanostructure: MBs as the diagnostic and split RNAi for treatment. The resulting recNANPs can dynamically respond to disease associated cellular environments and activate targeted TNAs through NOT logic (**Fig 26c**). The NOT gate implemented into the current recNANPs follows the truth table in which the release of TNAs is true only if the non-mutated gene is false. Thus, in the absence of a disease-associated trigger, the recNANPs remain inactive. However, recNANPs are equipped with sequence regions that can bind to the intracellular oncogene (*KRAS* G12D), inducing conformational changes that lead to the release of siRNAs against apoptosis inhibitor genes (**Fig 26d**). The G12D *KRAS* mutation is found in up to 35% of patients with pancreatic cancer[181], making it a valuable diagnostic marker tested in this work.

We demonstrate the design and production of recNANPs, along with the validation of their ability to intracellularly recognize prognostic cancer triggers and release RNAi inducers targeting apoptosis inhibitors. Our work highlights several innovative aspects of this technology. Firstly, we focus on the design, assembly, and efficient delivery of recNANPs using lipid carriers. This approach ensures effective transport of therapeutic payloads to target cells. Additionally, we emphasize specific RNAi activation based on pre-defined biomarkers, allowing for precise and tailored treatment strategies. Moreover, our study underscores the adaptability of recNANPs design, enabling simple replacement of therapeutic domains to address evolving therapeutic needs. Our findings contribute to advancing the field of RNAi therapies and nucleic acid technologies by offering a versatile and targeted approach for treating cancer and other diseases.

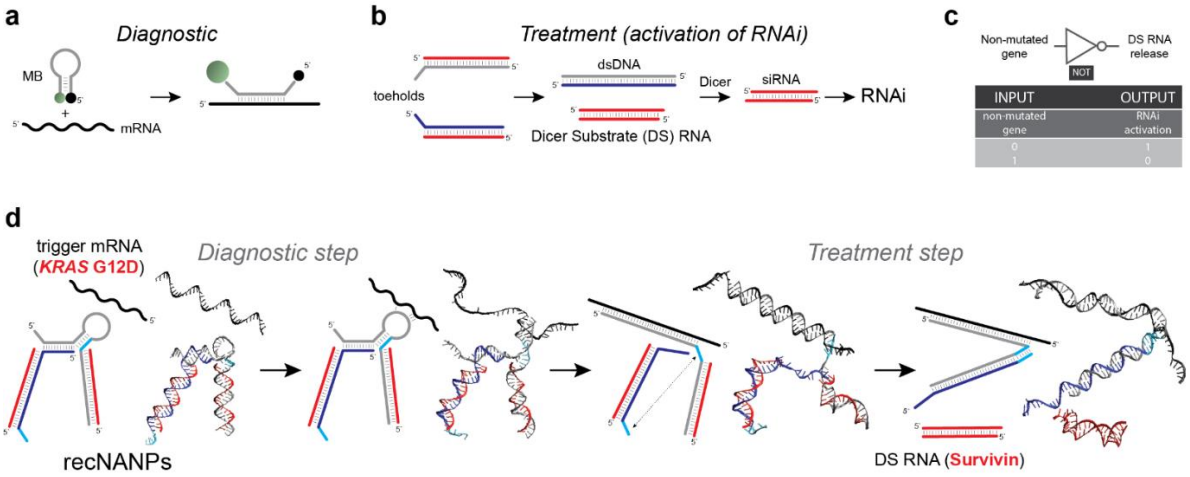

Figure 26. Modular four-stranded reconfigurable nucleic acid nanoparticles (recNANPs) for conditional activation of therapeutic RNAi responses upon interaction with a trigger mRNA. (a) Working principle of molecular beacons (MBs). (b) Working principles of split RNAi inducers. (c-d) Proposed design of recNANPs which act as a simple NOT logic gate (c) and allow for conditional activation of RNAi (d). In (d), 2D schematics and predicted 3D structures are shown for all constructs.

4.2. RESULTS AND DISCUSSION

Design and validation of recNANPs. For the *diagnostic step*, we selected MBs designed to exclusively recognize endogenous *KRAS* codon 12 mutation (GGT→GAT, G12D)[181-186]. The function of chosen MBs was validated in cells for specific detection of pancreatic cancer[187, 188]. For the *treatment* step, we have designed Dicer Substrate (DS) RNAs[189], using our established protocols[165], that upon intracellular dicing release siRNAs targeting Survivin. Survivin is a potent inhibitor of apoptosis present in 77% of pancreatic duct cell adenocarcinomas[190].

We have engineered and tested recNANPs assembled from four short, chemically synthesized oligos (**Fig 2a**), where DNA strand 2 incorporates the MB for G12D KRAS[187, 188] and is complementary to DS RNA sense (strand 1) sequence. We then elongated the sequence of the MB further at 5'-end to facilitate binding to DNA strand 3 which carries the complement for split DS RNA antisense (Strand 4). The interactions between complementary DNA toeholds highlighted in light blue, which are protected by the stem of inactive MB, are necessary for RNA-DNA hybrid re-association and DS RNA release after the diagnostic step is achieved. These toeholds become mutually accessible only upon complete binding and

opening of the MB on the target mRNA and this binding facilitates the release of DS RNA (duplex 1-4) through isothermal reassociation of separated RNA/DNA duplexes 1-2 and 3-4 (**Fig 26d**).

To optimize the assembly conditions of recNANPs, we explored various annealing protocols (**Fig. S29**), subsequently confirmed through electrophoretic mobility shift assays (EMSA). The stepwise assembly process involved the initial formation of duplexes 1+2 and 3+4, followed by their incubation at 16°C, which was found to be optimal due to the minimal presence of partial assemblies and unbound monomers compared to other conditions tested. Interestingly, recNANPs exhibited the potential to assemble even at lower temperatures (4°C to 12°C) immediately after combining the duplexes. Moreover, a significant proportion of recNANPs were still formed at higher temperatures (37°C and 45°C), indicating the potential for structural integrity even under conditions relevant to cellular delivery.

Cold chain storage is essential for maintaining the potency of therapeutic nucleic acids, which significantly increases transportation and handling costs. Previous studies have tested storage conditions for NANPs at various temperatures to identify the optimal protocol for preparing the materials and determining their structural stability over time[6, 191]. Additionally, we investigated the integrity of recNANPs structures after dehydration, storage at different temperatures, and subsequent rehydration (**SI Fig. 30**). For dehydration, we employed a straightforward protocol using SpeedVac, which centrifuges recNANPs while exposing them to heat and infrared radiation. Unfortunately, assembled recNANPs could not withstand drying and rehydration, leading to degradation and the formation of multiple nonspecific structures regardless of the conditions used to store the dried pellets (**Fig. S30E-F**). However, when maintained in solution, recNANPs demonstrated stability for up to nearly 72 hours at 4°C and room temperature (**SI Fig. S2G-H**). Meanwhile, the duplexes themselves exhibited stability after drying and storing for up to 72 hours at 4°C and 50°C, facilitating a clean assembly of recNANPs (**Fig. S30A-B**). Furthermore, duplexes in solution stored at RT or 50°C for similar time points displayed the same stability as dried duplexes (**Fig. 302C-D**). Therefore, long-term storage of recNANPs can be accomplished in the form of dehydrated duplexes. Upon rehydration, these duplexes can be mixed and

incubated to yield functional recNANPs. This approach ensures structural integrity and functional efficacy of recNANPs over extended periods, offering a practical solution for storage and subsequent use as therapies.

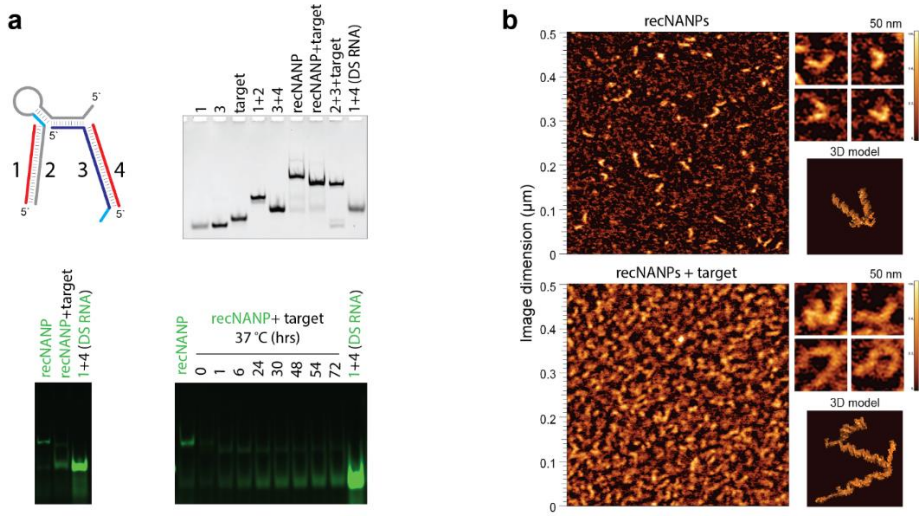

Figure 27. In vitro characterization of recNANPs. (a) Schematic of recNANPs and native-PAGE (with EtBr staining or Alexa 488 labeled recNANPs) for assessment of assembly and working principles of recNANPs. (b) Atomic force microscopy (AFM) of recNANPs and recNANPs incubated with target sequence, showing the morphology changes for inactive and activated state.

The activation of recNANPs upon interaction with mRNA fragments ("target") and release of DS RNAs was analyzed using EMSA and AFM (**Fig 27**). On the EMSA, the release of DS RNA and the formation of 2+3+target byproducts are clearly observed via disappearance of recNANPs and appearance of DS RNA bands. The AFM was employed to examine the structures of the recNANPs before and after activation with target strand, as shown in **Fig 27b**. When observed with AFM, the recNANPs alone displayed a uniform morphology, which was altered upon the introduction of the target. The distribution of morphologies encompassed DS RNAs and 2+3+target byproducts (corresponding representative 3D models shown).

Cellular Uptake, Specificity in Activation, and Silencing Activity. Two different cell lines were selected to assess the sequence-specific activation of recNANPs. PANC-1 cells, which carry the G12D KRAS mutation, were chosen as our target, and HEK-293FT cells were selected as the wild-type (WT) KRAS control cell line[181-186]. Lipofectamine 2000 served as the carrier in all studies. For cell investigations,

uptake of recNANPs conjugated with Alexa 488 (to strand 1) was confirmed *via* fluorescent microscopy (**Fig 29a-b**). The relative expression of Survivin in both cell lines was demonstrated to be comparable (**Fig 29c** and **Fig 30**). Western blots were used to evaluate specificity, release, and efficacy of recNANPs in delivering DS RNA (Survivin) versus DS RNA (Survivin) alone. In PANC-1 cells after 72 hours, at concentrations of 25 and 50 nM, the expression of Survivin was significantly decreased when treated with both the DS RNAs and recNANPs, indicating that the recNANPs are equally effective as DS RNAs in downregulating Survivin through the RNAi pathway (**Fig 28d**). Notably, we attempted to mimic kidneys function by replacing media with fresh one during incubation period which resulted in effect on Survivin observed. Thus, recNANPs showed long lasting effect in downregulating Survivin in PANC-1. Cell viability remained unaffected post-treatment (**Fig 32**). Conversely, when HEK-293FT cells were treated with the same concentrations of recNANPs and DS RNAs, only the DS RNA exhibited a notable effect on Survivin expression, suggesting that the recNANPs remain inactive in WT *KRAS* cells and demonstrated the specificity of the recNANPs (**Fig 28d** and **Fig 33**). Interestingly, recNANPs needed around 5 to 7.5nM for complete silencing of Survivin in the situation of no media changed or kidney failure without significantly affecting normal cells, HEK-293FT **(Fig 33)**.

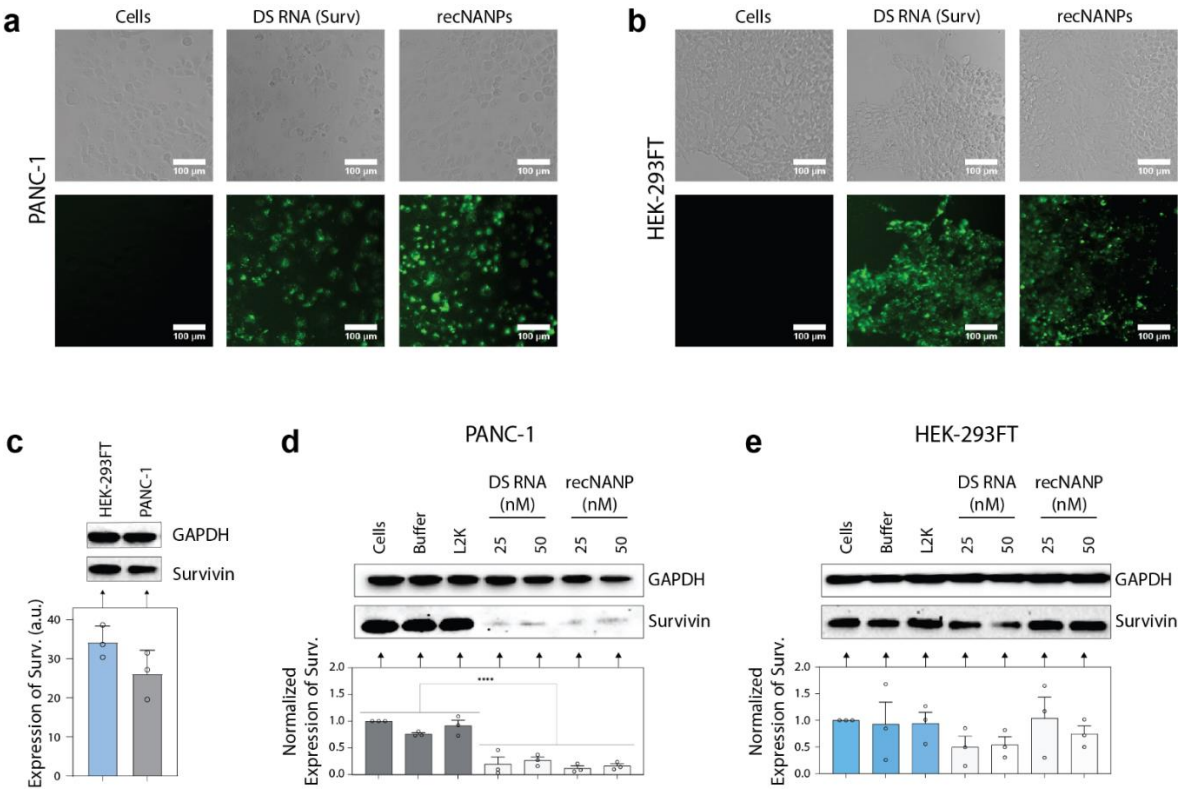

Figure 28. Cellular and specificity in activation of recNANPs. (a-b) Microscopy of uptake in PANC-1 and HEK-293FT cells of labeled DS RNAs and recNANPs after 72 hours of incubation. (c) Relative expression of Survivin in PANC-1 and HEK-293FT cells. Expression of Survivin in (d) PANC-1 and (e) HEK-293FT cells after treatment with DS RNA and recNANPs with media replaced after 24 hours for total of 72 hours incubation, analyzed by western blots. Representative immunoblots demonstrate changes in expressions of Survivin at the predicted size of 16.5 kDa (SI Fig. S4-S5). Each bar represents the mean of N=3 biological repeats ± SEM. Asterisks indicate statistical significance (one-ways ANOVA, $p<0.0001$).

4.3. METHODS

4.3.1. Purification of DNA and RNA monomers:

DNA and RNA strands were purchased from Integrated DNA Technologies, Inc. Each strand was purified through denaturing polyacrylamide gel electrophoresis (PAGE, 8%), in the presence of 8 M urea, 89 mM tris-borate, 2 mM EDTA. Bands were then visualized using UV shadowing, extracted, and eluted out into 300 mM NaCl, 89 mM tris-borate, and 2 mM EDTA overnight at 4 °C. The following day, the samples were mixed with 2× volumes of 100% ethanol and chilled to -20 °C for a minimum of 3 h. The samples were then spun at 14,000g for 30 min and supernatant was disposed. An additional washing was done by adding 90% ethanol, centrifuging at 14 000g, and discarding the supernatant. Finally, the samples were

processed using SpeedVac to evaporate any remaining ethanol. Then, the strands were redispersed in endotoxin-free water, and the concentrations were measured using a NanoDrop 2000.

4.3.2. Synthesis of recNANPs:

The synthesis of the recNANPs nanoparticle is a two-step process wherein strands 1+2 and 3+4 is assembled separately as intermediates, which are then combined in an incubation step. For step one of the assemblies, each intermediate is combined in equimolar ratios in assembly buffer (89 mM tris-borate, 2 mM $MgCl_2$, 50 mM KCl), heated to 95 °C for 2 min, and then incubated at RT for 20 min. Step two requires an equimolar combination of intermediates 1+2 and 3+4 at 16 °C for 10 minutes. To confirm the assembly of all structures, they were run in a non-denaturing native-PAGE (8%, 37.5:1) in 89 mM tris-borate (pH 8.2), 2 mM $MgCl_2$ at 4 °C followed by ethidium bromide total staining and visualization on a ChemiDoc MP Imaging System.

4.3.3. Triggering activation of the recNANPs to release dsRNA using a target monomer:

Once verification of the recNANPs assembly was completed, a mock target sequence monomer was introduced at a 1:1 ratio of recNANPs:monomer to induce the conformational change and release of the DS RNA. Once the two samples were mixed, they were incubated for 72 hours at 37 °C and aliquots were taken at different timepoints, quickly frozen on dry ice for storage, and then run on a native-PAGE to investigate at what point the DS RNA is released.

4.3.4. Physicochemical characterization of recNANPs:

Atomic force microscopy (AFM) was utilized to investigate the morphology of the recNANPs. Mica, which had been freshly cleaved, was treated with 1-(2-aminopropyl) silatrane (APS) according to established protocols, and AFM was then conducted as described in previous papers.

4.3.5. Molecular dynamic simulations:

Discovery Studio Visualizer built the initial structures of each step of the recNANPs and its activation. Two Amber force fields, DNA.OL15[192] and RNA.OL3[193], were used to simulate DNA and RNA strands, respectively. Energy minimization was applied to repair atomic crashes in the initial structures of each

step. In each TMD simulation, two nucleotides in a base pair in the starting conformation were dissociated and were re-paired with target nucleotides. To complete the branch migration in the recognition step, 42 consecutive TMD simulations were applied while the siRNA release process in the therapeutic step were performed by 37 consecutive TMD simulations. Each TMD simulation was conducted by 3000 steps with 2 fs timestep. The force constant in the TMD simulations was adjusted between 2.0 kcal/molÅ and 20.0 kcal/molÅ. Both energy minimization and TMD simulations were performed by Amber simulation package[194].

4.3.6. Cellular uptake of recNANPs:

Strand 1 of the recNANPs was labeled with Al488 for these studies, and microscopy was used to visualize the uptake of the Al488-labeled recNANPs into PANC-1 and HEK-293FT. Each of the cell lines were seeded at a density of 40,000 cells per well in a 24-well plate containing 200 µL of media and was further maintained for 24 hours at 37°C with 5% CO_2 in a humidified incubator. Sample preparation of the recNANPs and DS RNA plus Lipofectamine 2000 included a 30-minute incubation time at room temperature before transfection. Sample preparation of the recNANPs and DS RNA plus DOTAP was done following the manufacturer's guidelines and using a 1:10 w/w ratio and a 30 minutes incubation period at room temperature. After the incubation periods, sample volumes were brought up to 50 µL and were then transfected into the cells. The cells were treated with either DS RNA, recNANPs, Lipofectamine 2000, or DOTAP alone as controls and incubated for 48 hours at 37 °C with 5% CO_2. Afterward, the cells were washed with phosphate buffered saline (1X PBS, pH 7.4) and visualized to assess the presence of the Al488 fluorophore-labeled recNANPs or DS RNA using the EVOS FL system and a GFP Light Cube.

4.3.7. Specific gene silencing of Survivin:

PANC-1 and HEK-293FT cells were cultured in 24-well plates at a seeding density of 40,000 cells per well and maintained for 24 hours at 37° C and 5% CO_2. After 24 hours, the cells were transfected with either DS RNA or recNANPs at 25 and 50 nM concentrations using either Lipofectamine 2000 or DOTAP

as the transfection agent. They were left to incubate in a humidified incubator for 72 hours at 37 °C and 5% CO_2 with media changed following first 24 hours after treatments added. Once the incubation period ended, the cells were washed using 1X PBS and detached using 0.25% trypsin-EDTA. The cells were spun down at 500g for 5 minutes, washed once with PBS, and lysed by using Triton lysis buffer (50 mM Tris-pH 8.0, 150 mM NaCl, and 1% TX-100). The cell lysates were then tested for protein concentration using a BCA assay and evaluated for expression of Survivin by western blot analysis. Samples were electrophoresed using Bio-Rad and transferred onto membranes. The membranes were blocked with 5% mild for 1 hour and then incubated overnight at 4 °C with primary antibodies for Survivin (Abcam, Cat # EPY2880Y, kDA of 16.5) and the housekeeping gene, Glyceraldehyde-2-phosphate dehydrogenase (GAPDH) (Santa Cruz, Cat # sc-47724, kDA of 37).

The blots were then washed and incubated in the presence of HRP-conjugated secondary anti-rabbit, and anti-mouse antibodies (Cells signaling, Cat# 7074P2), respectively. Bound enzymes were detected using a Western Pico ECL kit and the Bio-Rad Chemi-Doc imaging system. Western blots were quantified using the ImageLab software (Bio-Rad).

Similarly, without media change, PANC-1 cells, after 24 hours of plating were treated with 2.5 to 7.5 nM DS RNA or recNANPs. Proteins were extracted and western blot was performed according to protocol listed above.

4.3.8. PANC-1 and HEK-293FT cell Maintenance:

Cells were maintained in Dulbecco's modified Eagle's medium, supplemented with 5% heat-inactivated FBS and penicillin/streptomycin (100 U/ml-100 µg/ml).

4.4. CONCLUSION

The need for more precise and effective therapeutics is paramount for patients dealing with resistive cancers, and conditionally activated nanoparticles are a step in the right direction in limiting off-target effects. Our construct can release its therapeutic moiety in the specifically targeted cells that are in a

diseased state by using a molecular beacon that is complementary to the mutated KRAS oncogene in pancreatic cancer.

We demonstrated that our recNANPs are efficient in down regulating Survivin. With much smaller concentration, our recNANPs can significantly affect protein expression of Survivin. Furthermore, when used in combination with the current therapeutic option for pancreatic cancer, gemcitabine, cell viability was impacted more than when gemcitabine was used alone. We have also shown the recNANPs construct is robust and modular by having control over the therapeutic moieties that are released upon activation.

This system is simple, modular, and can be customized with different triggers, targets, and therapeutic moieties. As such, it makes the recNANPs a viable therapeutic candidate for diseased cells that are not limited to cancer cells, or in the regulation of only one therapeutic target. For example, the extensions on the molecular beacon could be further extended to hold multiple DS RNAs that each target a different cellular mechanism that can aid in the fight against the targeted disease.

Author Contributions

Y.I.A., A.H., M.C., conducted experiments and analyzed data. K.A.A. and M.A.D. designed and supervised the study and analyzed data. All authors discussed the progress of research, interpreted data, and wrote the manuscript.

Sequences used in this work:

recNANPs activated by KRAS, against Survivin

Strand 1:

5’pGGACCACCGCAUCUCUACAUUCAAG

Strand 2:

5’TATCGTCAAGGCACTCTTGCCTACGCCATCAGCTCCGTAGGCTTGAATGTAGAGATGCGGT GGTCC

Strand 3:

5’CAAGAGTGCCTTAAGGACCACCGCATCTCTACATTCAAGCCTAC

Strand 4:

5’CUUGAAUGUAGAGAUGCGGUGGUCCUU

DS RNA against Survivin

Sense (Strand 1):

5’ pGGACCACCGCAUCUCUACAUUCAAG

Antisense (Strand 4):

5’CUUGAAUGUAGAGAUGCGGUGGUCCUU

Alexa488 labeled sense (Al488 Strand 1):

5’GGACCACCGCAUCUCUACAUUCAAG/3AlexF488N/

recNANPs activated by KRAS, against BCL2

Strand 1:

5’pGUACAUCCAUUAUAAGCUGUCGCAG

Strand 2:

5’TATCGTCAAGGCACTCTTGCCTACGCCATCAGCTCCGTAGGTTCTGCGACAGCTTATAATG

GATGTAC

Strand 3:

5’CAAGAGTGCCTTAAGTACATCCATTATAAGCTGTCGCAGCCTAC

Strand 4:

5’CUGCGACAGCUUAUAAUGGAUGUACUU

DS RNA against BCL2

Sense (Strand 1):

5’pGUACAUCCAUUAUAAGCUGUCGCAG

Antisense (Strand 4):

5’CUGCGACAGCUUAUAAUGGAUGUACUU

SUPPORTING FIGURES

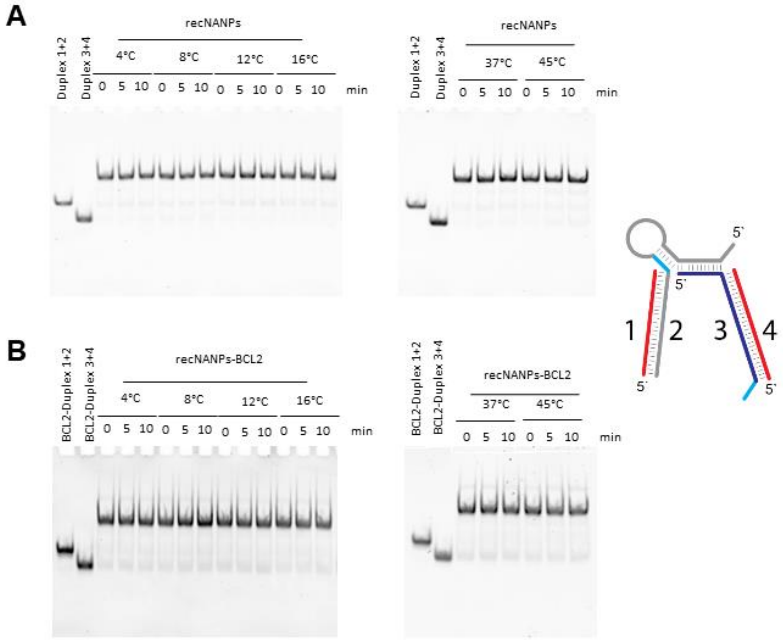

Figure 29. Assembly conditions of recNANPs. (A) recNANPs (Surv) and (B) recNANPs (BCL2) at 4-8-12-16-37 and 45°C from 0 to 10 minutes Figure S2. Relative stability of recNANPs when stored at 4°C, room temperature (RT), and 50°C for durations ranging from 24 to 72 hours, using native PAGE (8%). (A and B) The stability of speed-vac-dried recNANPs and duplexes were investigated when stored at 4°C and 50°C, with the recNANPs assembled using dried duplexes stored from 24 to 72 hours. (C and D) Similarly, duplexes in solution were examined when stored at RT and 50°C, with recNANPs assembled using these stored duplexes from each time points. (E and F) Dried assembled recNANPs was evaluated when stored at 4°C and 50°C from 24 to 72 hours, as well as the stability of recNANPs in solution stored at 4°C, RT, and 50°C at corresponding time points (G and H).

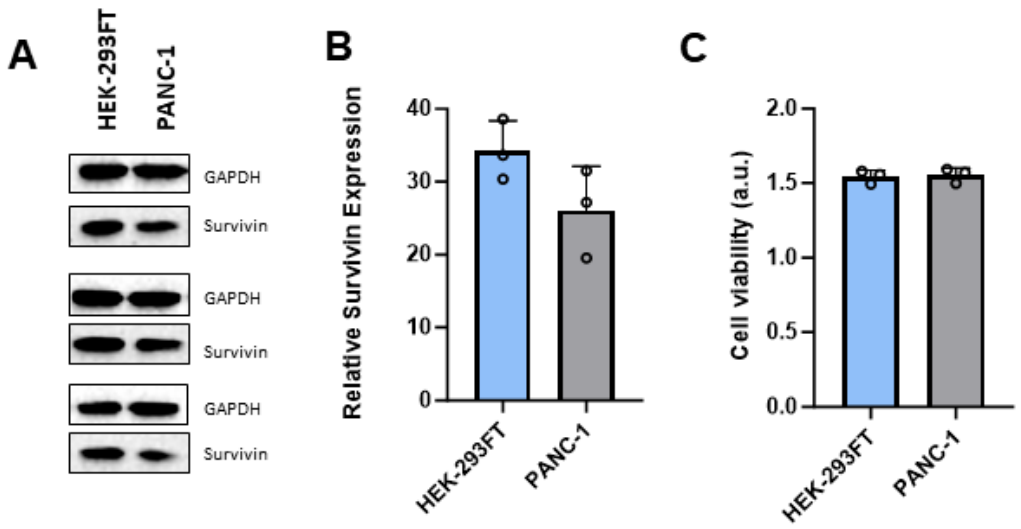

Figure 30. Relative expression of Survivin in HEK-293FT and PANC-1 and relative cell viability. A) Western blat analysis of Surv expression in HEK-293FT and PANC-1 cells. B) Expression quantification of Surv in HEK-293FT and PANC-1 cells. C) Cell viability in each cell line. Data presented as mean ± SEM (N=3).

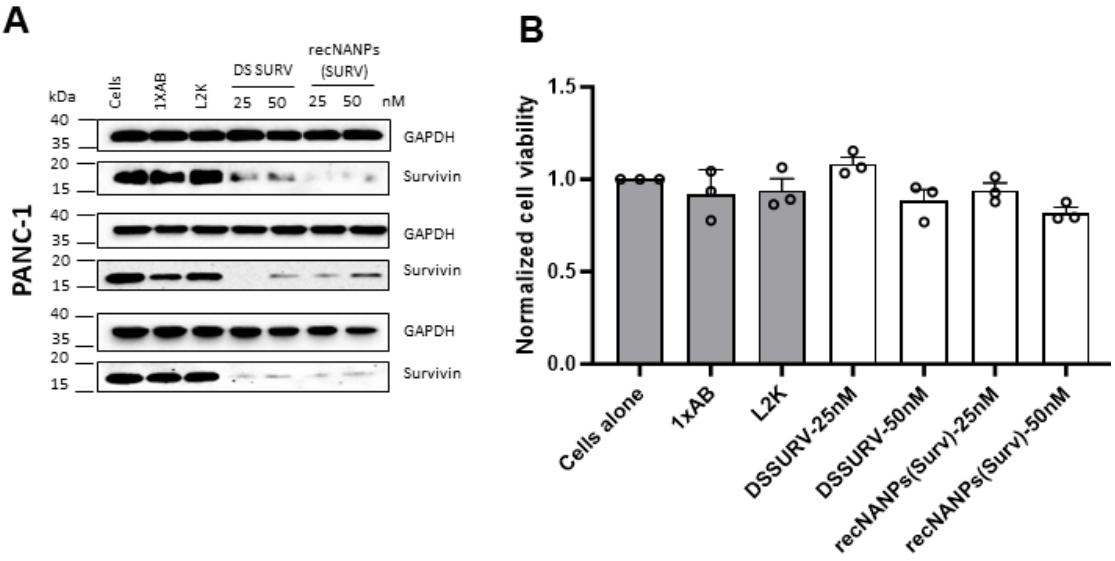

Figure 31. Detection of Survivin expression in PANC-1 cells and cell viability under treatment with 25 and 50nM DS RNAs or recNANPs with media changed 24 hours after transfection and total incubation of 72 Hours. (A) Immunoblotting for detection of Survivin in PANC-1 cells. (B) Correlation of cell viability to each treatment in PANC-1 cells. Data presented as Mean ± SEM (N=3).

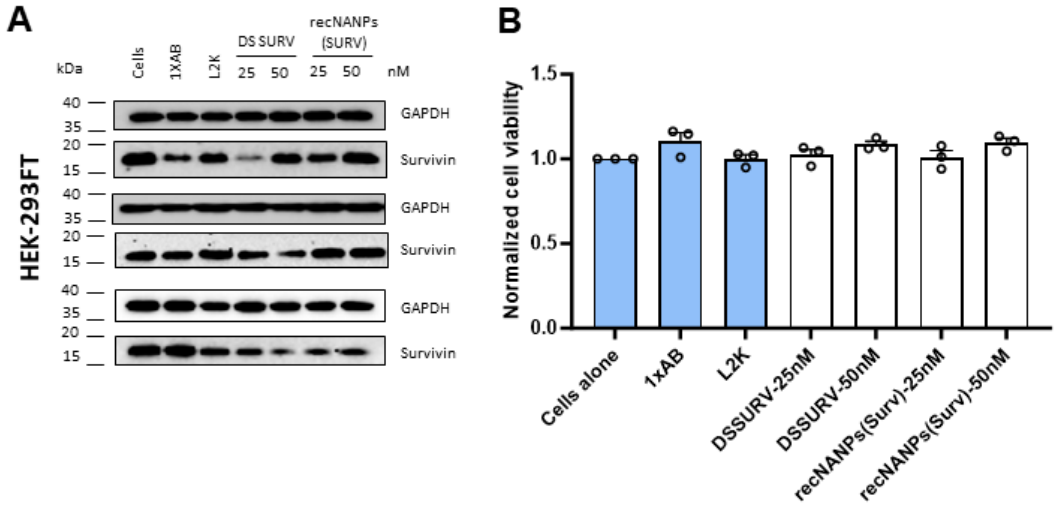

Figure 32. Detection of Survivin expression in HEK-3293FT cells and cell viability under treatment with 25 and 50nM DS RNAs or recNANPs with media changed 24 hours after transfection and total incubation of 72 Hours. (A) Immunoblotting for detection of Survivin in HEK-3293FT cells. (B) Correlation of cell viability to each treatment in HEK-3293FT cells. Data presented as Mean ± SEM (N=3).

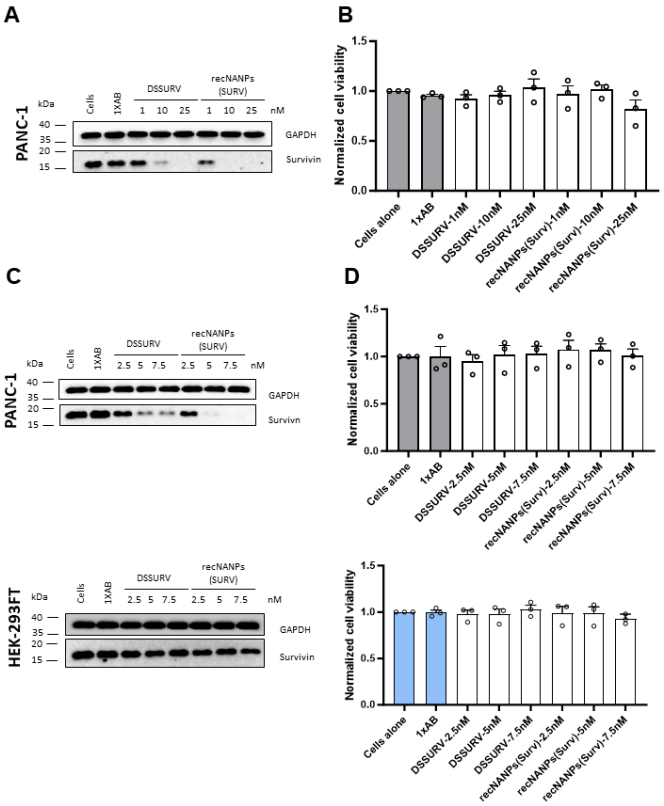

Figure 33. Detection of Survivin expression in PANC-1 and HEK-293FT cells and cell viability under different concentrations of DS RNAs and recNANPs after 48 hours incubation. (A-B) Immunoblotting for detection of Survivin in PANC-1 cells from 1 to 25nM with cells viability under same treatments. (C-D) Immunoblotting of PANC-1 and HEK-293FT with their viability when treated at 2.5 to 7.5nM for 48 hours. Data presented as Mean ± SEM (N=3).

5 CHAPTER 5: CONCLUSIONS

The work presented in this thesis is centered on advancing our understanding of the influence of carriers on biological responses to nucleic acid nanoparticles. Additionally, the thesis incorporates the use of conditional activation mechanisms within the design of nucleic acid nanoparticles to produce a dynamic therapeutic platform. Both pursuits are aimed at enhancing specificity and elucidating the biological behavior of these nanoparticles. As outlined in the introduction, the thesis addresses several key challenges in nucleic acid nanotechnology, including delivery, immune response, and specificity. Through systematic investigation and innovative approaches, this work contributes to overcoming these hurdles and advancing the field of nucleic acid-based therapeutics.

FUTURE PROSPECTS

By employing advanced techniques such as organoids and three-dimensional cell culturing, researchers can recreate physiological conditions more closely resembling human tissues, enhancing the predictive value of preclinical studies. Additionally, recreating tumor microenvironments through co-culturing techniques allows for the study of interactions between different cell populations, providing valuable insights into the efficacy and safety of therapeutic interventions. Researchers would be able to investigate whether nanoformulations exhibit uptake preferences for specific cell types over others and assess the differential impact of these formulations on various cell types. This exploration could provide valuable insights into the cellular targeting capabilities of the nanoformulations and their potential implications for therapeutic efficacy and safety. By elucidating how different cell types interact with and respond to nanoformulations, researchers can optimize the design and formulation of nanotherapeutics to enhance their specificity, efficacy, and biocompatibility for targeted disease treatment. Overall, these advancements in model systems contribute to more informed decision-making during the translational process, ultimately increasing the likelihood of successful clinical translation of nanotherapeutic platforms. The advancement of nanomedicine has opened avenues for engineering biological systems at the molecular level, allowing for the design of systems capable of orchestrating protein synthesis and

regulation. By exerting control over these molecular processes, researchers aim to manipulate cellular pathways, regulate phenotypes, and influence cell-to-cell communications[195]. This precise control holds promise for the development of targeted therapies, which are increasingly recognized as essential for mitigating off-target effects and associated toxicities of novel formulations.

Furthermore, incorporation of conditionally activated materials to increase precision and reduce off-target effects by enabling localization to the site of disease. Conditionally activated nanomaterials have been a lucrative goal in nanotechnology for therapeutics. Wherein the ability to control whether a therapeutic particle releases its treatment is dependent on the presence of the intended target to trigger activation of the particle. A few examples of activation triggers may include pH activation, temperature activation, or activation in response to the presence of proteins[196-198], RNA[147, 199], small molecules-riboswitches-[200], or different wavelengths of light[201, 202]. Only upon association with the trigger, or activation conditions, would the nanomaterial activate. Nanomaterials that respond to biological and chemical stimuli associated with pathogenic states have a sophisticated method that results in more precise treatment options.

For example, some pathological triggers or markers can lead to a conditioned and deliberate response wherein the triggers can be viral antigens or oncogenic factors resulting in specificity and sensitivity of detection and treatment of the pathogenic diseases and malfunctioning cells[203]. The nanomaterials could integrate the release of therapeutics targeting several essential genes to trigger cell death, or activation of a cell mechanism that calls the immune system for help.

Nanobiotechnologies play a pivotal role in this endeavor by harnessing the intricate mechanisms of biological systems. By leveraging the versatility and specificity of biological components, such as nucleic acids and proteins, nanobiotechnologies enable the creation of more efficient therapeutic designs. Through innovative approaches that capitalize on the inherent properties of biological systems, researchers strive to achieve enhanced precision and efficacy in therapeutic interventions.

As the field of nanomedicine continues to evolve, the integration of biological principles with engineering concepts offers unprecedented opportunities for the development of personalized and targeted treatments. By unlocking the potential of molecular-level manipulation, researchers aim to revolutionize healthcare and address unmet medical needs with greater precision and effectiveness.

This dissertation encompassed a comprehensive evaluation of the interaction between amine-terminated PAMAM dendrimers and cubic NANPs, shedding light on the dynamics governing their immune recognition and response. The work in this dissertation aimed to elucidate how different generations of dendrimers affect the immune profile elicited by NANPs, thereby contributing to the broader understanding of nanoparticle-based therapeutics. Further mechanistic studies will need to be conducted to uncover the mechanisms involved in cellular uptake to reveal how the dendriplexes are avoiding detection from the reporter cell lines. It must first be determined whether the dendriplexes are in the endosomes. Then, investigations into whether the dendrimers are hindering recognition from TLRs of the NANPs are occurring. It appears, from the data presented within this thesis, that generations 3 and 7 of the dendrimers have the highest impact on immune recognition in PBMCs. As such, it would be relevant to explore the binding affinity and strength that each dendrimer generation has with the NANPs, and whether this is impacting the release of the NANPs from the delivery vehicle. Also, the impact that the charge ratio (N/P) has on the uptake efficiency and immune recognition should be considered and explored as well to test whether this will affect how and if the dendrimers will release the NANPs after being complexed at weaker or stronger ratios.

Furthermore, this dissertation offered novel insights into a reconfigurable nucleic acid nanoparticle, uniquely designed to be conditionally activated upon detection of a specific disease biomarker. This innovative approach represents a significant advancement in the field of nucleic acid-based therapeutics, offering a tailored and precise method for targeting diseased cells while minimizing off-target effects. Through meticulous experimentation and characterization, the dissertation illuminated the abilities of the conditionally activated recNANPs. To expand on this work, different molecular beacons could be

incorporated into the recNANP design to target different disease models. The recNANPs could also be redesigned to carry multiple dicer substrate RNAs, each targeting a key protein associated with a diseased state mechanism. As such, multiple dicer substrates would result in multiple pathways being manipulated upon the binding of the molecular beacon to its target. To improve on the validity of the recNANPs efficiency and robustness, a true wild-type pancreatic cell line could be used as a negative control along with the HEK-293FT cells to get a more accurate understanding of the recNANP's capabilities of activation. Furthermore, the lengths of the resulting antisense oligonucleotide between the molecular beacon and its target can be investigated to ensure incorporation of RNAse H to result in degradation of the disease marker target. By leveraging these design principles, their application can aid in the enhancement of precision medicine and targeted delivery strategies, ultimately advancing the field of nanomedicine and nucleic acid nanotechnologies.

REFERENCES

1. Afonin KA, Dobrovolskaia MA, Church G, Bathe M. Opportunities, Barriers, and a Strategy for Overcoming Translational Challenges to Therapeutic Nucleic Acid Nanotechnology. ACS Nano. 2020;14(8):9221-7. Epub 20200724. doi: 10.1021/acsnano.0c04753. PubMed PMID: 32706238; PMCID: PMC7731581.
2. Shu Y, Pi F, Sharma A, Rajabi M, Haque F, Shu D, Leggas M, Evers BM, Guo P. Stable RNA nanoparticles as potential new generation drugs for cancer therapy. Adv Drug Deliv Rev. 2014;66:74-89. Epub 20131122. doi: 10.1016/j.addr.2013.11.006. PubMed PMID: 24270010; PMCID: PMC3955949.
3. Li X, Bhullar AS, Binzel DW, Guo P. The dynamic, motile and deformative properties of RNA nanoparticles facilitate the third milestone of drug development. Adv Drug Deliv Rev. 2022;186:114316. Epub 20220505. doi: 10.1016/j.addr.2022.114316. PubMed PMID: 35526663; PMCID: PMC9257724.
4. Jasinski D, Haque F, Binzel DW, Guo P. Advancement of the Emerging Field of RNA Nanotechnology. ACS nano. 2017;11(2):1142-64. doi: 10.1021/acsnano.6b05737. PubMed PMID: PMC5333189.
5. Brumett R, Danai L, Coffman A, Radwan Y, Teter M, Hayth H, Doe E, Pranger K, Thornburgh S, Dittmer A, Li Z, Kim TJ, Afonin KA, Khisamutdinov EF. Design and Characterization of Compact, Programmable, Multistranded Nonimmunostimulatory Nucleic Acid Nanoparticles Suitable for Biomedical Applications. Biochemistry. 2024;63(3):312-25. Epub 20240125. doi: 10.1021/acs.biochem.3c00615. PubMed PMID: 38271599.
6. Beasock D, Ha A, Halman J, Panigaj M, Wang J, Dokholyan NV, Afonin KA. Break to Build: Isothermal Assembly of Nucleic Acid Nanoparticles (NANPs) via Enzymatic Degradation. Bioconjug Chem. 2023;34(6):1139-46. Epub 20230609. doi: 10.1021/acs.bioconjchem.3c00167. PubMed PMID: 37293781; PMCID: PMC10288440.
7. Panigaj M, Skelly E, Beasock D, Marriott I, Johnson MB, Salotti J, Afonin KA. Therapeutic immunomodulation by rationally designed nucleic acids and nucleic acid nanoparticles. Front Immunol. 2023;14:1053550. Epub 20230131. doi: 10.3389/fimmu.2023.1053550. PubMed PMID: 36798121; PMCID: PMC9927404.
8. Chandler M, Minevich B, Roark B, Viard M, Johnson MB, Rizvi MH, Deaton TA, Kozlov S, Panigaj M, Tracy JB, Yingling YG, Gang O, Afonin KA. Controlled Organization of Inorganic Materials Using Biological Molecules for Activating Therapeutic Functionalities. ACS Appl Mater Interfaces. 2021;13(33):39030-41. Epub 20210817. doi: 10.1021/acsami.1c09230. PubMed PMID: 34402305; PMCID: PMC8654604.
9. Jing Z, Du Q, Zhang X, Zhang Y. Nanomedicines and nanomaterials for cancer therapy: Progress, challenge and perspectives. Chemical Engineering Journal. 2022;446:137147. doi: https://doi.org/10.1016/j.cej.2022.137147.
10. Afzal O, Altamimi ASA, Nadeem MS, Alzarea SI, Almalki WH, Tariq A, Mubeen B, Murtaza BN, Iftikhar S, Riaz N, Kazmi I. Nanoparticles in Drug Delivery: From History to Therapeutic Applications. Nanomaterials (Basel). 2022;12(24). Epub 20221219. doi: 10.3390/nano12244494. PubMed PMID: 36558344; PMCID: PMC9781272.
11. Liu Q, Zou J, Chen Z, He W, Wu W. Current research trends of nanomedicines. Acta Pharm Sin B. 2023;13(11):4391-416. Epub 20230520. doi: 10.1016/j.apsb.2023.05.018. PubMed PMID: 37969727; PMCID: PMC10638504.
12. Smith BR, Edelman ER. Nanomedicines for cardiovascular disease. Nature Cardiovascular Research. 2023;2(4):351-67. doi: 10.1038/s44161-023-00232-y.
13. Casals E, Li S, Jia Z, Casals G, Zeng M. Editorial: Advanced functional nanomaterials for diagnosis, bioimaging, drug delivery and therapeutics. Frontiers in Molecular Biosciences. 2024;11. doi: 10.3389/fmolb.2024.1399695.

14. Sargent J. Cardiovascular disease: New nanomedicines for treating atherosclerotic plaques. Nat Rev Endocrinol. 2015;11(5):256. Epub 20150310. doi: 10.1038/nrendo.2015.35. PubMed PMID: 25752278.
15. He L, Mu J, Gang O, Chen X. Rationally Programming Nanomaterials with DNA for Biomedical Applications. Adv Sci (Weinh). 2021;8(8):2003775. Epub 20210224. doi: 10.1002/advs.202003775. PubMed PMID: 33898180; PMCID: PMC8061415.
16. Johnson MB, Chandler M, Afonin KA. Nucleic acid nanoparticles (NANPs) as molecular tools to direct desirable and avoid undesirable immunological effects. Adv Drug Deliv Rev. 2021;173:427-38. Epub 20210420. doi: 10.1016/j.addr.2021.04.011. PubMed PMID: 33857556; PMCID: PMC8178219.
17. Dobrovolskaia MA, Bathe M. Opportunities and challenges for the clinical translation of structured DNA assemblies as gene therapeutic delivery and vaccine vectors. Wiley Interdiscip Rev Nanomed Nanobiotechnol. 2021;13(1):e1657. Epub 2020/07/17. doi: 10.1002/wnan.1657. PubMed PMID: 32672007; PMCID: PMC7736207.
18. Bui MN, Brittany Johnson M, Viard M, Satterwhite E, Martins AN, Li Z, Marriott I, Afonin KA, Khisamutdinov EF. Versatile RNA tetra-U helix linking motif as a toolkit for nucleic acid nanotechnology. Nanomedicine. 2017;13(3):1137-46. Epub 20170104. doi: 10.1016/j.nano.2016.12.018. PubMed PMID: 28064006; PMCID: PMC6637421.
19. Afonin KA, Cieply DJ, Leontis NB. Specific RNA self-assembly with minimal paranemic motifs. J Am Chem Soc. 2008;130(1):93-102. Epub 20071212. doi: 10.1021/ja071516m. PubMed PMID: 18072767; PMCID: PMC4869885.
20. Stewart JM, Viard M, Subramanian HK, Roark BK, Afonin KA, Franco E. Programmable RNA microstructures for coordinated delivery of siRNAs. Nanoscale. 2016;8(40):17542-50. doi: 10.1039/c6nr05085a. PubMed PMID: 27714127; PMCID: PMC5510167.
21. Parlea L, Bindewald E, Sharan R, Bartlett N, Moriarty D, Oliver J, Afonin KA, Shapiro BA. Ring Catalog: A resource for designing self-assembling RNA nanostructures. Methods. 2016;103:128-37. Epub 20160426. doi: 10.1016/j.ymeth.2016.04.016. PubMed PMID: 27090005; PMCID: PMC6319925.
22. Chandler M, Panigaj M, Rolband LA, Afonin KA. Challenges to optimizing RNA nanostructures for large scale production and controlled therapeutic properties. Nanomedicine (Lond). 2020;15(13):1331-40. Epub 20200526. doi: 10.2217/nnm-2020-0034. PubMed PMID: 32452262; PMCID: PMC7304434.
23. Ke W, Hong E, Saito RF, Rangel MC, Wang J, Viard M, Richardson M, Khisamutdinov EF, Panigaj M, Dokholyan NV, Chammas R, Dobrovolskaia MA, Afonin KA. RNA-DNA fibers and polygons with controlled immunorecognition activate RNAi, FRET and transcriptional regulation of NF-kappaB in human cells. Nucleic Acids Res. 2019;47(3):1350-61. doi: 10.1093/nar/gky1215. PubMed PMID: 30517685; PMCID: PMC6379676.
24. Rackley L, Stewart JM, Salotti J, Krokhotin A, Shah A, Halman JR, Juneja R, Smollett J, Lee L, Roark K, Viard M, Tarannum M, Vivero-Escoto J, Johnson PF, Dobrovolskaia MA, Dokholyan NV, Franco E, Afonin KA. RNA Fibers as Optimized Nanoscaffolds for siRNA Coordination and Reduced Immunological Recognition. Adv Funct Mater. 2018;28(48). Epub 2019/07/02. doi: 10.1002/adfm.201805959. PubMed PMID: 31258458; PMCID: PMC6599627.
25. Sajja S, Chandler M, Fedorov D, Kasprzak WK, Lushnikov A, Viard M, Shah A, Dang D, Dahl J, Worku B, Dobrovolskaia MA, Krasnoslobodtsev A, Shapiro BA, Afonin KA. Dynamic Behavior of RNA Nanoparticles Analyzed by AFM on a Mica/Air Interface. Langmuir. 2018;34(49):15099-108. Epub 20180430. doi: 10.1021/acs.langmuir.8b00105. PubMed PMID: 29669419; PMCID: PMC6207479.
26. Johnson MB, Halman JR, Satterwhite E, Zakharov AV, Bui MN, Benkato K, Goldsworthy V, Kim T, Hong E, Dobrovolskaia MA, Khisamutdinov EF, Marriott I, Afonin KA. Programmable Nucleic Acid Based Polygons with Controlled Neuroimmunomodulatory Properties for Predictive QSAR Modeling. Small (Weinheim an der Bergstrasse, Germany). 2017;13(42). Epub 2017/09/19. doi: 10.1002/smll.201701255. PubMed PMID: 28922553; PMCID: PMC6258062.

27. Martinsen E, Jinnurine T, Subramani S, Rogne M. Advances in RNA therapeutics for modulation of ‘undruggable’ targets. Progress in Molecular Biology and Translational Science: Academic Press; 2024.
28. Zhu Y, Zhu L, Wang X, Jin H. RNA-based therapeutics: an overview and prospectus. Cell Death & Disease. 2022;13(7):644. doi: 10.1038/s41419-022-05075-2.
29. Moazzam M, Zhang M, Hussain A, Yu X, Huang J, Huang Y. The landscape of nanoparticle-based siRNA delivery and therapeutic development. Molecular Therapy. 2024;32(2):284-312. doi: https://doi.org/10.1016/j.ymthe.2024.01.005.
30. Liang X, Li D, Leng S, Zhu X. RNA-based pharmacotherapy for tumors: From bench to clinic and back. Biomedicine & Pharmacotherapy. 2020;125:109997. doi: https://doi.org/10.1016/j.biopha.2020.109997.
31. Mullard A. FDA approves landmark RNAi drug. Nat Rev Drug Discov. 2018;17(9):613. doi: 10.1038/nrd.2018.152. PubMed PMID: 30160250.
32. Scott LJ. Givosiran: First Approval. Drugs. 2020;80(3):335-9. doi: 10.1007/s40265-020-01269-0. PubMed PMID: 32034693.
33. Scott LJ, Keam SJ. Lumasiran: First Approval. Drugs. 2021;81(2):277-82. doi: 10.1007/s40265-020-01463-0. PubMed PMID: 33405070.
34. Kallend D, Stoekenbroek R, He Y, Smith PF, Wijngaard P. Pharmacokinetics and pharmacodynamics of inclisiran, a small interfering RNA therapy, in patients with hepatic impairment. J Clin Lipidol. 2022;16(2):208-19. Epub 20220110. doi: 10.1016/j.jacl.2022.01.001. PubMed PMID: 35168913.
35. Chandler M, Johnson B, Khisamutdinov E, Dobrovolskaia MA, Sztuba-Solinska J, Salem AK, Breyne K, Chammas R, Walter NG, Contreras LM, Guo P, Afonin KA. The International Society of RNA Nanotechnology and Nanomedicine (ISRNN): The Present and Future of the Burgeoning Field. ACS Nano. 2021;15(11):16957-73. Epub 20211022. doi: 10.1021/acsnano.0c10240. PubMed PMID: 34677049; PMCID: PMC9023608.
36. Dobrovolskaia MA, Shurin M, Shvedova AA. Current understanding of interactions between nanoparticles and the immune system. Toxicol Appl Pharmacol. 2016;299:78-89. Epub 2016/01/08. doi: 10.1016/j.taap.2015.12.022. PubMed PMID: 26739622; PMCID: PMC4811709.
37. Chen L, Calin GA, Zhang S. Novel insights of structure-based modeling for RNA-targeted drug discovery. J Chem Inf Model. 2012;52(10):2741-53. Epub 2012/09/06. doi: 10.1021/ci300320t. PubMed PMID: 22947071; PMCID: PMC3869234.
38. Ezike TC, Okpala US, Onoja UL, Nwike CP, Ezeako EC, Okpara OJ, Okoroafor CC, Eze SC, Kalu OL, Odoh EC, Nwadike UG, Ogbodo JO, Umeh BU, Ossai EC, Nwanguma BC. Advances in drug delivery systems, challenges and future directions. Heliyon. 2023;9(6):e17488. Epub 20230624. doi: 10.1016/j.heliyon.2023.e17488. PubMed PMID: 37416680; PMCID: PMC10320272.
39. Avila YI, Chandler M, Cedrone E, Newton HS, Richardson M, Xu J, Clogston JD, Liptrott NJ, Afonin KA, Dobrovolskaia MA. Induction of Cytokines by Nucleic Acid Nanoparticles (NANPs) Depends on the Type of Delivery Carrier. Molecules. 2021;26(3). Epub 20210127. doi: 10.3390/molecules26030652. PubMed PMID: 33513786; PMCID: PMC7865455.
40. Li X, Chandler M, Avila YI, Arroyo-Becker SI, Patriarche G, Vargas-Berenguel A, Casas-Solvas JM, Afonin KA, Gref R. Nanoscale metal-organic frameworks for the delivery of nucleic acids to cancer cells. Int J Pharm X. 2023;5:100161. Epub 20230130. doi: 10.1016/j.ijpx.2023.100161. PubMed PMID: 36817971; PMCID: PMC9931914.
41. Abedi-Gaballu F, Dehghan G, Ghaffari M, Yekta R, Abbaspour-Ravasjani S, Baradaran B, Dolatabadi JEN, Hamblin MR. PAMAM dendrimers as efficient drug and gene delivery nanosystems for cancer therapy. Applied materials today. 2018;12:177-90.
42. Durymanov M, Reineke J. Non-viral Delivery of Nucleic Acids: Insight Into Mechanisms of Overcoming Intracellular Barriers. Front Pharmacol. 2018;9:971. Epub 2018/09/07. doi: 10.3389/fphar.2018.00971. PubMed PMID: 30186185; PMCID: PMC6111240.

43. Ke W, Afonin KA. Exosomes as natural delivery carriers for programmable therapeutic nucleic acid nanoparticles (NANPs). Adv Drug Deliv Rev. 2021;176:113835. Epub 20210616. doi: 10.1016/j.addr.2021.113835. PubMed PMID: 34144087; PMCID: PMC8440450.
44. Krämer M, Stumbé JF, Grimm G, Kaufmann B, Krüger U, Weber M, Haag R. Dendritic polyamines: simple access to new materials with defined treelike structures for application in nonviral gene delivery. ChemBioChem. 2004;5(8):1081-7.
45. Murphy DE, de Jong OG, Brouwer M, Wood MJ, Lavieu G, Schiffelers RM, Vader P. Extracellular vesicle-based therapeutics: natural versus engineered targeting and trafficking. Exp Mol Med. 2019;51(3):1-12. Epub 20190315. doi: 10.1038/s12276-019-0223-5. PubMed PMID: 30872574; PMCID: PMC6418170.
46. Nordmeier S, Ke W, Afonin KA, Portnoy V. Exosome mediated delivery of functional nucleic acid nanoparticles (NANPs). Nanomedicine. 2020;30:102285. Epub 20200808. doi: 10.1016/j.nano.2020.102285. PubMed PMID: 32781137; PMCID: PMC7680442.
47. O'Brien K, Breyne K, Ughetto S, Laurent LC, Breakefield XO. RNA delivery by extracellular vesicles in mammalian cells and its applications. Nat Rev Mol Cell Biol. 2020;21(10):585-606. Epub 20200526. doi: 10.1038/s41580-020-0251-y. PubMed PMID: 32457507; PMCID: PMC7249041.
48. Ofek P, Fischer W, Calderón M, Haag R, Satchi-Fainaro R. In vivo delivery of small interfering RNA to tumors and their vasculature by novel dendritic nanocarriers. The FASEB Journal. 2010;24(9):3122-34.
49. Wang H, Shi H-B, Yin S-K. Polyamidoamine dendrimers as gene delivery carriers in the inner ear: How to improve transfection efficiency. Experimental and therapeutic medicine. 2011;2(5):777-81.
50. Yin H, Kauffman KJ, Anderson DG. Delivery technologies for genome editing. Nat Rev Drug Discov. 2017;16(6):387-99. Epub 2017/03/25. doi: 10.1038/nrd.2016.280. PubMed PMID: 28337020.
51. Newton HS, Radwan Y, Xu J, Clogston JD, Dobrovolskaia MA, Afonin KA. Change in Lipofectamine Carrier as a Tool to Fine-Tune Immunostimulation of Nucleic Acid Nanoparticles. Molecules. 2023;28(11). Epub 20230601. doi: 10.3390/molecules28114484. PubMed PMID: 37298960; PMCID: PMC10254523.
52. Juneja R, Vadarevu H, Halman J, Tarannum M, Rackley L, Dobbs J, Marquez J, Chandler M, Afonin K, Vivero-Escoto JL. Combination of Nucleic Acid and Mesoporous Silica Nanoparticles: Optimization and Therapeutic Performance In Vitro. ACS Appl Mater Interfaces. 2020;12(35):38873-86. Epub 20200818. doi: 10.1021/acsami.0c07106. PubMed PMID: 32805923; PMCID: PMC7748385.
53. Halman JR, Kim KT, Gwak SJ, Pace R, Johnson MB, Chandler MR, Rackley L, Viard M, Marriott I, Lee JS, Afonin KA. A cationic amphiphilic co-polymer as a carrier of nucleic acid nanoparticles (Nanps) for controlled gene silencing, immunostimulation, and biodistribution. Nanomedicine. 2020;23:102094. Epub 2019/11/02. doi: 10.1016/j.nano.2019.102094. PubMed PMID: 31669854; PMCID: PMC6942546.
54. Kim T, Afonin KA, Viard M, Koyfman AY, Sparks S, Heldman E, Grinberg S, Linder C, Blumenthal RP, Shapiro BA. In Silico, In Vitro, and In Vivo Studies Indicate the Potential Use of Bolaamphiphiles for Therapeutic siRNAs Delivery. Mol Ther Nucleic Acids. 2013;2(3):e80. Epub 20130319. doi: 10.1038/mtna.2013.5. PubMed PMID: 23511334; PMCID: PMC3615820.
55. Shi D, Beasock D, Fessler A, Szebeni J, Ljubimova JY, Afonin KA, Dobrovolskaia MA. To PEGylate or not to PEGylate: Immunological properties of nanomedicine's most popular component, polyethylene glycol and its alternatives. Adv Drug Deliv Rev. 2022;180:114079. Epub 20211210. doi: 10.1016/j.addr.2021.114079. PubMed PMID: 34902516; PMCID: PMC8899923.
56. Parlea L, Puri A, Kasprzak W, Bindewald E, Zakrevsky P, Satterwhite E, Joseph K, Afonin KA, Shapiro BA. Cellular Delivery of RNA Nanoparticles. ACS Comb Sci. 2016;18(9):527-47. Epub 20160826. doi: 10.1021/acscombsci.6b00073. PubMed PMID: 27509068; PMCID: PMC6345529.
57. Herrmann IK, Wood MJA, Fuhrmann G. Extracellular vesicles as a next-generation drug delivery platform. Nat Nanotechnol. 2021;16(7):748-59. Epub 20210701. doi: 10.1038/s41565-021-00931-2. PubMed PMID: 34211166.

58. Afonin KA, Re F, Boraschi D. Editorial: Delivering nucleic acids to immune and non-immune cells. Front Immunol. 2023;14:1237506. Epub 20230808. doi: 10.3389/fimmu.2023.1237506. PubMed PMID: 37614239; PMCID: PMC10443216.
59. Herwald H, Egesten A. On PAMPs and DAMPs. J Innate Immun. 2016;8(5):427-8. Epub 20160813. doi: 10.1159/000448437. PubMed PMID: 27522675; PMCID: PMC6738819.
60. Li D, Wu M. Pattern recognition receptors in health and diseases. Signal Transduct Target Ther. 2021;6(1):291. Epub 20210804. doi: 10.1038/s41392-021-00687-0. PubMed PMID: 34344870; PMCID: PMC8333067.
61. Gajewski TF, Schreiber H, Fu YX. Innate and adaptive immune cells in the tumor microenvironment. Nat Immunol. 2013;14(10):1014-22. doi: 10.1038/ni.2703. PubMed PMID: 24048123; PMCID: PMC4118725.
62. Park BS, Lee JO. Recognition of lipopolysaccharide pattern by TLR4 complexes. Exp Mol Med. 2013;45(12):e66. Epub 20131206. doi: 10.1038/emm.2013.97. PubMed PMID: 24310172; PMCID: PMC3880462.
63. Mortaz E, Adcock IM, Tabarsi P, Darazam IA, Movassaghi M, Garssen J, Jamaati H, Velayati A. Pattern recognitions receptors in immunodeficiency disorders. Eur J Pharmacol. 2017;808:49-56. Epub 20170114. doi: 10.1016/j.ejphar.2017.01.014. PubMed PMID: 28095323.
64. Kawai T, Akira S. The role of pattern-recognition receptors in innate immunity: update on Toll-like receptors. Nat Immunol. 2010;11(5):373-84. Epub 20100420. doi: 10.1038/ni.1863. PubMed PMID: 20404851.
65. Xu Y, Tao X, Shen B, Horng T, Medzhitov R, Manley JL, Tong L. Structural basis for signal transduction by the Toll/interleukin-1 receptor domains. Nature. 2000;408(6808):111-5. doi: 10.1038/35040600. PubMed PMID: 11081518.
66. Wang Y, Ludwig J, Schuberth C, Goldeck M, Schlee M, Li H, Juranek S, Sheng G, Micura R, Tuschl T, Hartmann G, Patel DJ. Structural and functional insights into 5'-ppp RNA pattern recognition by the innate immune receptor RIG-I. Nat Struct Mol Biol. 2010;17(7):781-7. Epub 20100627. doi: 10.1038/nsmb.1863. PubMed PMID: 20581823; PMCID: PMC3744876.
67. Chandler M, Jain S, Halman J, Hong E, Dobrovolskaia MA, Zakharov AV, Afonin KA. Artificial Immune Cell, AI-cell, a New Tool to Predict Interferon Production by Peripheral Blood Monocytes in Response to Nucleic Acid Nanoparticles. Small. 2022;18(46):e2204941. Epub 20221010. doi: 10.1002/smll.202204941. PubMed PMID: 36216772; PMCID: PMC9671856.
68. Dobrovolskaia MA, Afonin KA. Use of human peripheral blood mononuclear cells to define immunological properties of nucleic acid nanoparticles. Nat Protoc. 2020;15(11):3678-98. Epub 20201023. doi: 10.1038/s41596-020-0393-6. PubMed PMID: 33097923; PMCID: PMC7875514.
69. Hong E, Halman JR, Shah AB, Khisamutdinov EF, Dobrovolskaia MA, Afonin KA. Structure and Composition Define Immunorecognition of Nucleic Acid Nanoparticles. Nano Lett. 2018;18(7):4309-21. Epub 20180620. doi: 10.1021/acs.nanolett.8b01283. PubMed PMID: 29894623; PMCID: PMC6540121.
70. Dobrovolskaia MA, McNeil SE. Immunological properties of engineered nanomaterials. Nat Nanotechnol. 2007;2(8):469-78. Epub 20070729. doi: 10.1038/nnano.2007.223. PubMed PMID: 18654343.
71. Rebolledo LP, Ke W, Cedrone E, Wang J, Majithia K, Johnson MB, Dokholyan NV, Dobrovolskaia MA, Afonin KA. Immunostimulation of Fibrous Nucleic Acid Nanoparticles Can be Modulated through Aptamer-Based Functional Moieties: Unveiling the Structure-Activity Relationship and Mechanistic Insights. ACS Appl Mater Interfaces. 2024;16(7):8430-41. Epub 20240212. doi: 10.1021/acsami.3c17779. PubMed PMID: 38344840; PMCID: PMC10895590.
72. Ke W, Chandler M, Cedrone E, Saito RF, Rangel MC, de Souza Junqueira M, Wang J, Shi D, Truong N, Richardson M, Rolband LA, Dréau D, Bedocs P, Chammas R, Dokholyan NV, Dobrovolskaia MA, Afonin KA. Locking and Unlocking Thrombin Function Using Immunoquiescent Nucleic Acid Nanoparticles with Regulated Retention In Vivo. Nano Letters. 2022;22(14):5961-72. doi: 10.1021/acs.nanolett.2c02019.

73. Bila D, Radwan Y, Dobrovolskaia MA, Panigaj M, Afonin KA. The Recognition of and Reactions to Nucleic Acid Nanoparticles by Human Immune Cells. Molecules. 2021;26(14). Epub 20210712. doi: 10.3390/molecules26144231. PubMed PMID: 34299506; PMCID: PMC8306967.
74. Hong E, Halman JR, Shah A, Cedrone E, Truong N, Afonin KA, Dobrovolskaia MA. Toll-Like Receptor-Mediated Recognition of Nucleic Acid Nanoparticles (NANPs) in Human Primary Blood Cells. Molecules. 2019;24(6). Epub 2019/03/23. doi: 10.3390/molecules24061094. PubMed PMID: 30897721; PMCID: PMC6470694.
75. Turner MD, Nedjai B, Hurst T, Pennington DJ. Cytokines and chemokines: At the crossroads of cell signalling and inflammatory disease. Biochim Biophys Acta. 2014;1843(11):2563-82. Epub 20140602. doi: 10.1016/j.bbamcr.2014.05.014. PubMed PMID: 24892271.
76. Halman JR, Satterwhite E, Roark B, Chandler M, Viard M, Ivanina A, Bindewald E, Kasprzak WK, Panigaj M, Bui MN, Lu JS, Miller J, Khisamutdinov EF, Shapiro BA, Dobrovolskaia MA, Afonin KA. Functionally-interdependent shape-switching nanoparticles with controllable properties. Nucleic acids research. 2017;45(4):2210-20. Epub 2017/01/22. doi: 10.1093/nar/gkx008. PubMed PMID: 28108656; PMCID: PMC5389727.
77. Ke W, Hong E, Saito RF, Rangel MC, Wang J, Viard M, Richardson M, Khisamutdinov EF, Panigaj M, Dokholyan NV, Chammas R, Dobrovolskaia MA, Afonin KA. RNA-DNA fibers and polygons with controlled immunorecognition activate RNAi, FRET and transcriptional regulation of NF-κB in human cells. Nucleic acids research. 2019;47(3):1350-61. Epub 2018/12/06. doi: 10.1093/nar/gky1215. PubMed PMID: 30517685; PMCID: PMC6379676.
78. Johnson MB, Halman JR, Miller DK, Cooper JS, Khisamutdinov EF, Marriott I, Afonin KA. The immunorecognition, subcellular compartmentalization, and physicochemical properties of nucleic acid nanoparticles can be controlled by composition modification. Nucleic acids research. 2020;48(20):11785-98. Epub 2020/10/23. doi: 10.1093/nar/gkaa908. PubMed PMID: 33091133; PMCID: PMC7672449.
79. Messaoudi S, Greschner AA, Gauthier MA. Progress Toward Absorption, Distribution, Metabolism, Elimination, and Toxicity of DNA Nanostructures. Advanced Therapeutics. 2019;2(12):1900144. doi: https://doi.org/10.1002/adtp.201900144.
80. Zeng Y, Nixon RL, Liu W, Wang R. The applications of functionalized DNA nanostructures in bioimaging and cancer therapy. Biomaterials. 2021;268:120560. doi: https://doi.org/10.1016/j.biomaterials.2020.120560.
81. Kim J, Franco E. RNA nanotechnology in synthetic biology. Current Opinion in Biotechnology. 2020;63:135-41. doi: https://doi.org/10.1016/j.copbio.2019.12.016.
82. Green LN, Subramanian HKK, Mardanlou V, Kim J, Hariadi RF, Franco E. Autonomous dynamic control of DNA nanostructure self-assembly. Nature Chemistry. 2019;11(6):510-20. doi: 10.1038/s41557-019-0251-8.
83. Afonin KA, Viard M, Koyfman AY, Martins AN, Kasprzak WK, Panigaj M, Desai R, Santhanam A, Grabow WW, Jaeger L, Heldman E, Reiser J, Chiu W, Freed EO, Shapiro BA. Multifunctional RNA Nanoparticles. Nano Letters. 2014;14(10):5662-71. doi: 10.1021/nl502385k.
84. Khisamutdinov EF, Li H, Jasinski DL, Chen J, Fu J, Guo P. Enhancing immunomodulation on innate immunity by shape transition among RNA triangle, square and pentagon nanovehicles. Nucleic acids research. 2014;42(15):9996-10004. Epub 2014/08/06. doi: 10.1093/nar/gku516. PubMed PMID: 25092921; PMCID: PMC4150753.
85. Rackley L, Stewart JM, Salotti J, Krokhotin A, Shah A, Halman JR, Juneja R, Smollett J, Lee L, Roark K, Viard M, Tarannum M, Vivero-Escoto J, Johnson PF, Dobrovolskaia MA, Dokholyan NV, Franco E, Afonin KA. RNA Fibers as Optimized Nanoscaffolds for siRNA Coordination and Reduced Immunological Recognition. Advanced Functional Materials. 2018;28(48):1805959. doi: 10.1002/adfm.201805959.
86. Yang X, Wen Y, Wang L, Zhou C, Li Q, Xu L, Li L, Shi J, Lal R, Ren S, Li J, Jia N, Liu G. PCR-Free Colorimetric DNA Hybridization Detection Using a 3D DNA Nanostructured Reporter Probe. ACS Applied Materials & Interfaces. 2017;9(44):38281-7. doi: 10.1021/acsami.7b11994.

87. Zeng D, Zhang H, Zhu D, Li J, San L, Wang Z, Wang C, Wang Y, Wang L, Zuo X, Mi X. A novel ultrasensitive electrochemical DNA sensor based on double tetrahedral nanostructures. Biosensors and Bioelectronics. 2015;71:434-8. doi: https://doi.org/10.1016/j.bios.2015.04.065.
88. Zhu L, Liu Q, Yang B, Ju H, Lei J. Pixel Counting of Fluorescence Spots Triggered by DNA Walkers for Ultrasensitive Quantification of Nucleic Acid. Analytical Chemistry. 2018;90(11):6357-61. doi: 10.1021/acs.analchem.8b01146.
89. Douglas SM, Bachelet I, Church GM. A Logic-Gated Nanorobot for Targeted Transport of Molecular Payloads. Science. 2012;335(6070):831. doi: 10.1126/science.1214081.
90. Jiang Q, Song C, Nangreave J, Liu X, Lin L, Qiu D, Wang Z-G, Zou G, Liang X, Yan H, Ding B. DNA Origami as a Carrier for Circumvention of Drug Resistance. Journal of the American Chemical Society. 2012;134(32):13396-403. doi: 10.1021/ja304263n.
91. Du Y, Jiang Q, Beziere N, Song L, Zhang Q, Peng D, Chi C, Yang X, Guo H, Diot G, Ntziachristos V, Ding B, Tian J. DNA-Nanostructure–Gold-Nanorod Hybrids for Enhanced In Vivo Optoacoustic Imaging and Photothermal Therapy. Advanced Materials. 2016;28(45):10000-7. doi: https://doi.org/10.1002/adma.201601710.
92. Smith DM, Keller A. DNA in the Fight Against Infectious Diseases. Advanced NanoBiomed Research. 2020;n/a(n/a):2000049. doi: https://doi.org/10.1002/anbr.202000049.
93. Dobrovolskaia MA. Nucleic Acid Nanoparticles at a Crossroads of Vaccines and Immunotherapies. Molecules. 2019;24(24). Epub 2019/12/22. doi: 10.3390/molecules24244620. PubMed PMID: 31861154; PMCID: PMC6943637.
94. Chandler M, Johnson MB, Panigaj M, Afonin KA. Innate immune responses triggered by nucleic acids inspire the design of immunomodulatory nucleic acid nanoparticles (NANPs). Curr Opin Biotechnol. 2020;63:8-15. Epub 20191125. doi: 10.1016/j.copbio.2019.10.011. PubMed PMID: 31778882; PMCID: PMC7246180.
95. Veneziano R, Ratanalert S, Zhang K, Zhang F, Yan H, Chiu W, Bathe M. Designer nanoscale DNA assemblies programmed from the top down. Science. 2016;352(6293):1534. doi: 10.1126/science.aaf4388.
96. Li S, Jiang Q, Liu S, Zhang Y, Tian Y, Song C, Wang J, Zou Y, Anderson GJ, Han J-Y, Chang Y, Liu Y, Zhang C, Chen L, Zhou G, Nie G, Yan H, Ding B, Zhao Y. A DNA nanorobot functions as a cancer therapeutic in response to a molecular trigger in vivo. Nature Biotechnology. 2018;36(3):258-64. doi: 10.1038/nbt.4071.
97. Halman JR, Satterwhite E, Roark B, Chandler M, Viard M, Ivanina A, Bindewald E, Kasprzak WK, Panigaj M, Bui MN, Lu JS, Miller J, Khisamutdinov EF, Shapiro BA, Dobrovolskaia MA, Afonin KA. Functionally-interdependent shape-switching nanoparticles with controllable properties. Nucleic Acids Research. 2017;45(4):2210-20. doi: 10.1093/nar/gkx008.
98. Xiao T, Hou W, Cao X, Wen S, Shen M, Shi X. Dendrimer-entrapped gold nanoparticles modified with folic acid for targeted gene delivery applications. Biomaterials Science. 2013;1(11):1172-80.
99. Zarebkohan A, Najafi F, Moghimi HR, Hemmati M, Deevband MR, Kazemi B. Synthesis and characterization of a PAMAM dendrimer nanocarrier functionalized by SRL peptide for targeted gene delivery to the brain. European Journal of Pharmaceutical Sciences. 2015;78:19-30.
100. Guillot-Nieckowski M, Joester D, Stöhr M, Losson M, Adrian M, Wagner B, Kansy M, Heinzelmann H, Pugin R, Diederich F. Self-assembly, DNA complexation, and pH response of amphiphilic dendrimers for gene transfection. Langmuir. 2007;23(2):737-46.
101. Janiszewska J, Posadas I, Játiva P, Bugaj-Zarebska M, Urbanczyk-Lipkowska Z, Ceña V. Second generation amphiphilic poly-lysine dendrons inhibit glioblastoma cell proliferation without toxicity for neurons or astrocytes. PLoS One. 2016;11(11):e0165704.
102. Hou W, Wei P, Kong L, Guo R, Wang S, Shi X. Partially PEGylated dendrimer-entrapped gold nanoparticles: A promising nanoplatform for highly efficient DNA and siRNA delivery. Journal of Materials Chemistry B. 2016;4(17):2933-43.
103. Perez AP, Cosaka ML, Romero EL, Morilla MJ. Uptake and intracellular traffic of siRNA dendriplexes in glioblastoma cells and macrophages. International journal of nanomedicine. 2011;6:2715.

104. Su Y, Quan X, Li L, Zhou J. Computer simulation of DNA condensation by PAMAM dendrimer. Macromolecular Theory and Simulations. 2018;27(2):1700070.
105. Dobrovolskaia MA, Patri AK, Potter TM, Rodriguez JC, Hall JB, McNeil SE. Dendrimer-induced leukocyte procoagulant activity depends on particle size and surface charge. Nanomedicine (Lond). 2012;7(2):245-56. Epub 2011/10/01. doi: 10.2217/nnm.11.105. PubMed PMID: 21957862.
106. Dobrovolskaia MA, Patri AK, Simak J, Hall JB, Semberova J, De Paoli Lacerda SH, McNeil SE. Nanoparticle size and surface charge determine effects of PAMAM dendrimers on human platelets in vitro. Mol Pharm. 2012;9(3):382-93. Epub 2011/10/27. doi: 10.1021/mp200463e. PubMed PMID: 22026635; PMCID: PMC3624701.
107. Ilinskaya AN, Man S, Patri AK, Clogston JD, Crist RM, Cachau RE, McNeil SE, Dobrovolskaia MA. Inhibition of phosphoinositol 3 kinase contributes to nanoparticle-mediated exaggeration of endotoxin-induced leukocyte procoagulant activity. Nanomedicine (Lond). 2014;9(9):1311-26. Epub 2013/11/28. doi: 10.2217/nnm.13.137. PubMed PMID: 24279459; PMCID: PMC4035470.
108. Hong S, Leroueil PR, Janus EK, Peters JL, Kober MM, Islam MT, Orr BG, Baker JR, Jr., Banaszak Holl MM. Interaction of polycationic polymers with supported lipid bilayers and cells: nanoscale hole formation and enhanced membrane permeability. Bioconjug Chem. 2006;17(3):728-34. Epub 2006/05/18. doi: 10.1021/bc060077y. PubMed PMID: 16704211.
109. Leroueil PR, Berry SA, Duthie K, Han G, Rotello VM, McNerny DQ, Baker JR, Jr., Orr BG, Holl MM. Wide varieties of cationic nanoparticles induce defects in supported lipid bilayers. Nano Lett. 2008;8(2):420-4. Epub 2008/01/26. doi: 10.1021/nl0722929. PubMed PMID: 18217783.
110. Qin L, Cao D, Huang H, Ji G, Feng M, Chen J, Pan S. Improvement of Cellular Uptake and Transfection Ability of pDNA Using α-Cyclodextrin-Polyamidoamine Conjugates as Gene Delivery System. J Biomed Nanotechnol. 2016;12(2):261-73. Epub 2016/06/17. doi: 10.1166/jbn.2016.2155. PubMed PMID: 27305760.
111. Thomas TP, Majoros I, Kotlyar A, Mullen D, Holl MM, Baker JR, Jr. Cationic poly(amidoamine) dendrimer induces lysosomal apoptotic pathway at therapeutically relevant concentrations. Biomacromolecules. 2009;10(12):3207-14. Epub 2009/11/21. doi: 10.1021/bm900683r. PubMed PMID: 19924846; PMCID: PMC2805189.
112. Afonin KA, Viard M, Kagiampakis I, Case CL, Dobrovolskaia MA, Hofmann J, Vrzak A, Kireeva M, Kasprzak WK, KewalRamani VN, Shapiro BA. Triggering of RNA Interference with RNA–RNA, RNA–DNA, and DNA–RNA Nanoparticles. ACS Nano. 2015;9(1):251-9. doi: 10.1021/nn504508s.
113. Dobrovolskaia MA, McNeil SE. Understanding the correlation between in vitro and in vivo immunotoxicity tests for nanomedicines. J Control Release. 2013;172(2):456-66. Epub 2013/06/08. doi: 10.1016/j.jconrel.2013.05.025. PubMed PMID: 23742883; PMCID: PMC5831149.
114. Carmona-Ribeiro AM, Pérez-Betancourt Y. Cationic Nanostructures for Vaccines Design. Biomimetics (Basel). 2020;5(3). Epub 2020/07/11. doi: 10.3390/biomimetics5030032. PubMed PMID: 32645946; PMCID: PMC7560170.
115. Feng S, Zhang Z, Mo Y, Tong R, Zhong Z, Chen Z, He D, Wan R, Gao M, Mo Y, Zhang Q, Huang Y. Activation of NLRP3 inflammasome in hepatocytes after exposure to cobalt nanoparticles: The role of oxidative stress. Toxicol In Vitro. 2020;69:104967. Epub 2020/08/18. doi: 10.1016/j.tiv.2020.104967. PubMed PMID: 32805375.
116. Liu X, Lu B, Fu J, Zhu X, Song E, Song Y. Amorphous silica nanoparticles induce inflammation via activation of NLRP3 inflammasome and HMGB1/TLR4/MYD88/NF-kb signaling pathway in HUVEC cells. J Hazard Mater. 2021;404(Pt B):124050. Epub 2020/10/15. doi: 10.1016/j.jhazmat.2020.124050. PubMed PMID: 33053467.
117. Ilinskaya AN, Clogston JD, McNeil SE, Dobrovolskaia MA. Induction of oxidative stress by Taxol® vehicle Cremophor-EL triggers production of interleukin-8 by peripheral blood mononuclear cells through the mechanism not requiring de novo synthesis of mRNA. Nanomedicine. 2015;11(8):1925-38. Epub 2015/08/19. doi: 10.1016/j.nano.2015.07.012. PubMed PMID: 26282378; PMCID: PMC4652134.
118. Grimaldi C, Finco D, Fort MM, Gliddon D, Harper K, Helms WS, Mitchell JA, O'Lone R, Parish ST, Piche MS, Reed DM, Reichmann G, Ryan PC, Stebbings R, Walker M. Cytokine release: A workshop

proceedings on the state-of-the-science, current challenges and future directions. Cytokine. 2016;85:101-8. Epub 2016/06/17. doi: 10.1016/j.cyto.2016.06.006. PubMed PMID: 27309676.
119. Hofmann JN, Yu K, Bagni RK, Lan Q, Rothman N, Purdue MP. Intra-individual variability over time in serum cytokine levels among participants in the prostate, lung, colorectal, and ovarian cancer screening Trial. Cytokine. 2011;56(2):145-8. Epub 2011/07/19. doi: 10.1016/j.cyto.2011.06.012. PubMed PMID: 21764327; PMCID: PMC3185107.
120. Ma M, Percopo CM, Sturdevant DE, Sek AC, Komarow HD, Rosenberg HF. Cytokine Diversity in Human Peripheral Blood Eosinophils: Profound Variability of IL-16. J Immunol. 2019;203(2):520-31. Epub 2019/06/12. doi: 10.4049/jimmunol.1900101. PubMed PMID: 31182481; PMCID: PMC6664432.
121. Mueller SC, März R, Schmolz M, Drewelow B. Intraindividual long term stability and response corridors of cytokines in healthy volunteers detected by a standardized whole-blood culture system for bed-side application. BMC Med Res Methodol. 2012;12:112. Epub 2012/08/03. doi: 10.1186/1471-2288-12-112. PubMed PMID: 22853196; PMCID: PMC3494532.
122. Sahdo B, Fransén K, Asfaw Idosa B, Eriksson P, Söderquist B, Kelly A, Särndahl E. Cytokine profile in a cohort of healthy blood donors carrying polymorphisms in genes encoding the NLRP3 inflammasome. PLoS One. 2013;8(10):e75457. Epub 2013/10/08. doi: 10.1371/journal.pone.0075457. PubMed PMID: 24098386; PMCID: PMC3789710.
123. Zhou ZH, Han Y, Wei T, Aras S, Chaturvedi P, Tyler S, Rani MR, Ransohoff RM. Regulation of monocyte chemoattractant protein (MCP)-1 transcription by interferon-gamma (IFN-gamma) in human astrocytoma cells: postinduction refractory state of the gene, governed by its upstream elements. Faseb j. 2001;15(2):383-92. Epub 2001/02/07. doi: 10.1096/fj.00-0373com. PubMed PMID: 11156954.
124. Padgett LE, Araujo DJ, Hedrick CC, Olingy CE. Functional crosstalk between T cells and monocytes in cancer and atherosclerosis. J Leukoc Biol. 2020;108(1):297-308. Epub 2020/06/13. doi: 10.1002/jlb.1mir0420-076r. PubMed PMID: 32531833.
125. Dobrovolskaia MA, McNeil SE. Immunological and hematological toxicities challenging clinical translation of nucleic acid-based therapeutics. Expert Opin Biol Ther. 2015;15(7):1023-48. Epub 20150528. doi: 10.1517/14712598.2015.1014794. PubMed PMID: 26017628.
126. Suptela AJ, Radwan Y, Richardson C, Yan S, Afonin KA, Marriott I. cGAS Mediates the Inflammatory Responses of Human Microglial Cells to Genotoxic DNA Damage. Inflammation. 2023. Epub 20231226. doi: 10.1007/s10753-023-01946-8. PubMed PMID: 38148453.
127. Gupta A, Andresen JL, Manan RS, Langer R. Nucleic acid delivery for therapeutic applications. Advanced Drug Delivery Reviews. 2021;178:113834. doi: https://doi.org/10.1016/j.addr.2021.113834.
128. Delyanee M, Akbari S, Solouk A. Amine-terminated dendritic polymers as promising nanoplatform for diagnostic and therapeutic agents' modification: A review. European Journal of Medicinal Chemistry. 2021;221:113572. doi: https://doi.org/10.1016/j.ejmech.2021.113572.
129. Kannan RM, Nance E, Kannan S, Tomalia DA. Emerging concepts in dendrimer-based nanomedicine: from design principles to clinical applications. J Intern Med. 2014;276(6):579-617. Epub 20140731. doi: 10.1111/joim.12280. PubMed PMID: 24995512.
130. Wu LP, Ficker M, Christensen JB, Trohopoulos PN, Moghimi SM. Dendrimers in Medicine: Therapeutic Concepts and Pharmaceutical Challenges. Bioconjug Chem. 2015;26(7):1198-211. Epub 20150213. doi: 10.1021/acs.bioconjchem.5b00031. PubMed PMID: 25654320.
131. Frechet JM. Dendrimers and supramolecular chemistry. Proc Natl Acad Sci U S A. 2002;99(8):4782-7. doi: 10.1073/pnas.082013899. PubMed PMID: 11959930; PMCID: PMC122668.
132. Song C, Shen M, Rodrigues J, Mignani S, Majoral J-P, Shi X. Superstructured poly(amidoamine) dendrimer-based nanoconstructs as platforms for cancer nanomedicine: A concise review. Coordination Chemistry Reviews. 2020;421:213463. doi: https://doi.org/10.1016/j.ccr.2020.213463.
133. Gao Y, Shen M, Shi X. Interaction of dendrimers with the immune system: An insight into cancer nanotheranostics. VIEW. 2021;2(3):20200120. doi: https://doi.org/10.1002/VIW.20200120.
134. Bu J, Nair A, Iida M, Jeong WJ, Poellmann MJ, Mudd K, Kubiatowicz LJ, Liu EW, Wheeler DL, Hong S. An Avidity-Based PD-L1 Antagonist Using Nanoparticle-Antibody Conjugates for Enhanced

Immunotherapy. Nano Lett. 2020;20(7):4901-9. Epub 20200611. doi: 10.1021/acs.nanolett.0c00953. PubMed PMID: 32510959; PMCID: PMC7737517.
135. Myung JH, Gajjar KA, Saric J, Eddington DT, Hong S. Dendrimer-mediated multivalent binding for the enhanced capture of tumor cells. Angew Chem Int Ed Engl. 2011;50(49):11769-72. Epub 20111019. doi: 10.1002/anie.201105508. PubMed PMID: 22012872; PMCID: PMC3549433.
136. Xie J, Wang J, Chen H, Shen W, Sinko PJ, Dong H, Zhao R, Lu Y, Zhu Y, Jia L. Multivalent conjugation of antibody to dendrimers for the enhanced capture and regulation on colon cancer cells. Sci Rep. 2015;5:9445. Epub 20150330. doi: 10.1038/srep09445. PubMed PMID: 25819426; PMCID: PMC4377633.
137. Wu L-P, Ficker M, Christensen JB, Simberg D, Trohopoulos PN, Moghimi SM. Dendrimer end-terminal motif-dependent evasion of human complement and complement activation through IgM hitchhiking. Nature Communications. 2021;12(1):4858. doi: 10.1038/s41467-021-24960-6.
138. Afonin KA, Bindewald E, Yaghoubian AJ, Voss N, Jacovetty E, Shapiro BA, Jaeger L. In vitro assembly of cubic RNA-based scaffolds designed in silico. Nat Nanotechnol. 2010;5(9):676-82. Epub 20100829. doi: 10.1038/nnano.2010.160. PubMed PMID: 20802494; PMCID: PMC2934861.
139. Kowalski PS, Rudra A, Miao L, Anderson DG. Delivering the Messenger: Advances in Technologies for Therapeutic mRNA Delivery. Mol Ther. 2019;27(4):710-28. Epub 2019/03/09. doi: 10.1016/j.ymthe.2019.02.012. PubMed PMID: 30846391; PMCID: PMC6453548.
140. Chakravarthi BV, Nepal S, Varambally S. Genomic and Epigenomic Alterations in Cancer. Am J Pathol. 2016;186(7):1724-35. doi: 10.1016/j.ajpath.2016.02.023. PubMed PMID: 27338107; PMCID: PMC4929396.
141. Castro-Mondragon JA, Aure MR, Lingjaerde OC, Langerod A, Martens JWM, Borresen-Dale AL, Kristensen VN, Mathelier A. Cis-regulatory mutations associate with transcriptional and post-transcriptional deregulation of gene regulatory programs in cancers. Nucleic acids research. 2022;50(21):12131-48. doi: 10.1093/nar/gkac1143. PubMed PMID: 36477895; PMCID: PMC9757053.
142. Lee TI, Young RA. Transcriptional regulation and its misregulation in disease. Cell. 2013;152(6):1237-51. doi: 10.1016/j.cell.2013.02.014. PubMed PMID: 23498934; PMCID: PMC3640494.
143. Choi S, Lee G, Kim J. Cellular Computational Logic Using Toehold Switches. Int J Mol Sci. 2022;23(8). Epub 20220412. doi: 10.3390/ijms23084265. PubMed PMID: 35457085; PMCID: PMC9033136.
144. Xie Z, Liu SJ, Bleris L, Benenson Y. Logic integration of mRNA signals by an RNAi-based molecular computer. Nucleic acids research. 2010;38(8):2692-701. Epub 20100301. doi: 10.1093/nar/gkq117. PubMed PMID: 20194121; PMCID: PMC2860122.
145. Liang JC, Chang AL, Kennedy AB, Smolke CD. A high-throughput, quantitative cell-based screen for efficient tailoring of RNA device activity. Nucleic acids research. 2012;40(20):e154. Epub 20120718. doi: 10.1093/nar/gks636. PubMed PMID: 22810204; PMCID: PMC3488204.
146. Wachsmuth M, Findeiss S, Weissheimer N, Stadler PF, Morl M. De novo design of a synthetic riboswitch that regulates transcription termination. Nucleic acids research. 2013;41(4):2541-51. Epub 20121228. doi: 10.1093/nar/gks1330. PubMed PMID: 23275562; PMCID: PMC3575828.
147. Xie Z, Wroblewska L, Prochazka L, Weiss R, Benenson Y. Multi-input RNAi-based logic circuit for identification of specific cancer cells. Science. 2011;333(6047):1307-11. doi: 10.1126/science.1205527. PubMed PMID: 21885784.
148. Bindewald E, Afonin KA, Viard M, Zakrevsky P, Kim T, Shapiro BA. Multistrand Structure Prediction of Nucleic Acid Assemblies and Design of RNA Switches. Nano Lett. 2016;16(3):1726-35. doi: 10.1021/acs.nanolett.5b04651. PubMed PMID: 26926528.
149. Lee JH, Kim JA, Kwon MH, Kang JY, Rhee WJ. In situ single step detection of exosome microRNA using molecular beacon. Biomaterials. 2015;54:116-25. Epub 20150331. doi: 10.1016/j.biomaterials.2015.03.014. PubMed PMID: 25907045.

150. Ma Z, Wu X, Krueger CJ, Chen AK. Engineering Novel Molecular Beacon Constructs to Study Intracellular RNA Dynamics and Localization. Genomics Proteomics Bioinformatics. 2017;15(5):279-86. Epub 20170921. doi: 10.1016/j.gpb.2017.04.004. PubMed PMID: 28942262; PMCID: PMC5673673.
151. Marras SA, Kramer FR, Tyagi S. Multiplex detection of single-nucleotide variations using molecular beacons. Genet Anal. 1999;14(5-6):151-6. PubMed PMID: 10084107.
152. Tyagi S, Kramer FR. Molecular beacons: probes that fluoresce upon hybridization. Nat Biotechnol. 1996;14(3):303-8. doi: 10.1038/nbt0396-303. PubMed PMID: 9630890.
153. Peng XH, Cao ZH, Xia JT, Carlson GW, Lewis MM, Wood WC, Yang L. Real-time detection of gene expression in cancer cells using molecular beacon imaging: new strategies for cancer research. Cancer Res. 2005;65(5):1909-17. doi: 10.1158/0008-5472.CAN-04-3196. PubMed PMID: 15753390.
154. Wee SK, Sivalingam SP, Yap EPH. Rapid Direct Nucleic Acid Amplification Test without RNA Extraction for SARS-CoV-2 Using a Portable PCR Thermocycler. Genes (Basel). 2020;11(6). Epub 20200618. doi: 10.3390/genes11060664. PubMed PMID: 32570810; PMCID: PMC7349311.
155. Li X, Xiong X, Yi C. Epitranscriptome sequencing technologies: decoding RNA modifications. Nat Methods. 2016;14(1):23-31. doi: 10.1038/nmeth.4110. PubMed PMID: 28032622.
156. Johnsson N, Varshavsky A. Split ubiquitin as a sensor of protein interactions in vivo. Proceedings of the National Academy of Sciences of the United States of America. 1994;91(22):10340-4. PubMed PMID: 7937952.
157. Cassonnet P, Rolloy C, Neveu G, Vidalain PO, Chantier T, Pellet J, Jones L, Muller M, Demeret C, Gaud G, Vuillier F, Lotteau V, Tangy F, Favre M, Jacob Y. Benchmarking a luciferase complementation assay for detecting protein complexes. Nat Methods. 2011;8(12):990-2.
158. Shekhawat SS, Ghosh I. Split-protein systems: beyond binary protein-protein interactions. Curr Opin Chem Biol. 2011;15(6):789-97.
159. Afonin KA, Viard M, Martins AN, Lockett SJ, Maciag AE, Freed EO, Heldman E, Jaeger L, Blumenthal R, Shapiro BA. Activation of different split functionalities on re-association of RNA-DNA hybrids. Nature nanotechnology. 2013;8(4):296-304. doi: 10.1038/nnano.2013.44. PubMed PMID: 23542902; PMCID: 3618561.
160. Afonin KA, Desai R, Viard M, Kireeva ML, Bindewald E, Case CL, Maciag AE, Kasprzak WK, Kim T, Sappe A, Stepler M, Kewalramani VN, Kashlev M, Blumenthal R, Shapiro BA. Co-transcriptional production of RNA-DNA hybrids for simultaneous release of multiple split functionalities. Nucleic acids research. 2014;42(3):2085-97. doi: 10.1093/nar/gkt1001.
161. Afonin KA, Kasprzak WK, Bindewald E, Kireeva M, Viard M, Kashlev M, Shapiro BA. In silico design and enzymatic synthesis of functional RNA nanoparticles. Acc Chem Res. 2014;47(6):1731-41. doi: 10.1021/ar400329z.
162. Afonin KA, Viard M, Koyfman AY, Martins AN, Kasprzak WK, Panigaj M, Desai R, Santhanam A, Grabow WW, Jaeger L, Heldman E, Reiser J, Chiu W, Freed EO, Shapiro BA. Multifunctional RNA nanoparticles. Nano letters. 2014;14(10):5662-71. doi: 10.1021/nl502385k. PubMed PMID: 25267559; PMCID: 4189619.
163. Afonin KA, Viard M, Kagiampakis I, Case CL, Dobrovolskaia MA, Hofmann J, Vrzak A, Kireeva M, Kasprzak WK, KewalRamani VN, Shapiro BA. Triggering of RNA interference with RNA-RNA, RNA-DNA, and DNA-RNA nanoparticles. ACS Nano. 2015;9(1):251-9. Epub 20141218. doi: 10.1021/nn504508s. PubMed PMID: 25521794; PMCID: PMC4310632.
164. Dao BN, Viard M, Martins AN, Kasprzak WK, Shapiro BA, Afonin KA. Triggering RNAi with multifunctional RNA nanoparticles and their delivery. DNA and RNA Nanotechnology. 2015;1(1):27-38. doi: 10.1515/rnan-2015-0001.
165. Martins AN, Ke W, Jawahar V, Striplin M, Striplin C, Freed EO, Afonin KA. Intracellular Reassociation of RNA-DNA Hybrids that Activates RNAi in HIV-Infected Cells. Methods Mol Biol. 2017;1632:269-83. doi: 10.1007/978-1-4939-7138-1_18. PubMed PMID: 28730446; PMCID: PMC6941940.
166. Afonin KA, Viard M, Tedbury P, Bindewald E, Parlea L, Howington M, Valdman M, Johns-Boehme A, Brainerd C, Freed EO, Shapiro BA. The Use of Minimal RNA Toeholds to Trigger the

Activation of Multiple Functionalities. Nano Lett. 2016;16(3):1746-53. Epub 20160229. doi: 10.1021/acs.nanolett.5b04676. PubMed PMID: 26926382; PMCID: PMC6345527.
167. Rogers TA, Andrews GE, Jaeger L, Grabow WW. Fluorescent monitoring of RNA assembly and processing using the split-spinach aptamer. ACS synthetic biology. 2015;4(2):162-6. doi: 10.1021/sb5000725. PubMed PMID: 24932527.
168. Groves B, Chen YJ, Zurla C, Pochekailov S, Kirschman JL, Santangelo PJ, Seelig G. Computing in mammalian cells with nucleic acid strand exchange. Nature nanotechnology. 2016;11(3):287-94. doi: 10.1038/nnano.2015.278. PubMed PMID: 26689378; PMCID: 4777654.
169. Seelig G, Soloveichik D, Zhang DY, Winfree E. Enzyme-free nucleic acid logic circuits. Science. 2006;314(5805):1585-8. doi: 10.1126/science.1132493. PubMed PMID: 17158324.
170. Turberfield AJ, Mitchell JC, Yurke B, Mills AP, Jr., Blakey MI, Simmel FC. DNA fuel for free-running nanomachines. Physical review letters. 2003;90(11):118102. doi: 10.1103/PhysRevLett.90.118102. PubMed PMID: 12688969.
171. Machinek RR, Ouldridge TE, Haley NE, Bath J, Turberfield AJ. Programmable energy landscapes for kinetic control of DNA strand displacement. Nature communications. 2014;5:5324. doi: 10.1038/ncomms6324. PubMed PMID: 25382214.
172. Srinivas N, Ouldridge TE, Sulc P, Schaeffer JM, Yurke B, Louis AA, Doye JP, Winfree E. On the biophysics and kinetics of toehold-mediated DNA strand displacement. Nucleic acids research. 2013;41(22):10641-58. doi: 10.1093/nar/gkt801. PubMed PMID: 24019238; PMCID: 3905871.
173. Sulc P, Ouldridge TE, Romano F, Doye JP, Louis AA. Modelling toehold-mediated RNA strand displacement. Biophysical journal. 2015;108(5):1238-47. doi: 10.1016/j.bpj.2015.01.023. PubMed PMID: 25762335; PMCID: 4375624.
174. Zakrevsky P, Bindewald E, Humbertson H, Viard M, Dorjsuren N, Shapiro BA. A Suite of Therapeutically-Inspired Nucleic Acid Logic Systems for Conditional Generation of Single-Stranded and Double-Stranded Oligonucleotides. Nanomaterials (Basel). 2019;9(4). Epub 20190415. doi: 10.3390/nano9040615. PubMed PMID: 30991728; PMCID: PMC6526476.
175. Bindewald E, Hayes R, Yingling YG, Kasprzak W, Shapiro BA. RNAJunction: a database of RNA junctions and kissing loops for three-dimensional structural analysis and nanodesign. Nucleic acids research. 2008;36(Database issue):D392-7. PubMed PMID: 17947325.
176. Bindewald E, Grunewald C, Boyle B, O'Connor M, Shapiro BA. Computational strategies for the automated design of RNA nanoscale structures from building blocks using NanoTiler. Journal of molecular graphics & modelling. 2008;27(3):299-308. PubMed PMID: 18838281.
177. Krokhotin A, Houlihan K, Dokholyan NV. iFoldRNA v2: folding RNA with constraints. Bioinformatics. 2015;31(17):2891-3. doi: 10.1093/bioinformatics/btv221. PubMed PMID: 25910700; PMCID: PMC4547609.
178. Ding F, Sharma S, Chalasani P, Demidov VV, Broude NE, Dokholyan NV. Ab initio RNA folding by discrete molecular dynamics: from structure prediction to folding mechanisms. RNA. 2008;14(6):1164-73. doi: 10.1261/rna.894608. PubMed PMID: 18456842; PMCID: PMC2390798.
179. Rothemund PWK. Folding DNA to create nanoscale shapes and patterns. Nature. 2006;440(7082):297-302. doi: 10.1038/nature04586.
180. Geary C, Rothemund PWK, Andersen ES. RNA nanostructures. A single-stranded architecture for cotranscriptional folding of RNA nanostructures. Science (New York, NY). 2014;345(6198):799-804. doi: 10.1126/science.1253920.
181. Waters AM, Der CJ. KRAS: The Critical Driver and Therapeutic Target for Pancreatic Cancer. Cold Spring Harb Perspect Med. 2018;8(9). Epub 20180904. doi: 10.1101/cshperspect.a031435. PubMed PMID: 29229669; PMCID: PMC5995645.
182. Huang L, Guo Z, Wang F, Fu L. KRAS mutation: from undruggable to druggable in cancer. Signal Transduct Target Ther. 2021;6(1):386. Epub 20211115. doi: 10.1038/s41392-021-00780-4. PubMed PMID: 34776511; PMCID: PMC8591115.

183. Jancik S, Drabek J, Radzioch D, Hajduch M. Clinical relevance of KRAS in human cancers. J Biomed Biotechnol. 2010;2010:150960. Epub 20100607. doi: 10.1155/2010/150960. PubMed PMID: 20617134; PMCID: PMC2896632.
184. Kemp SB, Cheng N, Markosyan N, Sor R, Kim IK, Hallin J, Shoush J, Quinones L, Brown NV, Bassett JB, Joshi N, Yuan S, Smith M, Vostrejs WP, Perez-Vale KZ, Kahn B, Mo F, Donahue TR, Radu CG, Clendenin C, Christensen JG, Vonderheide RH, Stanger BZ. Efficacy of a Small-Molecule Inhibitor of KrasG12D in Immunocompetent Models of Pancreatic Cancer. Cancer Discov. 2023;13(2):298-311. doi: 10.1158/2159-8290.CD-22-1066. PubMed PMID: 36472553; PMCID: PMC9900321.
185. Mahadevan KK, LeBleu VS, Ramirez EV, Chen Y, Li B, Sockwell AM, Gagea M, Sugimoto H, Sthanam LK, Tampe D, Zeisberg M, Ying H, Jain AK, DePinho RA, Maitra A, McAndrews KM, Kalluri R. Elimination of oncogenic KRAS in genetic mouse models eradicates pancreatic cancer by inducing FAS-dependent apoptosis by CD8(+) T cells. Dev Cell. 2023;58(17):1562-77 e8. Epub 20230824. doi: 10.1016/j.devcel.2023.07.025. PubMed PMID: 37625403.
186. Riely GJ, Ladanyi M. KRAS mutations: an old oncogene becomes a new predictive biomarker. J Mol Diagn. 2008;10(6):493-5. Epub 20081002. doi: 10.2353/jmoldx.2008.080105. PubMed PMID: 18832458; PMCID: PMC2570631.
187. Kam Y, Rubinstein A, Nissan A, Halle D, Yavin E. Detection of endogenous K-ras mRNA in living cells at a single base resolution by a PNA molecular beacon. Mol Pharm. 2012;9(3):685-93. doi: 10.1021/mp200505k. PubMed PMID: 22289057.
188. Santangelo PJ, Yang L, Bao G. EARLY DETECTION OF PANCREATIC CANCER USING MOLECULAR BEACONS. 2003 Summer Bioengineering Conference,. 2003.
189. Rose SD, Kim DH, Amarzguioui M, Heidel JD, Collingwood MA, Davis ME, Rossi JJ, Behlke MA. Functional polarity is introduced by Dicer processing of short substrate RNAs. Nucleic acids research. 2005;33(13):4140-56. Epub 20050726. doi: 10.1093/nar/gki732. PubMed PMID: 16049023; PMCID: PMC1180746.
190. Satoh K, Kaneko K, Hirota M, Masamune A, Satoh A, Shimosegawa T. Expression of survivin is correlated with cancer cell apoptosis and is involved in the development of human pancreatic duct cell tumors. Cancer. 2001;92(2):271-8. doi: Doi 10.1002/1097-0142(20010715)92:2<271::Aid-Cncr1319>3.0.Co;2-0. PubMed PMID: WOS:000169943900009.
191. Tran AN, Chandler M, Halman J, Beasock D, Fessler A, McKeough RQ, Lam PA, Furr DP, Wang J, Cedrone E, Dobrovolskaia MA, Dokholyan NV, Trammell SR, Afonin KA. Anhydrous Nucleic Acid Nanoparticles for Storage and Handling at Broad Range of Temperatures. Small. 2022;18(13):e2104814. Epub 20220206. doi: 10.1002/smll.202104814. PubMed PMID: 35128787; PMCID: PMC8976831.
192. Galindo-Murillo R, Robertson JC, Zgarbova M, Sponer J, Otyepka M, Jurecka P, Cheatham TE, 3rd. Assessing the Current State of Amber Force Field Modifications for DNA. J Chem Theory Comput. 2016;12(8):4114-27. Epub 20160707. doi: 10.1021/acs.jctc.6b00186. PubMed PMID: 27300587; PMCID: PMC4980684.
193. Zgarbova M, Otyepka M, Sponer J, Mladek A, Banas P, Cheatham TE, 3rd, Jurecka P. Refinement of the Cornell et al. Nucleic Acids Force Field Based on Reference Quantum Chemical Calculations of Glycosidic Torsion Profiles. J Chem Theory Comput. 2011;7(9):2886-902. Epub 20110802. doi: 10.1021/ct200162x. PubMed PMID: 21921995; PMCID: PMC3171997.
194. Case DA, Cheatham TE, 3rd, Darden T, Gohlke H, Luo R, Merz KM, Jr., Onufriev A, Simmerling C, Wang B, Woods RJ. The Amber biomolecular simulation programs. J Comput Chem. 2005;26(16):1668-88. doi: 10.1002/jcc.20290. PubMed PMID: 16200636; PMCID: PMC1989667.
195. Afonin KA, Dokholyan NV. Editorial to "Molecular engineering of biomaterials programmed to operate in living systems". Adv Drug Deliv Rev. 2023;193:114669. Epub 20221215. doi: 10.1016/j.addr.2022.114669. PubMed PMID: 36529189; PMCID: PMC10015611.
196. Cella F, Wroblewska L, Weiss R, Siciliano V. Engineering protein-protein devices for multilayered regulation of mRNA translation using orthogonal proteases in mammalian cells. Nat Commun. 2018;9(1):4392. Epub 20181022. doi: 10.1038/s41467-018-06825-7. PubMed PMID: 30349044; PMCID: PMC6197189.

197. Matsuura S, Ono H, Kawasaki S, Kuang Y, Fujita Y, Saito H. Synthetic RNA-based logic computation in mammalian cells. Nat Commun. 2018;9(1):4847. Epub 20181119. doi: 10.1038/s41467-018-07181-2. PubMed PMID: 30451868; PMCID: PMC6242901.
198. Ono H, Kawasaki S, Saito H. Orthogonal Protein-Responsive mRNA Switches for Mammalian Synthetic Biology. ACS Synth Biol. 2020;9(1):169-74. Epub 20191213. doi: 10.1021/acssynbio.9b00343. PubMed PMID: 31765565.
199. Rinaudo K, Bleris L, Maddamsetti R, Subramanian S, Weiss R, Benenson Y. A universal RNAi-based logic evaluator that operates in mammalian cells. Nat Biotechnol. 2007;25(7):795-801. Epub 20070521. doi: 10.1038/nbt1307. PubMed PMID: 17515909.
200. Goldfless SJ, Belmont BJ, de Paz AM, Liu JF, Niles JC. Direct and specific chemical control of eukaryotic translation with a synthetic RNA-protein interaction. Nucleic Acids Res. 2012;40(9):e64. Epub 20120124. doi: 10.1093/nar/gks028. PubMed PMID: 22275521; PMCID: PMC3351163.
201. de Mena L, Rizk P, Rincon-Limas DE. Bringing Light to Transcription: The Optogenetics Repertoire. Front Genet. 2018;9:518. Epub 20181102. doi: 10.3389/fgene.2018.00518. PubMed PMID: 30450113; PMCID: PMC6224442.
202. Nakanishi H, Yoshii T, Kawasaki S, Hayashi K, Tsutsui K, Oki C, Tsukiji S, Saito H. Light-controllable RNA-protein devices for translational regulation of synthetic mRNAs in mammalian cells. Cell Chem Biol. 2021;28(5):662-74 e5. Epub 20210127. doi: 10.1016/j.chembiol.2021.01.002. PubMed PMID: 33508227.
203. Pardi ML, Wu J, Kawasaki S, Saito H. Synthetic RNA-based post-transcriptional expression control methods and genetic circuits. Adv Drug Deliv Rev. 2022;184:114196. Epub 20220311. doi: 10.1016/j.addr.2022.114196. PubMed PMID: 35288218.

APPENDIX A: Previously published material

This dissertation contains previously published material. The original published article can be found online.

Chapter 2:

Avila, Y. I., Chandler, M., Cedrone, E., Newton, H. S., Richardson, M., Xu, J., Clogston, J. D., Liptrott, N. J., Afonin, K. A., & Dobrovolskaia, M. A. (2021). Induction of Cytokines by Nucleic Acid Nanoparticles (NANPs) Depends on the Type of Delivery Carrier. **Molecules**, 26(3), 652. https://doi.org/10.3390/molecules26030652